Università degli Studi di Ferrara

DOTTORATO DI RICERCA IN

SCIENZE DELL'INGEGNERIA

CICLO ***XXX***

COORDINATORE Prof. Stefano Trillo

LINK DESING AND RESOURCE OPTIMIZATION FOR 5G WIRELESS SYSTEMS

Settore Scientifico Disciplinare ***ING-INF/03***

Dottorando:
Dott. Andres Ortega

Tutore:
Prof. Velio Tralli

Anni: 2014/2017

DEDICATION:

No podría expresar en pocas lineas todo el camino
que tuve que atravezar para estar aquí,
sin embargo la vida me enseñó que ningún camino
esta lleno de rosas y el mundo no es lo que aparenta ser.
He vivido hasta aquí para entregar mi esfuerzo a todos
mis seres queridos que han formado, forman y formarán
parte de mi vida
brindándome su aliento y apoyo en cualquier momento;
pero sobre todo, he vivido para entender una cosa sola
"el sacificio y el esfuerzo no tienen punto de comparación"
por eso, esta dedicatoria va para quienes
sacrificaron sus vidas para que yo esté aquí:
*** Juanito: Eres muy chiquito aún para entender, pero sé lo dificil*
que pasaste sin mí, y tu sacrifico será recompensado eternamente...
*** Flakita: Por su apoyo incondicional y sacrificar su porvenir*
dió paso a que yo esté aquí, y eso no lo hace cualquier mujer...
*** Mami: Diste todo por mi, y hasta mucho más de lo que te pedí*
Simplemente soy lo que soy por ti...

Introduction

The development of 5G wireless communications systems imposes more demanding challenges for mobile operators to support the data volume growth in the next few years, (up to three orders of magnitude with respect to long-term evolution (LTE) systems). Among them, the achievement of lower latency, higher energy efficiency, and scalability and flexibility of the network [1]. These more stringent requirements demand, more efficient modulation, coding, and multiple access schemes, in areas like cognitive radio, Internet of things and machine-to-machine communications [2].

Adaptive M-QAM modulation schemes have been chosen by Long-Term Evolution (LTE) to maximize network performance with a limited amount of spectrum. Depending on the signal-to-noise ratio (SNR), small or large constellations are adaptively used to achieve higher spectral efficiencies. However, the use of the M-QAM modulations may be restrictive to cover the quality of service (QoS) requirements of the expected massive connections in 5G environments. When it comes to massive connectivity, MIMO techniques [3], starting from Alamouti STBC scheme [4] are developed to give more capacity over network access legacy. Also the recent advances on the combination among spatial modulation and MIMO, and the use of beam-forming technique are an additional motivation towards optimization of 5G mobile communications [5].

To design such a system, is necessary to consider the effect of each block within the transmission system. As is known, the coding techniques are relevant in LTE systems. In this context, turbo codes and convolutional codes have been used to adapt the access network of LTE. However, today for the 5G mobile

communications, a parallel processing for coding channel called "Low-Density Parity-Check" (LDPC) codes has caught the attention [6]. These codes allow approaching the theoretical Shannon capacity with a reasonable complexity [7] in order to reduce packet loss of transmitted data. Moreover, several studies, using different rates and packet lengths, show that LDPC codes have a better performance than convolutional and turbo codes [8][9][10] currently used by LTE mobile systems. Thus, the needs of high reliability and spectral efficiency for 5G communications could be achieved through LDPC codes and high order modulations. An interesting scheme is proposed by Huawei Technologies in [11] called Sparse Code Multiple Access (SCMA), where the coding techniques and multidimensional modulations are combined in order to improve the Air Interface Ratio Transmissions for Multi-Access Schemes .

Another point to consider for the multiple-access scheme is the support to massive connectivity. In current 4G mobile networks, orthogonal frequency division multiplexing (OFDM) is used to transmit over the wireless channel with the aim of reduce the ISI interference when the number of users is increased. However, the high PAPR of this technology poses some challenges to meet 5G requirements. In an environment with thousands of users and devices transmitting and receiving information (such as expected for 5G systems), it is necessary to choose multiple access techniques that maintain a low PARP, e.g. PAPR$\leq$ 5 dB [1], without impairing BER performance, because the PAPR reduction techniques affect directly the system performance. One such technique, with a low PAPR over fading channels, is Interleaved Frequency Division Multiple Access (IFDMA) [12]. This technique can be consider as a special kind of a multi-carrier spread-spectrum scheme, which assigns each user overlapping but mutually orthogonal subcarriers. The increase in the number of subcarriers allows to increase system capacity in function of amount information and the number users.

In this context, Generalized Frequency Division Multiplexing (GFDM) [13] has been recently proposed for next generation mobile networks, derived from the filter-bank multicarrier (FBMC) approach [14]. It is based in multicarrier transmission with multiple time slots. Moreover, introducing non-orthogonal subcarri-

ers allows controlling different properties of the signal. A disadvantage of GFDM is its high PAPR, which may be higher than that of an OFDM using the same number of subcarriers [15]. This is because each GFDM has circular signals proprieties in time and frequency domain. In addition the effects of non-linearities in the transmission significantly impacts the trade-off between energy and spectral efficiency. Energy efficient transmission of signals with high peak-to-average-power ratio (PAPR) using power amplifiers produces out-of-band (OOB) emissions and performance degradation, thus reducing spectral efficiency.

In order to avoid such distortion effects, there is the need to use amplifiers with a large input back-off (IBO) in the transmitted signal which increases the energy consumption in mobile devices. Idealizing the model, we can investigate GFDM systems with non-linear channel in order to analyze the real effects in the uplink transmission and explore the effectiveness of some PAPR reduction techniques to mitigate OOB radiation and error performance degradation.

The 5G network needs to go soft in terms of Air interface in order to provide users with massive different services and quality of experience. To address these issues, the concept of Software Defined air Interface (SDAI) for 5G, that includes an intelligent controller and multiple configurable building blocks such as the multiple access, modulation and coding, spatial processing, synchronization and MU-MIMO techniques has been proposed. The building blocks have been brought from Matlab implementation to the SDR (Software Defined Radio) systems using a GNU Radio free platform and fully compatible with Matlab in order to reduce the computational complexity.

In this context, a link adaptation framework for 5G can be developed to find the optimal candidates sets for the implementation of the 5G air interface for different scenarios and objective requirements. In order to verify the theoretical concepts, we implemented the schemes designed for the air interface by using a SDR systems [16], considering a synchronization systems with adaptive LDPC codes [6] for MIMO transceiver [17], reducing in this way the processing complexity. The field research in Air interface for 5G is opening for future networks [18], considering a mix of techniques that provides more spectral efficiency [19], rate

transmission, reliability and capacity.

In addition MIMO 2x2 [4] and 3x4 are used in our experimental test using the Simulink toolkit over GNU Radio platform in order to demonstrate a real communications systems conserving the next generation concepts. This is a very important work for the future implementations on communications systems.

However, the overall capacity depends not only on the digital processing that is performed at the physical layer level, instead it depends substantially on the resources allotment in the network. If we use OFDMA (Orthogonal Frequency Division Multiple-Access) or any other orthogonal or non-orthogonal multi-access method [20] [21], they maintain the same concept that allow multiple users are allowed to transmit simultaneously on different subchannels during the same symbol period. This means that the network capacity can be increased [22] and managed by Resource Allocation Optimizer on the BS.

For this reason, Resource Allocation and Admission Control issues play a very important role and they are widely studied on the literature, with the aim of increasing the performance in the network and the cells capacity to support the users connectivity. In this context, the concept of femtocell [23] has been introduced with the objective of reducing the traffic demand on the network, increasing the rates due to the small dimension of the femtocells which provide the service to the neighbor users.

The heterogeneity of cellular [24] and other wireless networks will be a dominant trend in the near future. Even though the trend of increasing heterogeneity in wireless networks generates new possibilities for communication, by improving flexibility, capacity and energy efficiency, because of the increased possibility to communicate over short wireless links. It also introduces several challenges for the control and management.

In fact, reusing the same frequency in cellular networks to support simultaneous communications on different coexisting links has the potential to increase spectral efficiency, but at the same time it introduces harmful interference. In this scenario, when femtocell or D2D [24] users share the resources with cellular users (CUs), a two-level network is created. The cross-link interference can

be controlled by using suitably designed radio resource allocation (RRA) algorithms that coordinate on a short-time basis the use of slots, subcarriers and power among users, trying to optimize spectral efficiency and to guarantee a predefined level of QoS. On QoS-aware networks, on top of RRA algorithms, admission control (AC) mechanisms admits to the service only the users able to achieve the requested QoS, to further avoid interference and waste of resources.

The networks densification and micro networks (VANETS, Smart Meters, Smart Grids) will increase the use of large-scale data. The coverage of wireless and wired access networks will provide a high bandwidth services at low cost for end users. In this scenario, a hybrid fiber radio infrastructure for NAN Networks is proposed considering the future trends.

For this purpose it is necessary to consider the compatibility of radio systems with standard Passive Optical Networks (PON) systems, where the coexistence of the technologies Fiber&Wireless (FiWi) is guaranteed. It is also important to decide the optical infrastructure, where Dense-Wavelength-Division Multiplexing (DWDM) approach would support a much higher user density, but with large deployment cost.

In this context, we have proposed a novel adaptive modulation technique using M-QAM for wavelength-division multiplexing (WDM) [25]. The simulation is carried out in Matlab, in order to validate its performance prior to its implementation. With the design and the test set of parameters proposed in Chapter 3 the system is able to ensure high data transmission rates at long distances.

Advanced spectral efficient multilevel modulation formats combined with Mode-Locked Fiber Lasers (MLFL) [26] and Polarization division multiplexing (PDM) are essential for future large-capacity wavelength-division multiplexing (WDM) transmission systems.

Figure 1 presents a communication model with the general topics of the study carried out in this thesis, with all the techniques used at the level of physical layer, data link and application layer, for an optimal communications system that guides the future of the latest generation networks in 5G mobile communications systems. In this context, the processing for wireless and optical communications has

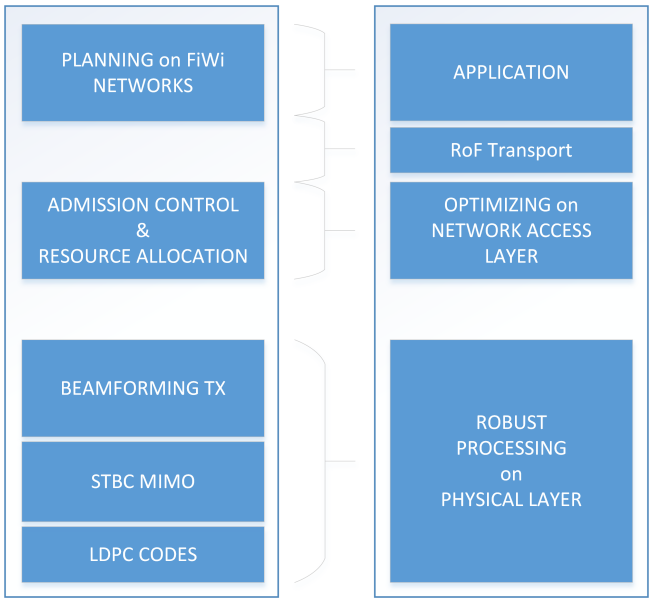

Figure 1: Enhancements for Next Generation Networks: Robustness, Reliability and Optimization in FiWi Networks

been developed in order to evaluate a GFDM scheme over non-linear channel and to design Optical Modulations as a solution for FiWi Networks and 5G Backhaul.

For the Network Access Layer a novel scenario with two-tier macro&femto cells is developed in order to investigate optimal algorithms, considering the interference, for admission control of users. Finally, the network planning is considered in the design of last generation networks in order to optimize the infrastructure that allows connectivity between Fiber Backhaul and Base Stations.

The thesis has many approaches from any of the levels cited above with the aim to design, evaluate and plan the future networks, and it is organized as follows: The Chapter 1, is oriented to Physical Layer Processing for the validation of different techniques such as PAPR reduction techniques, MIMO techniques and LDPC codes over schemes with 5G requirements. In this context, the work has been published in [27] and [28].

The Chapter 2 shows the investigation of the effects of pilot-aided channel estimation on the capacity of a two-tier HetNet with QoS-aware centralized ad-

mission control (AC) and radio resource allocation (RRA) algorithms that control the effects of cross-interference and optimize a service provider revenue in order to improve the capacity and performance in the system. This chapter shows the most relevant result of the thesis, as in literature does not exist the study of the effects of channel estimation errors on HetNet capacity. The work has been published in [29].

Finally, the Chapter 3 presents the investigation of planning method for FiWi networks and the processing schemes for optical link communications.

An optimal planning algorithm is based on Heuristics Process with georeferenced. The algorithm proposed provides the optimal location of BS in order to provide the 100% of connectivity with Advanced Metering Infrastructure (NAN) for Smart Meters Users. In addition, the algorithm provides the optimal distance between the BS and splitter device for the optical link, guarantying in this way the low cost of fiber. This work was published in [30].

On another hand, we propose a joint Multilevel Modulation and LDPC coding over Optical Systems for holistic 5G backhaul, where the systems is simulated with 4 parallel Mach Zehnder Modulators using a commercially available dual drive IQ modulator driven by eight binary signals combining with different amplitudes. This proposed design is of complex manufacture according to [31], [32], due to transceivers must have smaller footprints in order to reduce the power consumption. However, the simulated results show an interesting performance when the system is transmitted at 64-QAM up 80 km of distance. Those schemes are promising for high-speed multilevel modulations. The rate transmission achieved is 320 Gbps. This work has been published in [33].

Contents

List of Figures

List of Tables

Chapter 1

Transmission Schemes for 5G systems

1.1 Generalized Frequency Division Multiplexing (GFDM)

OFDM is the choise for multicarrier systems, but it suffers from significant strong spectral leakage even when using pulse shaping techniques or guard carriers to neighboring frequency bands.

Generalized Frequency Division Multiplexing (GFDM) has been recently proposed as a new waveform for next generation 5G mobile networks. GFDM is a non-orthogonal, block-based multi-carrier modulation scheme with circular signal properties in time and frequency domain, which can be efficiently implemented based on the fast Fourier transform (FFT) algorithm. A disadvantage of GFDM, similarly to the other multicarrier signals, is its high peak-to-average-power ratio (PAPR).

Peak-to-average power ratio (PAPR) is a key performance parameter of wireless communication schemes that impacts cost and energy efficiency of the hardware equipment. Large PAPR signals can easily saturate the transmit power amplifier and cause degradation in BER performance and out-of-band emissions.

For this reason, the performance of GFDM in presence nonlinearity effects in the transmission channel is investigated, with the aim to explore the effectiveness

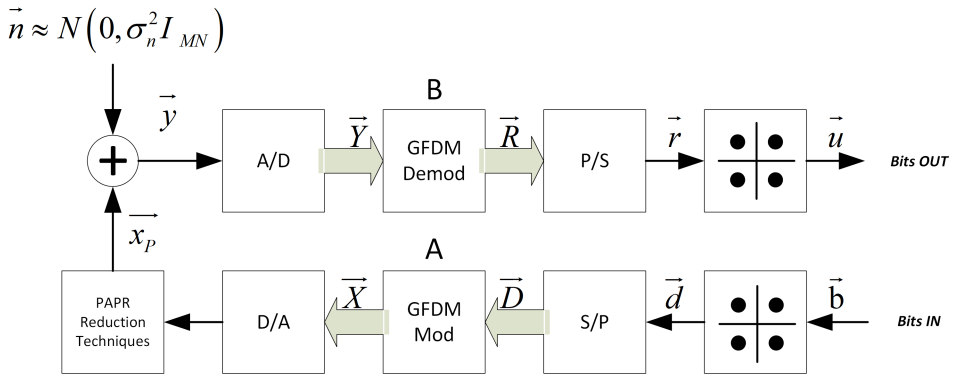

Figure 1.1: TX/RX block scheme for OFDM/GFDM

of some PAPR reduction techniques to mitigate OOB radiation and error performance degradation.

The GFDM scheme for Tx/Rx is as shown in the Figure 1.1. The binary source $\overline{b}$ are first mapped to a set of complex points, using 16-QAM modulation thus producing the serial data symbols $\overline{d}$. These symbols are then processed through a S/P block to convert them to a block of $KM \times 1$ parallel data symbols $\overline{D}$. The KM complex data symbols are distributed in M time slots and K frequency slots.

The subcarriers are modulated and the transmitted signal $\overline{x}_{[n]}$ is obtained through the superposition of all subcarriers signals weighted with the complex data symbols $\overline{d}_{k,m}$ as follows

$$\bar{x}_{[n]} = \sum_{m=0}^{M-1} \sum_{k=0}^{K-1} \bar{d}_{k,m} g_{T_x}[n] \tag{1.1}$$

Each subcarrier signal $g_{Tx}[n]$ is a shifted version, by mN and $k\frac{1}{N}$ in the time and frequency domain, respectively, of a circular filter $g[n]$:

$$g_{T_x}[n] = g[(n - mN)|_{MN}] e^{-i2\pi \frac{kn}{N}} \tag{1.2}$$

To avoid the aliasing, $\overline{D}$ is then upsampled. The Upconversion of the subcarriers can be done through the IFFT. The transmitted signal can be also rewritten [34] by using a linear matrix model according to:

$$\bar{X} = A\bar{D} \tag{1.3}$$

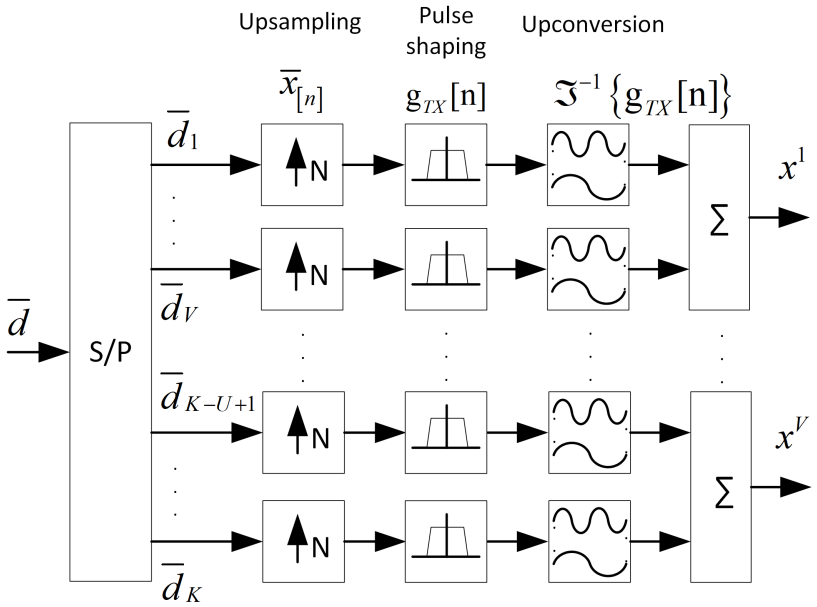

Figure 1.2: GFDM design scheme.

where the signal $\bar{X}$ transmitted contains the samples of $\bar{x}_{[n]}$ and A is a $KM \times KM$ transmitter matrix. A cyclic prefix (CP) should be also added to preserve the circular convolution, but in this paper it has no impact as multipath fading channel is not considered.

The signal is transmitted over a nonlinear channel with AWGN noise, as follows

$$\bar{y} = F_{NL}[\bar{x}_p] + \bar{n} \tag{1.4}$$

where $F_{NL}[.]$ in the nonlinear function characterizing the power amplifier, $\bar{n} \sim N\left(0, \sigma_n^2 I_{MN}\right)$ is the AWGN vector with noise variance σ_n^2 and I_{MN} is the $MN \times MN$ identity matrix. All the mathematical procedure described above is the GFDM design scheme, that it is shown in Figure 1.2.

It is important to clarify that $\bar{x}_p$ in the transmission scheme is the signal function of the different PAPR reduction techniques considered in this paper. In the next section we will explain how obtain $\bar{x}_p$ signal using the different PAPR reduction techniques.

There are three methods to design the receiver, i.e. by considering Matched Filter, Zero Forcing, MMSE processing. We have considered the Zero Forcing method [14] by using the receiver matrix $\bar{B}$ as the pseudo inverse matrix of $\bar{A}$. The output signal is defined as:

$$\bar{R} = B \cdot \bar{Y} \tag{1.5}$$

where

$$B = \left(A^H A\right)^{-1} A^H \tag{1.6}$$

and $\bar{Y}$ is the parallel vector of received data samples.

After parallel to serial conversion. The signal $\bar{r}$ is then demodulated to obtain the received bits $\bar{u}$.

1.2 PAPR Reduction Techniques

In this thesis, is consider different PAPR reduction techniques such as Clipping, Selected Mapping (SLM), Companding and interleaved frequency division multiple access (IFDMA), in order to compare the best efficiency in terms of PAPR, out-of band (OOB) emissions and BER over nonlinear channel. These schemes are under the sight of 5G requirements for the design of an uplink multiple-access systems using GFDM.

In a power amplifier when the input signal increases, also OOB radiation increases due to non-linear effect, thus resulting in interference between adjacent subcarriers. Below we discuss the different techniques used to reduce the PAPR, which will be analyzed in the next section. Here we describe clipping, companding and IFDMA techniques. SLM technique is illustrated in [35].

1.2.1 Clipping

Clipping is deliberately performed to limit the peaks in the signal to be transmitted over a non-linear channel. This operation causes non-linear degradation of

the signal and, without any countermeasure, a bad BER performance and out-of-band emissions. The clipped signal can be written as:

$$\bar{x}_{p[n]} = \begin{cases} \bar{x}_{[n]} & if \left|\bar{x}_{[n]}\right| \leq A_{max} \\ A_{max} e^{j\varphi(\bar{x}_{[n]})} & otherwise \end{cases} \tag{1.7}$$

where A_{max} is the clipping level and $\varphi(\bar{x}_{[n]})$ is the phase signal. Clipping is performed on a sufficiently oversampled signals (interpolation). The Clipping Ratio (CR) is defined as:

$$CR = \frac{A_{max}}{\sigma} = \frac{A_{max}}{\sqrt{E(\bar{x}_{[n]})^2}} \tag{1.8}$$

This parameter typically in the range $CR = 1 \approx 3$ should be selected as function of the system behavior. To reduce out-of-band emissions filtering is usually applied after clipping [36]. Since filtering may cause peak regrowth, the parameters of clipping and filtering should be jointly designed to obtain the wanted trade-off.

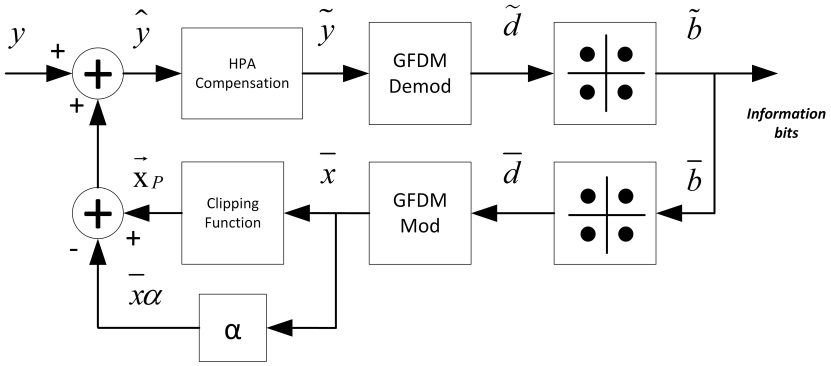

Figure 1.3: Functional scheme of the iterative receiver for clipped.

According to the Bussgang's theorem [1][37] for memoryless nonlinearities, the clipping effect produces an additive distortion noise, uncorrelated of $\bar{x}_{[n]}$, and an attenuation constant defined by:

$$\alpha = 1 - e^{-\gamma^2} + \sqrt{\frac{\pi}{2}} \cdot \gamma \cdot erf(\gamma) \tag{1.9}$$

where $\gamma = CR$. This fact can be exploited as in [38] to build an iterative detection algorithm at the receiver by estimating the received signal as follows:

$$\hat{y}[n] = \frac{1}{\alpha}(y[n] - d[n]) = x[n] - \tilde{w}[n] \tag{1.10}$$

where $\tilde{w}[n] = \frac{w[n]}{\alpha}$, and $w[n]$ is the additive distortion noise. If the receiver knows the clipping function, $d[n]$ can be estimated from $y[n]$ through the following algorithm:

Algorithm 1 Detection algorithm for clipping technique

Step 1 `Initialize: Recover the M-QAM symbols`

$d[n]$.

Step 2 `if:`

$\{x = A \cdot d[n]\} \geq Amp_{\max}$

`then`

Step 3 `for 1 : n-iter`

Step 4 $\hat{d}[n] = f_C(x) - \alpha \cdot x$

Step 5 $\hat{y}[n] = y(n) - \hat{d}[n]$

Step 6 $d[n] = B * \left(\frac{\hat{y}[n]}{\alpha}\right)$

Step 7 `end`

1.2.2 Companding

This technique is a variant of the clipping technique because it not only cuts the peaks, but amplifies the small values of the signals increasing the average power. In this context, we use as a non-linear function the μ-law that modifies the signal as follows:

$$\bar{x}_{c[n]} = \frac{V \log(1 + \mu|\bar{x}_{[n]}|/V)}{\log(1 + \mu)} e^{j\varphi(\bar{x}_{[n]})} \tag{1.11}$$

where V is the standard deviation of the GFDM signal $\sigma_{\tilde{x}[n]}$. This technique has a low complexity in terms of implementation, but has negative effects over OOB, as it introduces the distortion caused by the non-linear function used in the transmission. For this reason, the BER varies with signal amplitude resulting in a degradation of system performance.

1.2.3 IFDMA

Interleaved Frequency Division Multiple-Access(IFDMA) can be seen as a kind of multicarrier spread-spectrum scheme, where the users are identified by the subcarriers that they occupy. An IFDMA-symbol is obtained by compressing, the symbol time *(T)* to a chip time ($\tilde{T}$), with a compression factor of the signal equal to Q.

Thus, an IFDMA data block for one user consists of $L = K/Q$ modulated data symbols (as for OFDM, we consider a data block of $L \times M$ symbols, with $M = 1$) as shown in [12]. The data block is then shifted in the frequency domain, by applying DFT, and spreading is obtained, as shown in Fig. 3, by interleaving them over the K subcarriers (DFT-spreading technique). Finally the IFFT is applied to this block of K complex values.

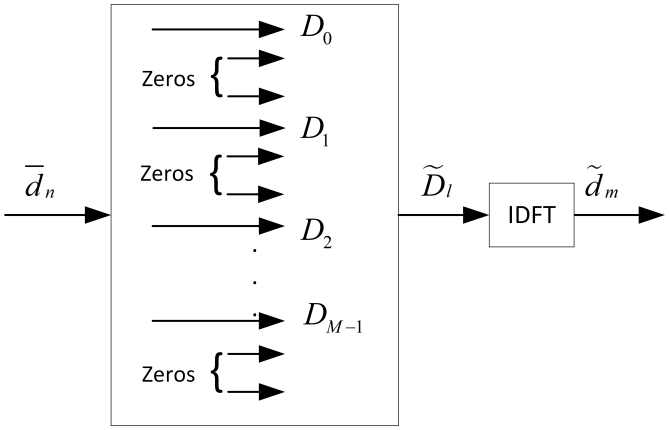

Figure 1.4: Subcarrier Mapping Scheme for IFDMA: K is total number of subcarriers $K > L$ and $\tilde{T} = TL/K$ is the symbols duration.

By looking at Fig. 3, the data symbols $\bar{d}$ are transformed through DFT to frequency domain samples D_k, and the interleaved signal sequence $\tilde{D}_l$ is obtained through zero insertion:

$$\tilde{D}_l = \begin{cases} D_{l/Q}, & l = 0, Q, 2Q, \dots \\ 0, & otherwise \end{cases} \tag{1.12}$$

The low complexity of the IFDMA technique compared with Clipping and Companding techniques is due to that there is no need to compensate for distortion at the receiver.

It smooths the high peaks in the transmitted signals, thus reducing the effects of the nonlinear channel. In this way more spectral efficiency could be achieved. This will be evaluated in the next section.

1.2.4 Peak-Average-Power-Ratio Analysis

The results of the simulations were performed in MATLAB, where were considered the following parameters for all techniques: $M = 15$ time slots, $K = 128$ frequency slots, 16 QAM modulation mapping, raised cosine pulse shaping with roll-off factor 0.1. Having in mind uplink applications, the transmitter is configured to use only $K/4 = 32$ consecutive frequency slots. When IFDMA is used for comparison the parameters are set as follows: $Q = 4$ $L = 128$. Each simulation run is made of 2000 data blocks.

In Figure 1.5 PAPR distribution is shown for GFDM with the different PAPR reduction techniques. The best performance is obtained by clipping and companding techniques with suitable choice of clipping ratio and compression parameters, thus addressing the 5G requirements (PAPR$\leq 5dB$). At the value of CCDF= 0.01 the figure shows that a gain of 8-9 dB approximately is achievable with respect to GFDM without PAPR reduction technique. In addition, there is a gain of 6 dB approximately with respect to IFDMA technique. In the figure, clipping ratios of 1.25 and 2.5 are considered, whereas companding is based on the μ-law where the quantization parameter μ is taken between 8 and 32. The case of $\mu = 32$, achieves a gain of 1.2 dB with respect to $\mu = 8$ in terms of PAPR at CCDF= 0.01.

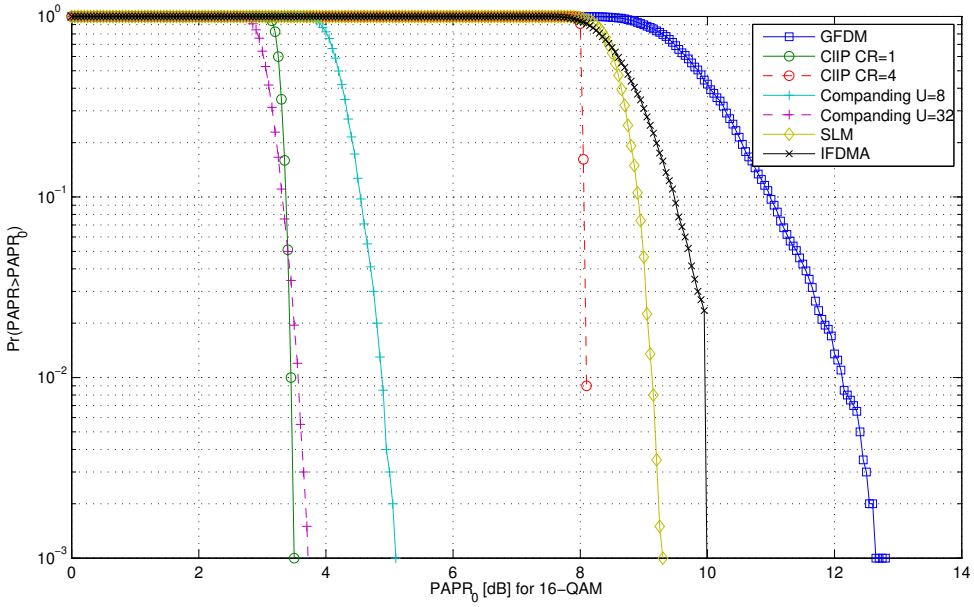

Figure 1.5: PAPR for GFDM and different PAPR reduction techniques.

Regarding IFDMA and SLM techniques, PAPR reduction is obtained without introducing any distortion in the transmitted signal. The gain is limited to 2-3 dB but there is no need to recover distortion at the receiver.

1.2.5 PSD Analysis

The power spectral density (PSD) analysis allows a qualitative evaluation of the performance in terms of spectral efficiency, by showing the OOB radiation [39] generated by the signal. Here, in the Figures 1.6 and 1.7, we show the PSD of the GFDM signal with and without PAPR reduction techniques before the transmission through a power amplifier. The effect of the power amplifier will be considered in the next subsections. In the figures the PSD is evaluated by considering an oversampling factor of 8 and by normalizing the bandwidth occupied by all the subcarriers to 1 MHz.

We note from the Figures 1.6 and 1.7 that SLM and PTS techniques do not

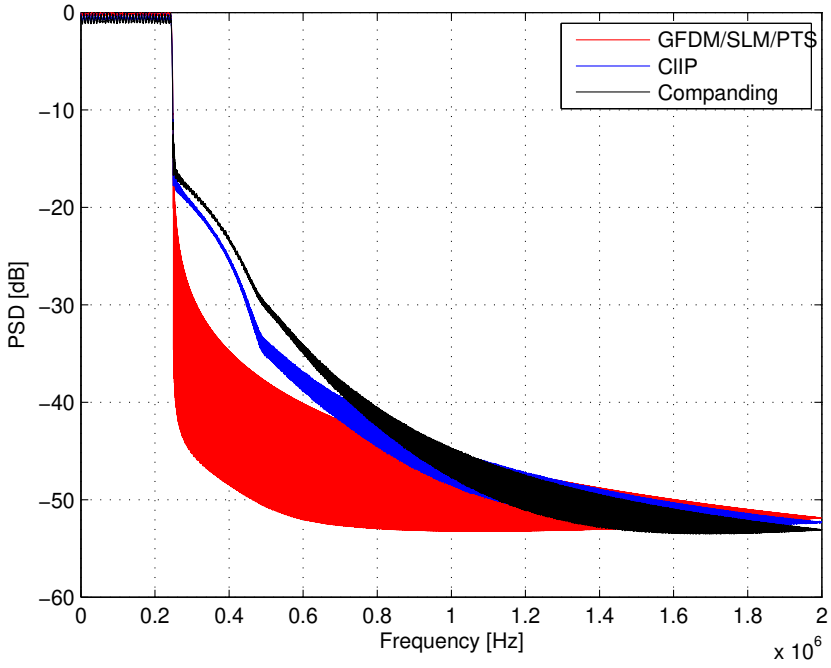

Figure 1.6: PSD of GFDM, SLM, CLIP and Companding techniques.

change the spectrum of GFDM. This is very important because these techniques do not increase of the OOB noise floor. However, less useful information can be transmitted with the same power, due to the redundancy introduced. The clipping and companding techniques increase the OOB noise floor before transmission through the power amplifier, but may support a better bandwidth efficiency, compared to GFDM, in presence of a nonlinear amplifier.

IFDMA has the lowest OOB emission, but the signal is spread over the entire bandwidth. The main advantage of IFDMA with respect to others techniques is the possibility to use in cognitive radio applications where transmission parameters can be adapted to the environment in order to reduce the interference between primary and secondary users.

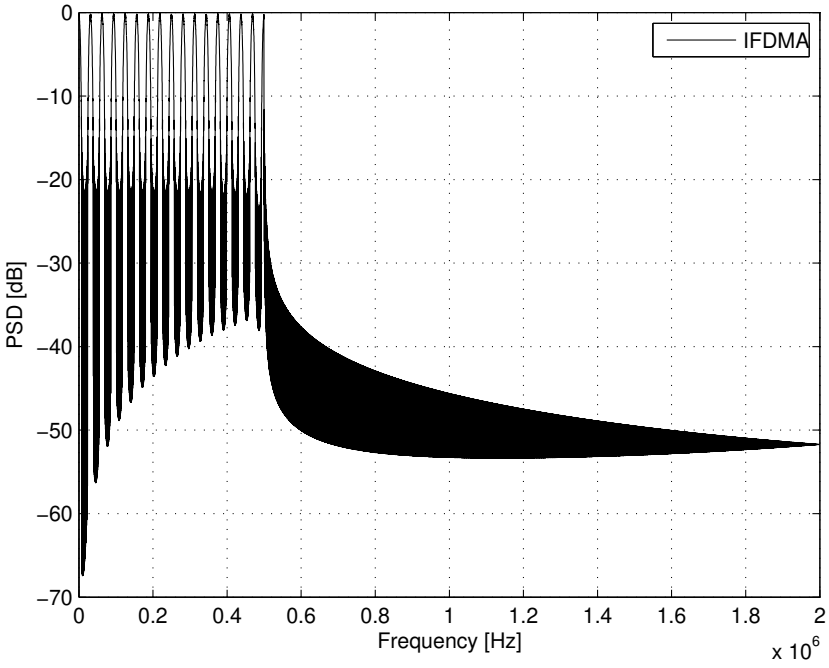

Figure 1.7: PSD of IFDMA tecnhnique.

1.2.6 BER vs IBO analysis

In real communications systems, the performance must be evaluated in presence of a high power amplifier at the transmission side, thereby causing nonlinear distortion effects in the system. The distortion arises when the system works over the non-linear or saturation zone of the amplifier.

To define the working point on the amplifier the input backoff (IBO) in dB is defined as:

$$IBO = 10 * log_{10} \frac{P_{max}^{in}}{P_{in}} \tag{1.13}$$

where $P_{max}^{in} = (A_{sat})^2/2$, and A_{sat} is the saturation level at the input of the power amplifier. However, for future works is possible to apply the HPA nonlinearity conditions using the Saleh model [40] in order to shown a real effect of the transmission system.

Figure 1.8(a) shows the BER performance as function of the IBO for GFDM with and without clipping or companding, OFDM and IFDMA, when the Eb/N0 parameter is set at 12dB, being $SNR = E_b/N_0 + 10\log_{10}(\log_2 D)$, where D is the modulation index. The clipping ratio is set to 1.25 or 2.5, whereas companding works with $\mu = 4$.

The results show that the system is degraded when the IBO level is low, but when the IBO level increases, the BER achieves the floor corresponding to the performance of the system without the nonlinear amplification at the given Eb/N0.

The BER floor is approximately 10^{-4} for all techniques with the exception of companding. This can be easily checked also in Figure 1.9 where the BER performance is evaluated in a linear channel for GFDM with clipping and clipping+filtering, and with different clipping ratios. When the receiver iteratively compensates for the distortion caused by clipping, the BER loss due to clipping can be almost recovered. However, the use of filtering, as expected, introduces BER degradation, since the receiver is not optimized for this case.

The performance of the system with clipping improves when the CR increases. On the other hand, PAPR increases when the CR increases. Hence, a trade-off should be found between CR = 1 and CR = 3. With CR = 1 the clipping technique can be used to optimize the PAPR level and to improve performance at the low IBO levels (see Fig. 1.9), but a larger CR is better to keep the BER low when filtering is needed. A more complete point of view can be gained in the next subsection considering a quantitative analysis of OOB radiation.

From Fig. 1.8(a) we can see that a 2 dB gain in terms of IBO is obtained at BER= 10^{-3} and with CR=1.25. The performance of the system with companding is quite poor without a receiver able to compensate for nonlinear degradation. In [41] is used a Polynomial-Based Compressing technique for PAPR Reduction, but the computational complexity is very high in comparison with our iterative technique based on clipping. The performance system can be improved by reducing the CR factor as is shown in the Figure 1.8(a).

In this context, IFDM is a technique to be considered and analyzed, because can to support the non linear degradation without iterative detection algorithm.

1.2.7 OOB leakage vs IBO analysis

GFDM can improve the out-of-band (OOB) radiation with respect to OFDM by using pulse shaping for the subcarriers. This can reduce the OOB radiation in order to not affect adjacent signals or neighbouring cells. In this regard, [42] show relevant results for OOB control in terms of interference variance by using 1 and 6 guard carriers. The choice of pulse shaping also affects BER performance of GFDM which is investigated in [34] when the roll-off factor of the pulse shaping filter is varied of 0.1 to 0.5 and standard receiver techniques, i.e. the MF, ZF, and MMSE, are used. To prevent rate loss the tail-biting is applied, and the cyclic prefix (CP) is added in order to prevent the multi-path effects in channel.

We evaluate here the amount of OOB emissions through the OOB leakage with reference in [39] defined as:

$$OOB = \frac{|B|}{|\overline{B}|} \frac{\int_{f\in B} P(f)df}{\int_{f\in \bar{B}} P(f)df} \tag{1.14}$$

where $\mathcal{B}$ and $\overline{\mathcal{B}}$ are in-band and out-of-band set of frequencies, respectively, and $P(f)$ is the PSD.

In Fig. 1.8(b), the OOB leakage is plotted as function of OBO comparing the behavior of GFDM e the different PAPR reduction techniques. When the IBO level is low, the systems works near the saturation zone, and the companding technique can not support high power levels. The inefficiency of this system was demonstrated in the previous BER performance analysis. When the IBO tends to infinity OOB leakage tends to a floor that measures the OOB emission in a linear channel. In addition, clipping without filtering does not reduce OOB leakage, even if it improves the PAPR. SLM technique reduces OOB emissions of 1-2 dB in the nonlinear working zone. Clipping+filtering provides substantial improvements. When CR=2.5 the OOB leakage of GFDM is reduced in both the linear and the nonlinear zone. When CR=1.6 the improvement is only in the region of small IBO. With the system settings of our simulation about 2 dB gain of power efficiency is achieved by using clipping+filtering with a suitable choice of CR between 1.5 and 2.5.

The table 1.1 summarizes the parameters used for the simulations carried out in Matlab:

Table 1.1: **List of parameters used in Matlab for GFDM Systems**

Number of subcarriers (K)	128
Number of subsymbols (M)	15
Frequency of carrier (f_c)	1MHz
Oversampling frequency ($\updownarrow$)	4
Oversampling factor (L)	8
Roll-off factor (α)	0.1
Modulations order D	16-QAM
E_b/N_0	12dB
Number of blockcs	2000
μ-law (μ)	4
Clipping Ratio (CR)	1.25 to 2.5 dB
Maximum Amplitude of signal (A_{max},)	1

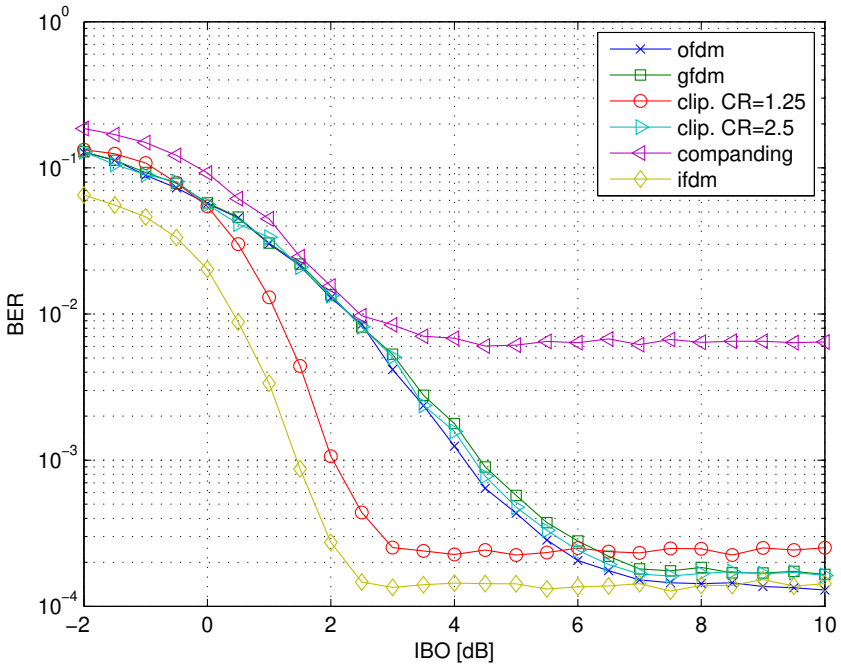

(a)

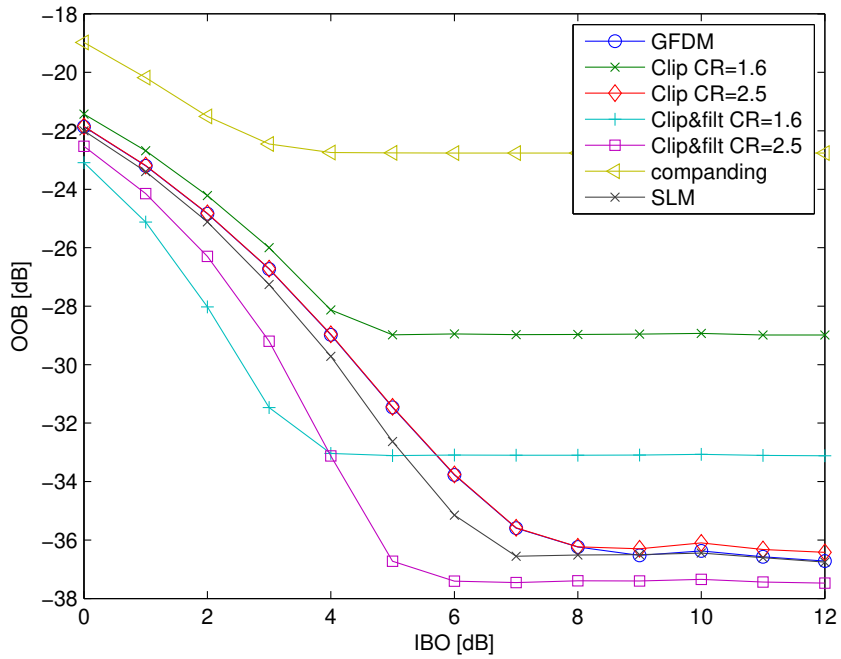

(b)

Figure 1.8: Evaluation of PAPR reduction techniques in GFDM System over linear channel, with (a) BER vs IBO, and (b) OOB leakage vs IBO.

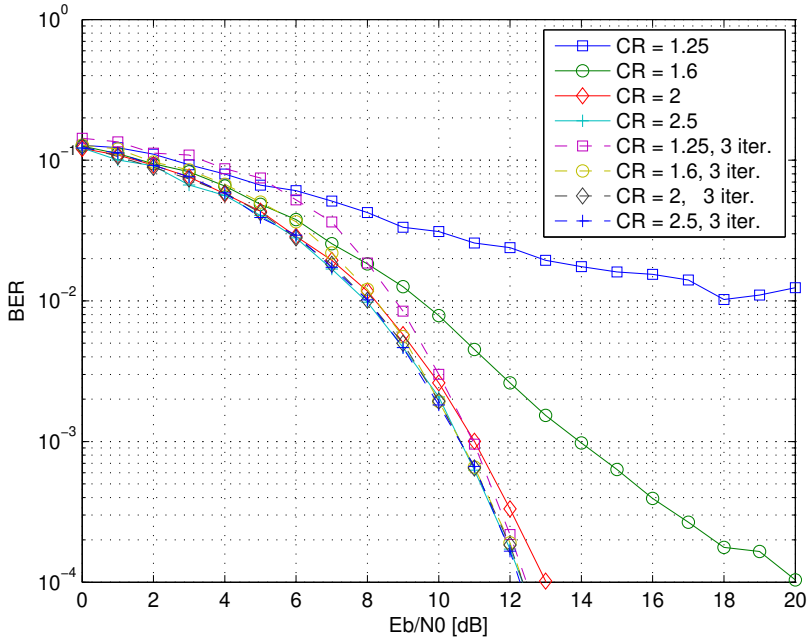

(a)

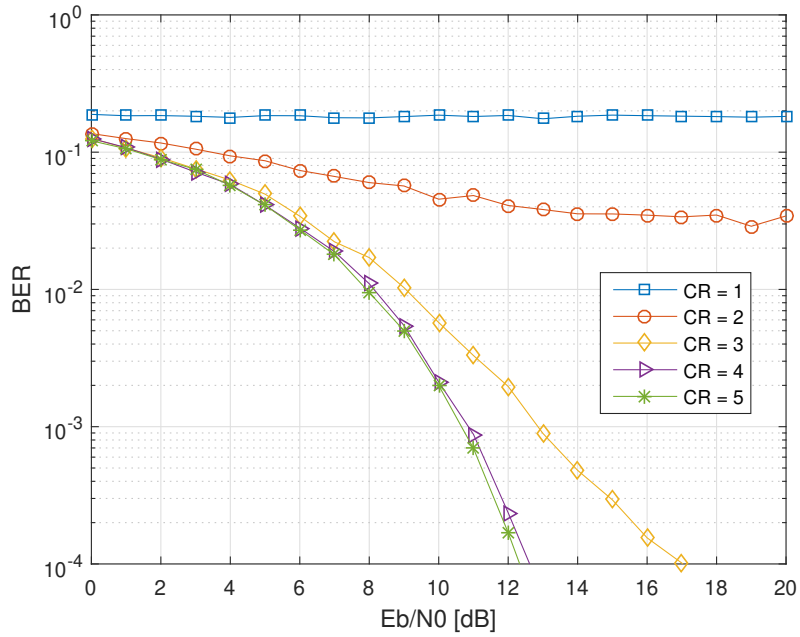

(b)

Figure 1.9: BER Performance for GFDM over linear channel, with (a) clipping, with and without iterative detection, and (b) clipping+filtering.

1.3 Experimental Evaluation via Software Defined Radio System

The legacy access networks should provide higher capacity, rate and spectral efficiency due to high demand of data transmission. However, in the actuality, the systems should be tested under real conditions, for this reason, the transitions from analog to digital by radio communications are implemented in Software-Defined Radio (SDR).

The Software Defined Radio increases the flexibility via programmable hardware and it provides a robust signal processing, where previously it was not possible to be developed, i.e FEC codes using parallel processing.

Motivated by these considerations, we have decided to combine different techniques in order to build a coding schemes, that they today have won the attention for 5G communications.

In this context, LDPC codes are combined with multi-antenna techniques in order to improve the reliability and capacity in the communication system for massive connectivity. The current hardware is able to support NT x NR antennas at the transmitter and receiver respectively, this allows us to create different MIMO configurations with variable number of antennas.

MIMO techniques such as Alamouti-STBC offer some benefits such as greater network access capabilities that help to make transmission more reliable, while LDPC coding provides higher transmission reliability due to a good error correction codes and offer an approximation to the limit of capacity established by Shannon. In this context, the system can support high quality of information and high rates in the transmission.

The proposal is to design a TX/RX communication system over Software Defined Radio as is shown in Figure1.10. This system is implemented in GNU Radio which has the Simulink support platform with graphical interface; in order to achieve a better performance in the signal processing. In this context, we have used initially two devices NI-USRP 2920 to achieve the base transmission MIMO 2X2. However, is necessary to use an expansion cable with the aim of connecting

the two devices, in addition, via software the synchronization protocol is set for to use different NT and NR antennas. In the next section is explained the configuration process for two devices. The power transmission for each device is limited at 30dB.

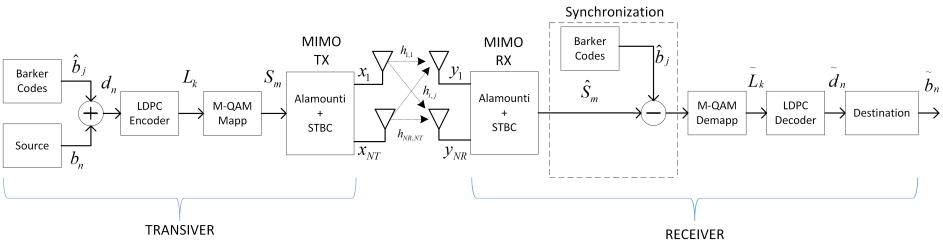

Figure 1.10: System Block Diagram using LDPC-MIMO channel.

1.3.1 Synchronization Process

In order to know the header frame sent, training sequences are added for the synchronization process. In this context before coding process the sequences are introduced at the transmitter's side. The training sequences are codewords bits with auto correlation properties, which should be known in the receiver and transceiver respectively.

The Barker codes are subsets of sequences used for data synchronization in digital communications. There are different Barker codes lengths, being the maximum length $l = 13$ as is shown in the Table 1.2.

The process to build the frame in the transmitter side, results from the addition of training sequence $\widehat{b_j} \in \{0, 1\} \forall j = [1, ..., 4l-1]$ and the source information $b[u]$, where the amount of information to be sent are 32400 random bits.

The training sequence or Header is defined by Unipolar Barker Code where their length is 4-times incremented due to the correlation properties. When the length sequence is increase, the synchronization improves.

In order to obtain the synchronization process using Barker Codes in the receiver side, the correlations between the training sequence and the receiver signal

Table 1.2: Barker Codes

Code Length	Barker Code
1	[-1]
2	[-1 1]
3	[-1 -1 1]
4	[-1 -1 1 -1]
5	[-1 -1 -1 1 -1]
7	[-1 -1 -1 1 1 -1 1]
11	[-1 -1 -1 1 1 1 -1 1 1 -1 1]
13	[-1 -1 -1 -1 -1 1 1 -1 -1 1 -1 1 -1]

is applied in the following equation [43]:

$$\Re_m = \left| \sum_{j=1}^{l-1} \widehat{b}_j \hat{S}_{m+j} \right|^2 \tag{1.15}$$

Where $\hat{S}_m$ is the received signal after MIMO scheme. In this context, $\widehat{b}_j$ is obtained through a signal processing where $t_i \in \{-1, 1\} \forall i = [1, ..., l-1]$ is initially converted to a binary data type in this way: $b_i \in \{0, 1\} \forall i = [1, ..., l-1]$, after this signal is multiplied to 4 times its length as in the transmitter $\widehat{b}_j \in \{0, 1\} \forall j = [1, ..., 4l-1]$. Finally the multiplied signal is modulated with the aim of converting to symbols as is shown in Fig. 1.11.

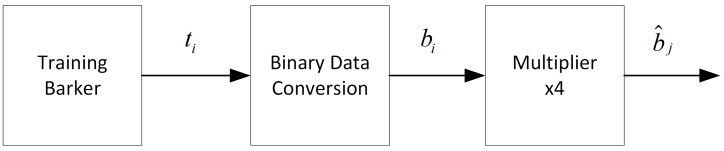

Figure 1.11: Barker Code Symbol Generation.

In order to detect the frame start, the maximum value of the correlation is obtained according to the length of the Barker Code in this way:

$$J = \underset{m}{\text{argmax}} \Re_m \tag{1.16}$$

Then, from the maximum value onwards the signal to be demodulated by M-QAM decoder will be: $\hat{S}_{m+j}$

1.3.2 Synchronization using NI-USRP

Some applications require synchronization across multiple USRP (Universal Software Radio Peripheral) devices. In this work, we will used two NI-USRP-2920, ready to work over GNU Radio Platform and synchronized using a MIMO cable.

For a transceiver to be considered MIMO-capable, each channel in the system must meet two basic requirements:

1. The sample clocks must be synchronized and aligned.

2. DSP operations must be performed on samples aligned in time from the same sample clock edge

The Figure 1.12 shows the configuration used, where a single Gigabit Ethernet(GigE) interface can be used to communicate with both USRP devices. The USRP connected to the GigE acts as a switch and routes data to/from both USRP devices. It will also handle time synchronization of the data so the sample alignment process is transparent to the user.

1.3.3 Phase Alignment with NI 2x2 MIMO System

In the transmitter side, due to the components in the scheme such as amplifiers, filters, place additional requirements on the systems, since its contribute to phase error and phase offsets that vary with time. In addition to sample and sample clock alignment the system must maintain a known phase relationship between each RF input or output. Due to phase ambiguities caused by phased-locked loops which are used for up and down-conversion, some calibration may be required to determine this phase relationship. Thus, applications that require RF phase alignment may require periodic calibration.

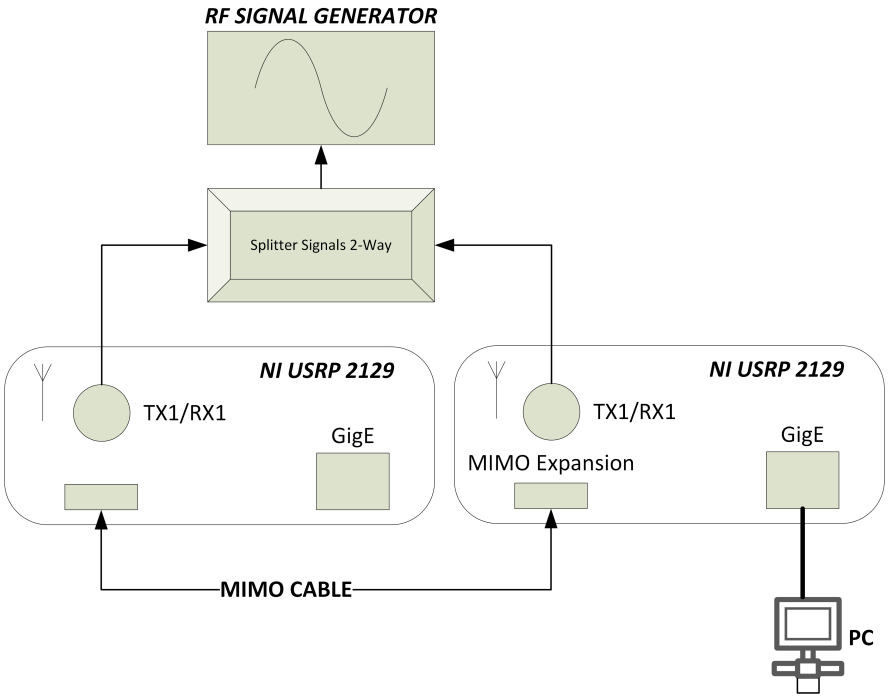

Figure 1.12: NI-USRP 2x2 Reference Design.

In this context, UHD API allows you to select synchronization settings for each USRP device. These settings are also exposed through GNU Radio blocks. GNU Radio Compnion (GRC) is used for this basic illustration.

Figure 1.13(a) shows a flowgraph that receives two streams from two unsynchronized USRP devices. Notice in Figure 1.14 that there are obvious phase and frequency differences between the two signals. This is a result of variations in the two unsynchronized reference clocks. Here is applied to one of the USRP devices internal reference crystals to amplify the frequency variation between the two units.

A single UHD block is used in the GRC flowgraph that is shown in Figure 1.13(b). The block parameters are configured to set up a 2x2 MIMO system. As example, the settings of interest to be configured over Simulink platform in order to linking devices are:

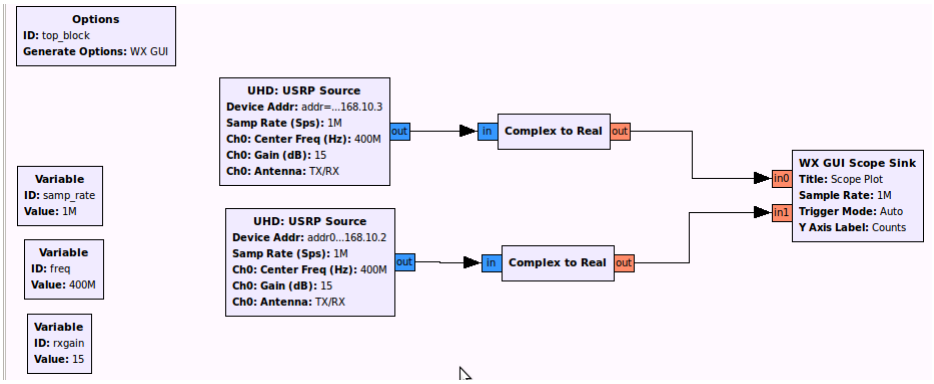

(a)

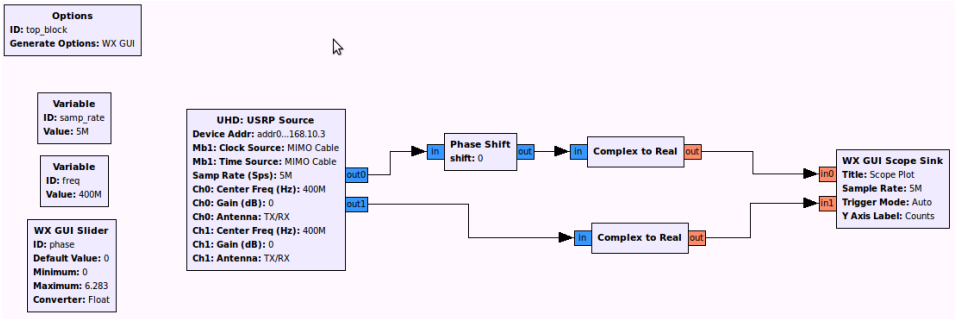

(b)

Figure 1.13: GRC Reception with two NI-USRP 2129, with (a) Un-Synchronized , and (b) Synchronized .

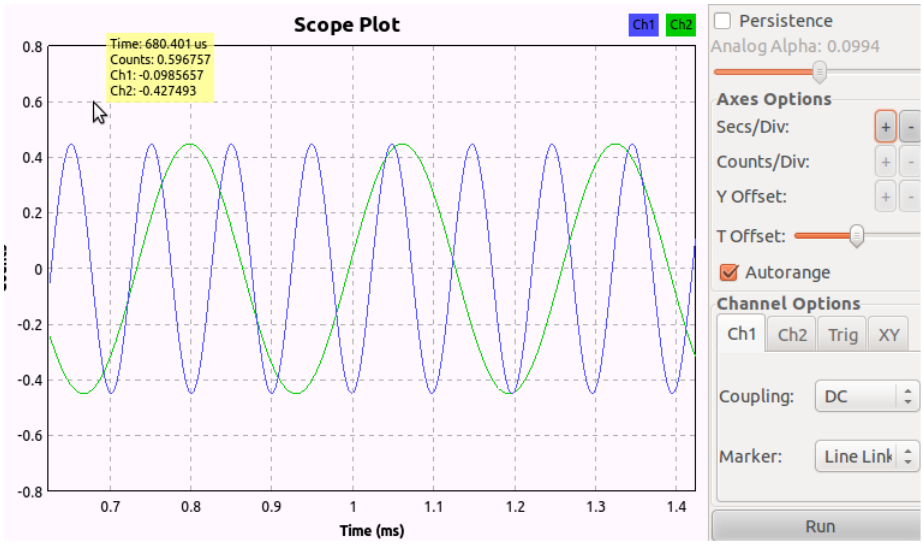

Figure 1.14: Un-Synchronized USRP devices, phase descompesation.

```
Device addr:  addr0=192.168.10.2,addr1=192.168.10.3
Sync = don't sync
Num Mboards = 2
Mb0 Clk Src = Default
Mb0 Time Src = Default
Mb1 Clk Src = MIMO Cable
Mb1 Time Src = MIMO Cable
```

These settings configure the first USRP device, Mb0, which corresponds to the first entry in the address string, to use its default reference for clocking and timing. The second USRP(Mb1) is configured to accept its frequency and timing reference from the MIMO cable. The signals are provided by Mb0. All other standard settings such as center frequency and gain assignments apply as well.

Figure 1.15 shows the signals with phase correction applied. In this plot, it is clear the MIMO connection has enabled the frequency and time references to be synchronized. The random phase offset is corrected with a complex phase shift in the flowgraph. In real applications, this phase correction would be implicitly generated with algorithms such as maximum-ratio combining (MRC), or periodic calibration.

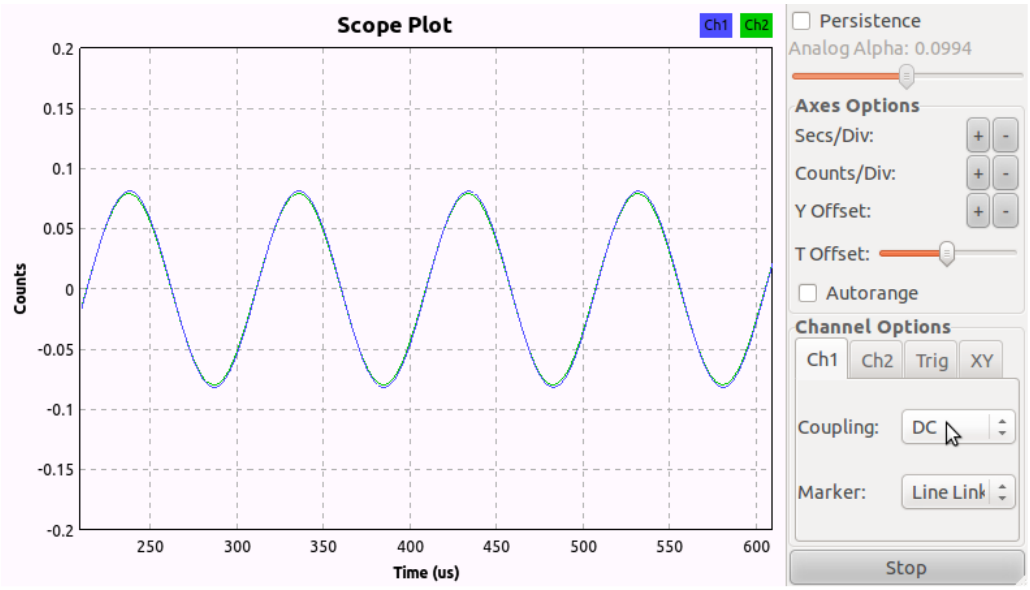

Figure 1.15: Time Domain Received Signal with Phase Compesation.

1.3.4 LDPC codes design

Low density parity check (LDPC) is considered into linear block codes, providing a close capacity to Shannon's Theory, which are suitable to work when the interference is increased. An additional motivation with the use of LDPC codes, is shown the performance for ergodic fading, in particular, to MIMO fading channels, where substantially will depend on the number of antennas [44]. For this reason, combining coding and modulation is an interesting approach for the future wireless communications, however the practical implementation can be a limiting when the number of devices increases proportionally with the computational complexity.

In this section we start with the desig of the LDPC codes. The redundancy bits are introduced in order to build the codeword. In this way, parity-check matrix H generates the codeword to be sent through G is $n \times k$ sparse matrix, if and only if:

$$H = [A, I_{k-n}] \tag{1.17}$$

where A is a matrix $(k-n) \times n$ and $I_{(k-n)}$ is the identity matrix. Therefore, with the aim to obtain the G matrix, the Gauss-Jordan method is applied from H matrix in this way:

$$G = [I_n, A^T] \tag{1.18}$$

where G is orthogonal to H, therefore must satisfy the next equation:

$$G \cdot H^T = 0 \tag{1.19}$$

In the transmission side, the source information vector $d[n]$ is multiplied by G_{nxk} in order to build a codeword of length $n < k$.

The data rate is multiplied by the code rate $R = n/k$, and thus is decreased by the addition of $(k-n)$ redundant bits. The parity check matrix could be generated in several ways. In this paper, we generate the H matrix from irregular Gallager codes, according to the bit stream transmitted, where $n = u + 4l = 32400$, $k = 64800$ resulting a H matrix of dimension $k - n$ x k.

In addition to the matrix representation, LDPC codes can be described using a graphical representation. A bipartite graph, called Tanner graph [45][46] is used for this propose as is show in Figure 1.16. LDPC codes can be decoded iteratively, using a relatively low powered microprocessor by using lookup tables (LUT). This process can be developed in two forms: hard-decision or soft-decision. In the first case, the decoder makes the decision based on the value of 1 or 0 of a single bit. In the second case, the decoder is able to discriminate among a set of quantized logical values between 0 and 1, allowing it to offer better performance than hard-decision [45].

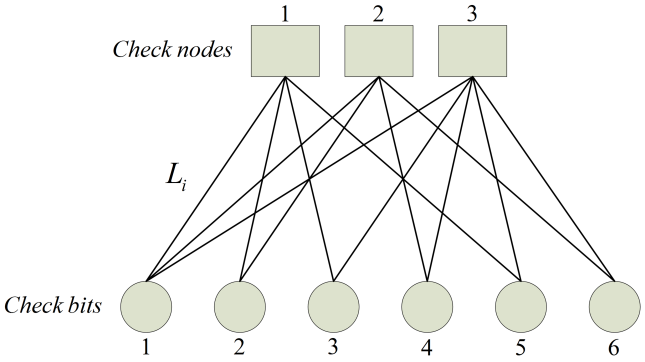

Figure 1.16: Tanner graph.

Soft-decision decoder is based on the idea of belief propagation, which performing inference on graphical models. Thus, a Sum-Product decoding algorithm (SPA) [45] that is used in our simulations, is applied and the probabilities are expressed as log-likelihood ratios (LLR) as messages between symbol and parity-check nodes. In our proposal, we use soft decision through LUT according to model proposes in [47]. In this case, the combining of Gray code with LUT returns a binary value with the aim of representing the metrics as log likelihood:

$$L_i = r_i + \sum_{j \in A_i} E_{j,i} \tag{1.20}$$

Where L_i is the translation from LLR back to probabilities, r_i is the priori message probabilities and $E_{j,i}$ is the extrinsic probability from check node j to bit

node i.

$$r_i = \begin{cases} \log \frac{p}{1-p}, u = 1 \\ \log \frac{1-p}{p}, u = 0 \end{cases} \tag{1.21}$$

Where u is the incoming bit when p has the probability of receiving a bit zero or a bit one. $E_{j,i}$ is the LLR of the probability that bit i causes parity-check j to be satisfied.

$$E_{j,i} = \log \left[\frac{1 + \prod \tanh\left(M_{j,i}/2\right)}{1 - \prod \tanh\left(M_{j,i}/2\right)} \right] \tag{1.22}$$

Where, $M_{j,i}$ is the the messages sent from the bit nodes to the check nodes. In order to avoid sending back to each check node information which it already has, the message from i-th node to the j-th check node is the sum in 1.20 without the component $E_{j,i}$ in this way:

$$M_{j,i} = \sum_{j' \in A_i, j' \neq j} E_{j',i} + r_i \tag{1.23}$$

Where j' is the check node repeated in the region A_i

1.3.5 Alamouti-STBC scheme for MIMO Channels

Space-Time Block Coding (STBC) has been developed to provide reliable transmission for multiple input multiple output (MIMO) antenna system, even more with the combination of other techniques in order to achieve the multi-diversity antennas.

STBC is a complex orthogonal space-time code where the principal aim is to achieve the diversity of antennas and it implement a efficient detection per-symbol on the receiver through maximum likelihood (ML).

Given an information of binary sequence $d_n = [d_0, ..., d_n] \rightarrow d_n \in \{0, 1\}$, we can obtain the corresponding codewords $L_k = [L_0, ..., L_k] \rightarrow L_k = 2d_n$ by the matrix multiplication $L = d^T \cdot G$, where G is the generator matrix of the LDPC code developed in previous section. In order to encode the information sequence

we would have to compute the generator matrix G, therefore the computational complexity is reduce using the LDPC blocks in Simulink platform.

Next,the codewords are mapped with a stream of QAM symbols to produce M parallel spatial streams of symbols. In addition, the scheme is designed with $N_T = 2$, $N_R = 2$ and $N_T = 3$, $N_R = 4$ as show in the Figure 1.10, where N_T and N_R are the antennas number of transceiver and receiver respectively.

Then, the complex matrix of Alamouti-STBC MIMO 2x2 is defined by X in this way:

$$\mathbf{X} = \begin{pmatrix} x_1 & -x_2^* \\ x_2 & x_1^* \end{pmatrix} \tag{1.24}$$

Where x_1 and x_2 are two consecutive symbols. The first column represents the symbols to be transmitted by the first antenna and the second column represents the symbols to be transmitted by the second antenna over two time instants. We assume M-QAM modulation, the transmitted signals from the first and the second antenna are $x_1 = s_1 + j \cdot s_2$ and $x_2 = s_3 + j \cdot s_4$; where $s_i, i \in \{1, ..., M\}$ are the binary information symbols.

The channel entries are complex i.e., $h_{1,1} = {h^R}_{1,1} + j{h^I}_{1,1}$, where ${h^R}_{1,1}$ and ${h^I}_{1,1}$ represents the real and imaginary part respectively. Then, the channel matrix for MIMO 2x2 can be written in this way:

$$\mathbf{H} = \begin{pmatrix} h_{1,1} & h_{1,2} \\ h_{2,1} & h_{2,2} \end{pmatrix} \tag{1.25}$$

For the received signal we express as $\mathbf{Y} = \mathbf{HX} + \mathbf{n}$, where $\mathbf{n}$ is the Gaussian noise with independent real and imaginary components. The signal received signal can be rewrite as follows:

$$\begin{aligned} y_1 &= h_{1,1}x_1 + h_{1,2}x_2 + n_1 \\ y_2 &= h_{2,1}x_1 + h_{2,2}x_2 + n_2 \end{aligned} \tag{1.26}$$

Then inserting the symbols, the signal is rewritten as:

$$\begin{aligned} \Re\{y_1\} &= {h^R}_{1,1}s_1 - {h^I}_{1,1}s_2 + {h^R}_{1,2}s_3 - {h^I}_{1,2}s_4 \\ I\{y_1\} &= {h^I}_{1,1}s_1 + {h^R}_{1,1}s_2 + {h^I}_{1,2}s_3 + {h^R}_{1,2}s_4 \\ \Re\{y_2\} &= {h^R}_{2,1}s_1 - {h^I}_{2,1}s_2 + {h^R}_{2,2}s_3 - {h^I}_{2,2}s_4 \\ I\{y_2\} &= {h^I}_{2,1}s_1 + {h^R}_{2,1}s_2 + {h^I}_{2,2}s_3 + {h^R}_{2,2}s_4 \end{aligned} \tag{1.27}$$

For MIMO 3x4 case it follows in the same way, considering that the first column represents the symbols to be transmitted by the first antenna, and so on until the last column in correspondence with the total transmission antennas. Then, the channel matrix is defined as:

$$\mathbf{H} = \begin{pmatrix} h_{1,1} & \dots & h_{1,NT} \\ \vdots & \ddots & \vdots \\ h_{NR,1} & \cdots & h_{NR,NT} \end{pmatrix} \tag{1.28}$$

The received signal is defined by:

$$\begin{aligned} y_1 &= h_{1,1}x_1 + h_{1,2}x_2 + h_{1,3}x_3 + n_1 \\ y_2 &= h_{2,1}x_1 + h_{2,2}x_2 + h_{2,3}x_3 + n_2 \\ y_3 &= h_{3,1}x_1 + h_{3,2}x_2 + h_{3,3}x_3 + n_3 \\ y_4 &= h_{4,1}x_1 + h_{4,2}x_2 + h_{4,3}x_3 + n_4 \end{aligned} \tag{1.29}$$

Then, we can to rewrite the Equation 1.29 in the next way:

$$\begin{aligned} \Re\{y_1\} &= h^R{}_{1,1}s_1 - h^I{}_{1,1}s_2 + h^R{}_{1,2}s_3 - h^I{}_{1,2}s_4 + h^R{}_{1,3}s_5 - h^I{}_{1,3}s_6 \\ I\{y_1\} &= h^I{}_{1,1}s_1 + h^R{}_{1,1}s_2 + h^I{}_{1,2}s_3 + h^R{}_{1,2}s_4 + h^I{}_{1,3}s_5 + h^R{}_{1,3}s_6 \\ \Re\{y_2\} &= h^R{}_{2,1}s_1 - h^I{}_{2,1}s_2 + h^R{}_{2,2}s_3 - h^I{}_{2,2}s_4 + h^R{}_{2,3}s_5 - h^I{}_{2,3}s_6 \\ I\{y_2\} &= h^I{}_{2,1}s_1 + h^R{}_{2,1}s_2 + h^I{}_{2,2}s_3 + h^R{}_{2,2}s_4 + h^I{}_{2,3}s_5 + h^R{}_{2,3}s_6 \\ \Re\{y_3\} &= h^R{}_{3,1}s_1 - h^I{}_{3,1}s_2 + h^R{}_{3,2}s_3 - h^I{}_{3,2}s_4 + h^R{}_{3,3}s_5 - h^I{}_{3,3}s_6 \\ I\{y_3\} &= h^I{}_{3,1}s_1 + h^R{}_{3,1}s_2 + h^I{}_{3,2}s_3 + h^R{}_{3,2}s_4 + h^I{}_{3,3}s_5 + h^R{}_{3,3}s_6 \\ \Re\{y_4\} &= h^R{}_{4,1}s_1 - h^I{}_{4,1}s_2 + h^R{}_{4,2}s_3 - h^I{}_{4,2}s_4 + h^R{}_{4,3}s_5 - h^I{}_{4,3}s_6 \\ I\{y_4\} &= h^I{}_{4,1}s_1 + h^R{}_{4,1}s_2 + h^I{}_{4,2}s_3 + h^R{}_{4,2}s_4 + h^I{}_{4,3}s_5 + h^R{}_{4,3}s_6 \end{aligned} \tag{1.30}$$

LDPC-STBC 3x4 performance: In the Figure 1.17 shows the BER performance using the combination among LDPC codes, STBC MIMO 3x4 and M-QAM modulation modeling over Rayleigh channel. The simulated results shown that the system improves around $4dB$ with respect to systems with uncoded over AWGN channel, when the index modulation is increased. This is an important contribution because the LDPC-MIMO technique reduce the interference significantly and BER distortion in presence of random channels where it becomes necessary the use of coding channel. In addition, MIMO 3x4 is easily adapted to the

initial configuration: MIMO 2x2 when we used the devices, being very important to confront the performance system in terms of capacity.

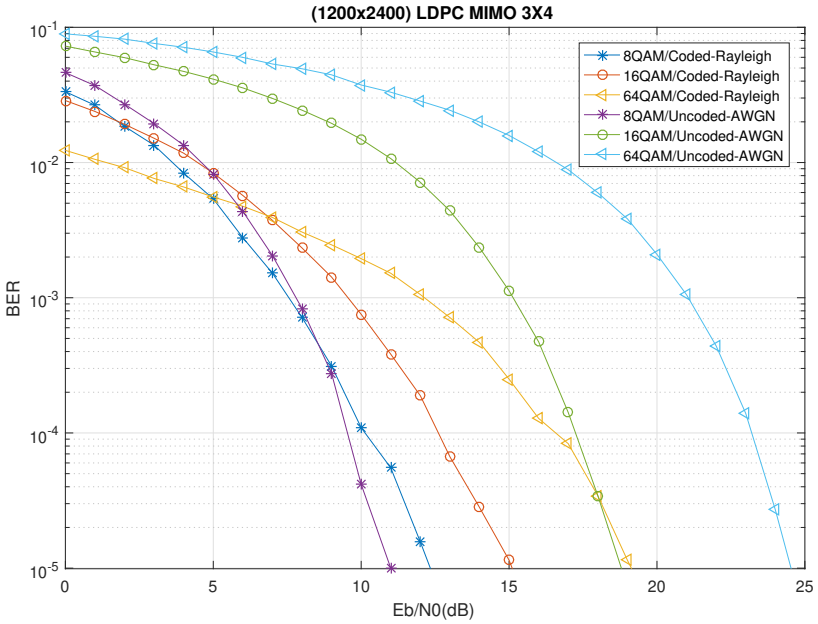

Figure 1.17: M-QAM-LDPC-MIMO 3x4.

LDPC-Alamounti 2x2 performance: On the other hand, the Figure 1.18 shows the simulation with MIMO 2x2 over Rayleigh channel following the same parameters of Figure 1.17. The simulated results show that the system worsen about $13dB$ of SNR for all cases with respect to Figure 1.17. Therefore the system outperform significantly the distortion when the antennas number in the receiver is increased. The gain obtained with MIMO 3x4 provides the possibility to work with greater capacity in the system without a trade-off of interference and distortion. For this reason is very important to choose the correct modulation index. We can see that between 8QAM and 16QAM there is no significant gain in terms of SNR, however between 16QAM and 64QAM there is about of 5dB of gain in terms of SNR. Thus 16QAM could have a better performance in the system with respect to other modulations.

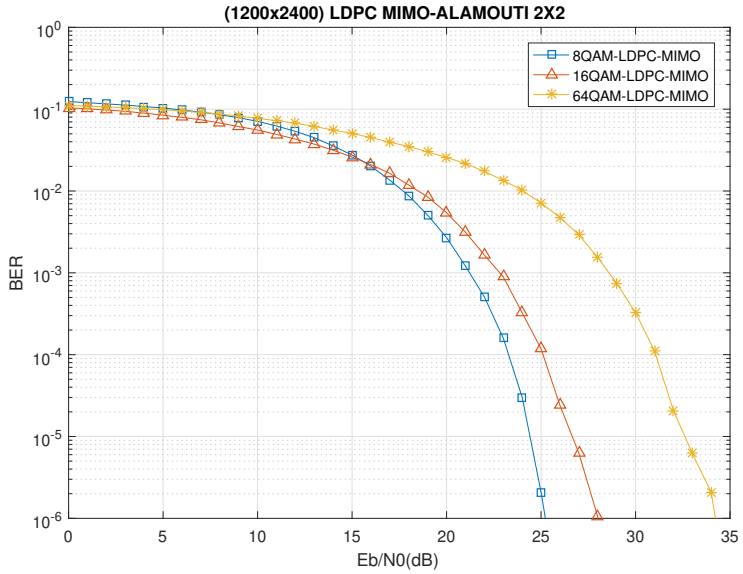

Figure 1.18: M-QAM-LDPC-MIMO 2x2.

LDPC-MIMO 3x4 performance using Rayleigh fading channel: The Figure 1.19 shows the experimental results over SDR systems obtained through the Tables 1.3 and 1.4 respectively. When the channel Rayleigh is used, we can see similar results with respect to simulated results showed in Figure 1.17. In this context, to work with real systems like SDR allows to implemented real systems of high complexity and parallel processing when the LDPC codes are used.

$16QAM(SNR)$	rate(1/2)	rate(2/3)	rate(3/4)	rate(5/6)
-5	0.3406	0.3397	0.3377	0.3402
0	0.2205	0.2211	0.2179	0.2219
5	0.1033	0.1055	0.1043	0.1075
10	0.0205	0.0216	0.0205	0.0220
15	3.08e-04	3.27e-04	2.9e-04	4.08e-04
20	0	0	0	0

Table 1.3: BER Experimental measurements by 16QAM LDPC-MIMO

$64AM(SNR)$	rate(1/2)	rate(2/3)	rate(3/4)	rate(5/6)
-5	0.3940	0.3949	0.3943	0.3960
0	0.3115	0.3116	0.3118	0.3130
5	0.2014	0.2021	0.2031	0.2045
10	0.1036	0.1029	0.1039	0.1046
15	0.0279	0.0281	0.0282	0.0294
20	10.2e-04	11.3e-04	11.1e-04	11.7e-04
25	0	0	0	0

Table 1.4: BER Experimental measurements by 64QAM LDPC-MIMO

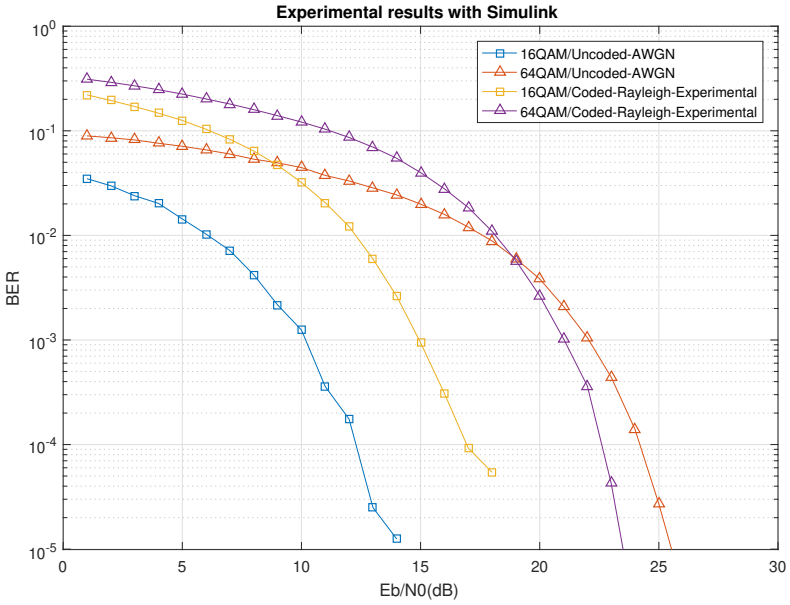

Figure 1.19: 16/64-QAM-MIMO 3x4

Capacity Analysis on MIMO channels: In order to obtain the capacity over MIMO channels using the proposed design we can compute the ergodic capacity as SNR is varied, when CSI is not know at the transmitter side. **H** is a random matrix being the capacity randomly time-varying. Our simulation assume that the random channel is an ergodic process. We consider the following statistical notion

(1.31) [3]:

$$\bar{C} = E\{C(H)\} = E\left\{log_2 \det\left(I_{NT} + \frac{SNR}{NT} H^T H\right)\right\} \tag{1.31}$$

Where the $\mathbf{I}_{NT}$ is defined as the identity matrix that it changes according to the number of antennas to be transmitted and the SNR is defined by $\frac{P_{TX}}{\sigma^2}$.

For the experimental results, by varying the level of SNR in a range of 0 dB to 20 dB, we capture the power of the signal in order to insert these values in the ergodic formula.

Figure 1.20 shown the ergodic capacity results that is achieved with MIMO 2x2 / 3x4 simulated and experimental MIMO 3x4. Is shown a similar performance of the simulated and experimental curve. In addition a gain of $6bps/Hz$ with respect to MIMO 2x2 when the SNR=16dB.

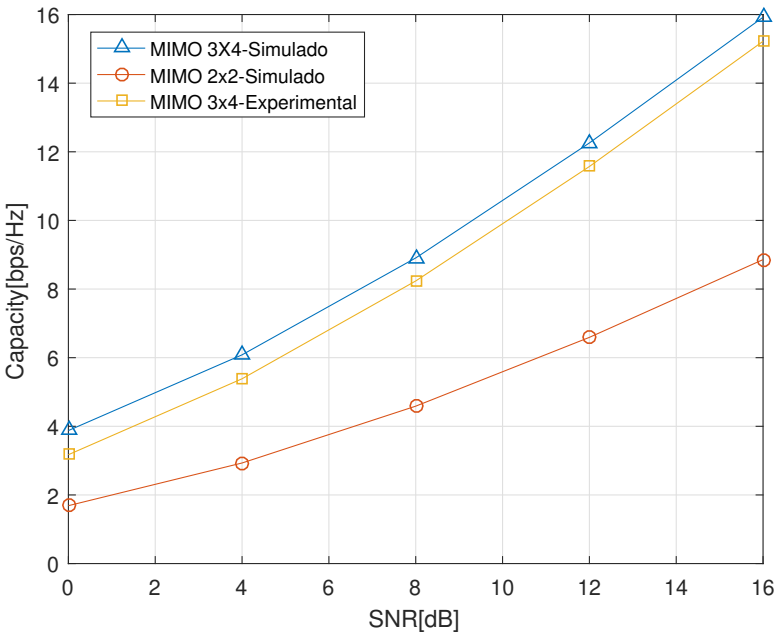

Figure 1.20: Channel capacity.

These results have a great relevance due to that is demonstrated by the use of SDR systems, that it is possible to close the gap from theory to practice. The transmission system has been built with advanced processing techniques, responding

in this way to the requirements for a last generation access network. However, the problem does not end there, because when the CSI is available at the transmitter, the power allocation is necessary at the transmitter.

This study is carried out in the following section, including the real effects on the channel for an OFDMA system when CSI is known. The Resource Allocation problem includes sub-channels and total power allocation for multi-users, therefore this analysis can be extended to the use of beamforming and MU-MIMO techniques over wireless systems with multi-users and multi-cell coordination in order to optimized the network resources.

Chapter 2

Optimization of Access Network in Heterogeneous scenario

In 5G Mobile Communications the data rate of user equipments (UEs) will tremendously grow with the inclusion of multimedia traffic, increasing in this way, the interference among multi-users and deteriorating the system performance in terms of QoS.

On the access network side, the management of communication resources, intercell and intersystem interference, and network selection becomes more complex due to the increasing number of overlaying systems equipped with varying capabilities.

OFDM is an efficient way to combat the harmful intersymbol interference (ISI) using adaptive modulation [48] over fading channel. However, this technique does not allow an increasing the subcarriers in order to achieve greater capacity in the system and it brings problems in terms of PAPR as we mentioned before. Massive MIMO [49] have gained much attention on the development of next-generation wireless communication for improved spectral efficiency in terms of PHY layer transmission.

There are many methods to enhance the resource allocation and minimize the intra-cell interference, either by optimizing subcarrier allocation [50], bit rate[51], power allocation [52].

In [22] a scenario with a heterogeneous macro/femto/D2D wireless networks is considered. When both femtocells and D2D links are included in the resource sharing optimization, the optimization problem becomes more complicated and for this reason the optimal solution for this network structure has not been obtained yet.

In [53] a low complexity QoS-aware joint AC and RRA strategy has been proposed for cellular networks with underlayed D2D communications. A QoS constraint on the average rate is considered in the optimization of both AC and RRA. However, this work does not consider the presence of small-cells or femtocells in the scenario.

In [54] an OFDMA HetNet including femtocells is investigated, where local CSI overhearing enables the femto-base stations to mitigate the interference to nearby macrocell users in the downlink.

The idea of downlink and uplink decoupling in multi-antenna two-tier Hetnets is investigated in [55] for 5G applications, showing the benefits obtained in terms of rate coverage in both macro and femto-cells. In [56] scalable admission and power control methods for D2D communications underlaying cellular networks are proposed to increase the reuse of frequency resources while maintaining QoS to all users.

In the literature outlined above, the rate performance of Hetnets is investigated without considering the degradation due to the channel estimation error at the receiver and the overhead of pilot-aided estimation. In a OFDM receiver, channel state information is needed to perform demodulation and equalization. The insertion of pilot symbols during the transmission plays an important role: the part of radio resources spent for pilot transmission reduces spectral and power efficiency, and the estimation error reduces the link capacity [57].

A scenario of HetNets (Heterogeneous Networks) with Macro/Femto cells for Uplink/Downlink using OFDM is simulated in order to provide QoS for each user and the optimization is done with multiuser to allocate the subchannels and the total power to the users while satisfying the bit error rate (BER). The load traffic can be decreased and therefore the interference also using the concept of device-to-

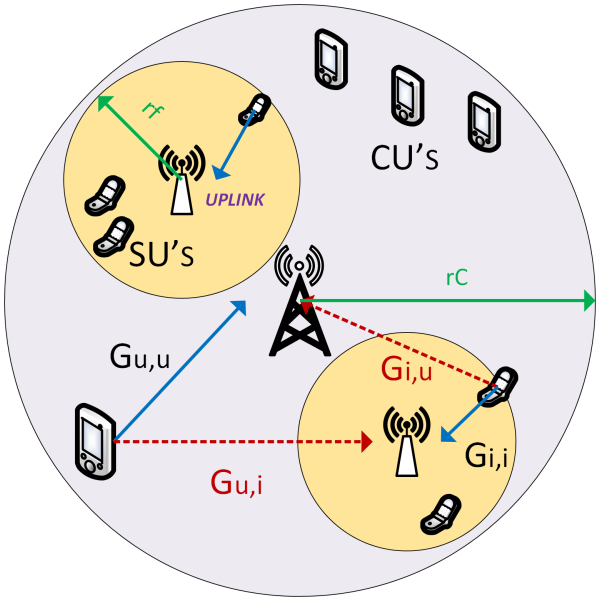

Figure 2.1: Cellular network model. The lines with arrows denote the wireless links in the uplink: useful link (solid), interfering link (dashed).

device (D2D), migrating in this way towards a model of Heterogeneous Networks (HetNets) [24], where the main idea is reduce the load through D2D devices and femtocells, guaranteeing a greater throughput in the system and increasing the capacity [22] of future mobile networks.

Nowadays, the heterogeneous networks (HetNets) [22] with device-to-device (D2D) communications and femtocells allows to reduce the traffic, the interference management and the energy consumption due to the base station; guaranteeing a greater throughput in the system and a correct power allocation from the base station.

We consider a two-tier cellular network using OFDMA, as in Fig. 2.1. In the network there are K cellular users (CUs), uniformly distributed in the macrocell and connected to the base station (BS), D small-cell users (SUs), each one assigned to a femtocell, and F femtocells. The femtocell access points (AP) are uniformly placed in the macrocell region limited by the circles of radii r_i and r_c, where r_c is the macrocell radius. The SUs are uniformly distributed inside the

femtocells, $D_F = D/F$ per femtocell. Femtocell radius is r_f.

The available OFDMA bandwidth is divided into S orthogonal subchannels with bandwidth ΔB, where the elementary resource unit is the resource block (RB), composed of one subchannel and one time slot, and each subchannel includes 12 OFDM subcarriers with $\Delta B = 180$ kHz, as in LTE cellular systems. All the available RBs are shared among the coexisting CUs and SUs communications. We assume that the network is fully loaded and the SUs can only be served in sharing (not orthogonal) mode with CUs. Hence, a RB can be allocated to either a CU in orthogonal mode or to a couple CU and SU in sharing mode. Sharing mode communications are affected by cross-interference as in the case illustrated in Fig. 2.1 for the uplink scenario.

We finally assume that the network supports a QoS-aware centralized resource management that controls resource assignment to all users in order to limit the effects of cross-interference and optimize the revenue for the service provider, while guaranteeing a predefined level of QoS. The QoS requirement is defined in terms of minimum average bit-rate, denoted with q_k, $k = 1, \ldots, K$, for the CUs and q'_d, $d = 1, \ldots, D$, for the SUs, respectively. The correspondent revenue for the service provider is denoted with w_k for the CUs and w'_d for the SUs, respectively. As in the system investigated in [53], the resource management is based on a radio resource allocation (RRA) algorithm that efficiently allocates RBs, slot by slot, and an admission control (AC) algorithm that determines which users can be served by the network in a long-term period, under QoS requirements. If the system is properly loaded by the AC algorithm, the RRA algorithm works to guarantee the QoS requirement. In this case the network capacity and service provider revenues depend on the outcome of the AC algorithm. If we use the binary variables x_k and z_d to indicate whether (1) or not (0) the CU k and the SU d are admitted in the system, respectively, the network capacity becomes:

$$C_N \geq \sum_{k=1}^{K} x_k q_k + \sum_{d=1}^{D} z_d q'_d \tag{2.1}$$

whereas the aggregate utility of the service provider is given by $U(x, z) = \sum_{k=1}^{K} x_k w_k + \sum_{d=1}^{D} z_d w'_d$ where $x = [x_1 \ldots, x_K]$ and $z = [z_1 \ldots, z_D]$. Another metric

of interest is the admission-rate given by $R_C = \sum_{k=1}^{K} x_k/K$ and $R_S = \sum_{d=1}^{D} z_d/D$ for the CUs and SUs, respectively. If all the users have the same QoS requirement $q_k = q'_d = q$, the network capacity is simply given by $C_N \geq (R_C K + R_S D)q$.

Network capacity and admission rate depend on the AC algorithm which is based on a suitable rate model used to estimate the average bit-rate on each link when used in either orthogonal mode or sharing mode. The AC algorithm is briefly described in the next Section. The rate model will be defined in Section IV, for both the ideal case of perfectly known CSI at each receiver and the realistic case of imperfect CSI [58] at the receiver obtained through a pilot symbol aided channel estimation.

2.1 Admission Control

The aim the AC is to select a set of CUs and SUs which can be supported by the heterogeneous cellular network with guaranteed QoS, i.e. long-term average rate, and which maximizes the total revenue. In this work we consider a reformulated version the AC algorithm originally proposed in [53] for a cellular system with underlaying device-to-device communications. In this Section we illustrate the optimization problem from which the algorithm is derived. The details of the algorithm, which is a low-complexity greedy algorithm based on clustering and iterative linear programming that achieves a solution near to the optimum, can be found in [53].

The basic assumption behind AC is the knowledge of the average bit-rate achieved by each user in orthogonal mode or when it shares the RB with each other user of the other cellular tier. This is what we call "rate-model". Let us denote with $c_k^{(d)}$, with $k = 1, \ldots, K$, $d = 0, \ldots, D$, the average rate of CU k when it shares the RB with SU d ($d = 0$ meaning CU in orthogonal mode) and with $c'^{(k)}_d$ the average rate of SU d when it shares the RB with CU d.

In a suitably long time interval let us denote with α_k the fractional amount of RBs per slot allocated to CU k, and with $\beta_d^{(k)}$ the fractional amount of RBs per slot

that CU k shares with SU d. The following resource sharing constraint

$$\sum_{d=1}^{D} \beta_d^{(k)} \leq \alpha_k, \quad \forall k \tag{2.2}$$

must hold, and the total amount of allocated RBs per slot must not exceed the total number S, i.e.,

$$\sum_{k=1}^{K} \alpha_k \leq S \tag{2.3}$$

The average rate achieved by the CU k when it shares the RBs with a set of SUs having $\beta_d^{(k)} > 0$ must be larger than the rate requirement q_k, i.e.,

$$\left(\alpha_k - \sum_{d=1}^{D} \beta_d^{(k)}\right) c_k^{(0)} + \sum_{d=1}^{D} \beta_d^{(k)} c_k^{(d)} \geq q_k \tag{2.4}$$

where the first term accounts for the rates achieved in orthogonal mode. On the other hand, the rate achieved by the SU d must be larger than the rate requirement q'_d, i.e.,

$$\sum_{k=1}^{K} \beta_d^{(k)} c'^{(k)}_d \geq q'_d \tag{2.5}$$

The AC algorithm looks for the solution of the following mixed integer linear problem:

$$\max_{x,z,\alpha,\beta \geq 0} \; U(x,z) \tag{2.6a}$$

$$\text{s.t.} \;\; (2.2), (2.3), (2.4), (2.5) \tag{2.6b}$$

where $\beta = [\beta_d^{(k)},\ d = 1,\ldots,D,\ k = 1,\ldots,K]$ and $\alpha = [\alpha_k,\ k = 1,\ldots,K]$. The AC maximizes the total revenue of the service provider and when the revenue from each user is proportional to the required average rate, it maximizes the network capacity.

2.2 Rate model

In an OFDMA multi-user scenario the long-term achievable data-rate is dependent on the statistical distribution and on the correlation of the short-term fading in all useful and interfering links, and on how the RRA algorithm works. Since its evaluation is an hard task, the long-term data-rate is usually estimated (e.g. in [59]) by considering the average channel conditions of direct and interfering links, by also taking into account the multi-user diversity gain captured by the underlaying RRA. We first introduce the rate-model used in [53], which assumes that the CSI is perfectly known at the receiver without the need of channel estimation. It is shown that this model is sufficiently reliable when the underlying RRA algorithm assigns the resources by maximizing the weighted average sum rate with a QoS constraint for each single CU or SU. After, we will extend this model to include the effects of the redundancy introduced by pilot symbol assisted channel estimation and the effects of channel estimation error.

2.2.1 Perfect CSI

Let $G_{u,i}$ be the *long-term* power gain of the channel between the transmitter of the user u, either CU or SU, and the receiver of user i. Let $\Upsilon_u^{(0)}$ be the SNR of user u in orthogonal mode , and $\Upsilon_u^{(i)}$ be the SINR of user u when it shares the channel with user i. They are given by

$$\Upsilon_u^{(i)} = \begin{cases} \frac{G_{u,u}P_u}{\sigma^2} & \text{if } i = 0 \\ \frac{G_{u,u}P_u}{\sigma^2 + G_{i,u}P_i} & \text{otherwise} \end{cases} \tag{2.7}$$

where P_u is the power budget of user u, and σ^2 is the noise power. The average rate achievable by the user u over one RB can be obtained according to the following model

$$c_u^{(i)} = A_2 \Delta B \log_2(1 + A_1 \Upsilon_u^{(i)}) \tag{2.8}$$

where the parameter A_1 accounts for the multi-user diversity gain captured by the RRA algorithm and the SNR-gap of the adaptive modulation and coding (AMC)

used at the physical layer. According to [53] [60], it is defined as $A_1 = \ln(\varsigma(K + D))/a_1$. The parameter A_2 depends on the AMC only.

2.2.2 Pilot-symbol-aided CSI estimation

When pilot-symbol-aided CSI estimation is implemented to allow OFDM coherent detection and synchronization, a part of the transmitted symbols in each RB is used as pilots, thus reducing the amount of symbols and the amount of power available for the transmission of useful data. Moreover, since channel estimation is not perfect, a residual estimation error acts as additional noise that degrades the link performance.

We assume that a minimum mean square error (MMSE) estimator is used at each receiver to estimate the impulse response of the frequency-selective channel, which is optimal with respect to link capacity [61]. It is shown in [57] that the mean square error, i.e. the variance of the estimation error, in case of equipowered and equispaced pilots, is given by

$$\sigma_e^2 = \sum_{l=1}^{L} \left[\frac{1}{p_l} + \frac{P_P}{\sigma_n^2} \right]^{-1} \tag{2.9}$$

where P_P is the total power received over pilot symbols, σ_n^2 is the noise power per subcarrier (over one RB $\sigma^2 = 12\sigma_n^2$) and $\{p_0, \ldots, p_L\}$ is the power-delay profile of the channel. PDP is a exponential function that depends of the sample time for each Resource Block in order to determined the number of taps. $T_s = 1\mu s$ and $decay = T_s \cdot \Delta B \cdot S$, where the number of taps is $5 \cdot decay$. In this context, the power-delay profile is defined by the follow equation as is shown in the Fig.2.2 :

$$p_l = \frac{e^{-1/decay}}{\sum_l e^{-1/decay}} \tag{2.10}$$

The discrete-time impulse response is modeled with $L + 1$ independent taps with zero-mean complex-Gaussian tap gains with variance p_l, and $\sum_l p_l = 1$. It is also shown in [57] that the instantaneous (short-term) signal-to-noise ratio in a given subcarrier (or RB in our case) at the receiver is given by

$$\rho = \frac{P_D^{(\mathrm{RB})}(1 - \sigma_e^2)}{\sigma^2 + P_D^{(\mathrm{RB})}\sigma_e^2} g^2 \tag{2.11}$$

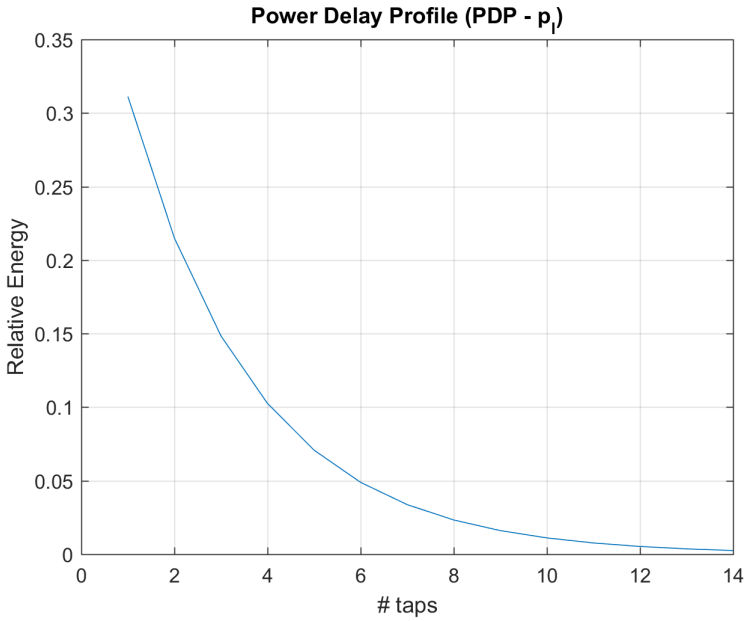

Figure 2.2: Energy Relative of Power-Delay-Profile.

where $P_D^{(\mathrm{RB})}$ is the average power received over the data symbols of the RB and g is the instantaneous fading variable, with unit variance, in the given subcarrier.

We apply these results to reformulate the SINR and the rate-model in (2.7) and (2.8) for a system with pilot-symbol assisted CSI estimation. By using the long-term average components of (2.11) and by including the interference, the SINR of user u when it shares the channel with user i becomes

$$\Upsilon_u^{(i)} = \begin{cases} \frac{G_{u,u}\eta_p P_u(1-\sigma_e^2)}{\sigma^2+G_{u,u}\eta_p P_u\sigma_e^2} & \text{if } i = 0 \\ \frac{G_{u,u}\eta_p P_u(1-\sigma_e^2)}{\sigma^2+G_{u,u}\eta_p P_u\sigma_e^2+G_{i,u}\eta_p P_i} & \text{otherwise} \end{cases} \tag{2.12}$$

where η_p is the power efficiency, i.e. the ratio between the power used over RB data symbols and the total power P_u,. The average rate achievable by the user u over one RB is therefore given by

$$c_u^{(i)} = A_2\eta_b\Delta B\log_2(1 + A_1\Upsilon_u^{(i)}) \tag{2.13}$$

where η_b is the bandwidth efficiency of channel estimation given by the ratio between the number of data symbols in one RB and the total number of symbols in

one RB, which can also be written as

$$\eta_b = 1 - \mu = 1 - N_P/N$$

where N_P is the number of pilots in one RB and N the total number of symbols in one RB.

To introduce flexibility in the use of pilots, we consider the possibility of allocate different amounts of power to pilot and data symbols. If we used the same power level for all symbols, the power per RB allocated to pilots would be μP_u. To differentiate the power level for pilots, we allocate to them a power equal to $\alpha\mu P_u$, where α is a power allocation parameter which can be different from 1. In this way, the power efficiency becomes

$$\eta_p = 1 - \alpha\mu$$

In order to set up the parameters for pilot-aided channel estimation we refer to LTE configuration [62] for uplink and downlink as is shown in Fig. 2.3. For the uplink, we consider the use of 12 pilot symbols per RB, placed over 12 adjacent subcarriers. As the RB has 12x7 symbols, we set $\mu = N_P/N = 1/7$. By assuming that in a loaded network the users transmit over non more than one assigned RB, the power received over pilots by each user u becomes $P_P = G_{u,u}\alpha\mu P_u$. For the downlink, we consider the use of 4 pilot symbols per RB, placed over equispaced subcarriers inside the RB. Hence, we set $\mu = N_P/N = 1/21$. As the base stations transmit over all the available bandwidth, the power received over pilots by each user u becomes $P_P = G_{u,u}\alpha\mu S P_u$. Unless otherwise stated, we use in the results $\alpha = 1$.

For the channel impulse response we consider an exponential power-delay profile with decay time equal to 1 microsecond. The number of taps of the discrete channel depends on transmission bandwidth, which is taken as ΔB for the uplink and $S\,\Delta B$ for the downlink.

Simulations are carried out for both uplink and downlink by fixing the number of CUs to $K = 50$ and the number of RUS to $S = 15$, and by varying either the number D of SUs or the number F of femtocells. The weights w_k of the CUs

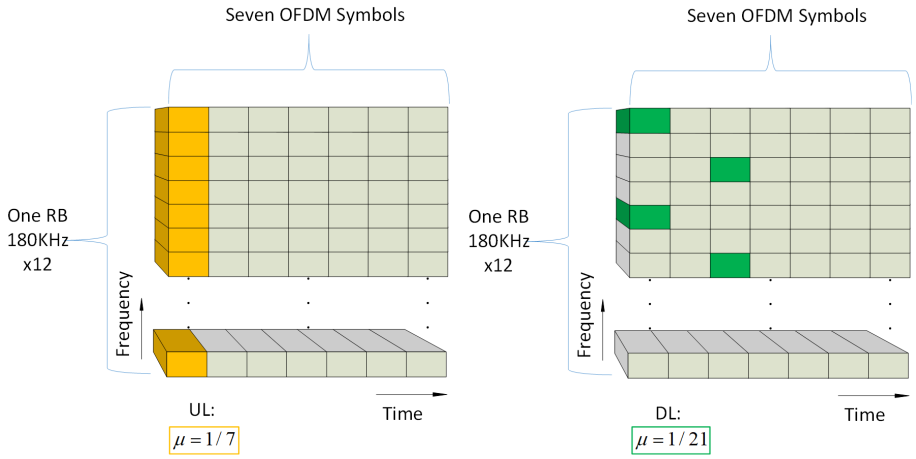

(a) Uplink (b) Downlink

Figure 2.3: Resource Block with pilot-added symbols.

are uniformly distributed in $[0.5, 1]$, whereas the weights w'_d of SUs are uniformly distributed in $[0.25, 0.5]$, in order to prioritize CUs. The required average rates q_k and q'_d for both CUs and SUs are set to 256 kbps. The other important system model parameters are listed in Table 2.1.

Table 2.1: **List of parameters used in Matlab for HetNet Scenario**

Macrocell radius (r_c)	500m
Femtocell radius (r_f)	30m
r_i	150m
Macro/Femtocell path loss	$128.1 + 37.6log_{10}(d[km])$
a_1	2.061
A_2	0.945
ς	0.5
Subchannel bandwidth (ΔB)	180KHz
CU and SU power budget (P_u)	10 dBm
Noise variance (σ^2)	$3.360 \cdot 10^{-15}$
Minimum rate (q_k, q'_d)	256 kbps

Figures 2.4(a) and 2.4(b) show the admission rate (%), as function of the number D_F of SUs per femtocell, for uplink and downlink, respectively. The number F of femtocells varies from 1 to 5. The results show that in the uplink, by increasing D_F and F, the admission rate of SUs decreases due to interference level caused by users into the femtocell. On the other hand, the CUs maintain a constant value of admission rate, because they are prioritary with respect to SUs. When we set $D_F = 10$, in the worst case with $F = 5$, the system can only admit 10% of SUs. By looking at the total number of SUs admitted, this number does not exceeds 6.

In the downlink (Figure 2.4(b)), the behavior is different: the admission rate of SUs is quite large, but both SUs' and CUs' admission rates suffer the increase of the number of SUs. The admission rate of CUs drops from 75% to 65% when the number of femtocells is increasing from $F = 1$ to $F = 5$.

Figures 2.5(a) and 2.5(b) show the same results as for the scenario of Figures 2.4(a) and 2.4(b), but in the case of perfect CSI, i.e. in the absence of channel estimation error. We first note that admission rate changes: it increases for the CUs and the difference is significant for the downlink. If the number of admitted CUs in the system increases, less space is left to admitted SUs whose number decreases. In the scenario investigated, the penalty due to channel estimation error is around 22% for downlink CUs and around 10% for uplink CUs.

In the last two figures, Figures 2.6(a) and 2.6(b), we investigate the option of allocating different power levels to pilot and data sysmbols, by using different values of the pilot amplification coefficient α. The case study is for $K = 50$ CUs and $D_F \cdot F = 10 \cdot F$ SUs for $F = 1, 2, 3$. The results show that there is an optimal value for the power allocated to pilots. This is obtained with $\alpha = 2$ for the uplink and with $\alpha = 4$ for the downlink. By using this optimal value, we are able to recover a significant part of the penalty with respect to perfect CSI. This penalty is reduced to 8% and to 13% for CUs in the uplink and downlink, respectively.

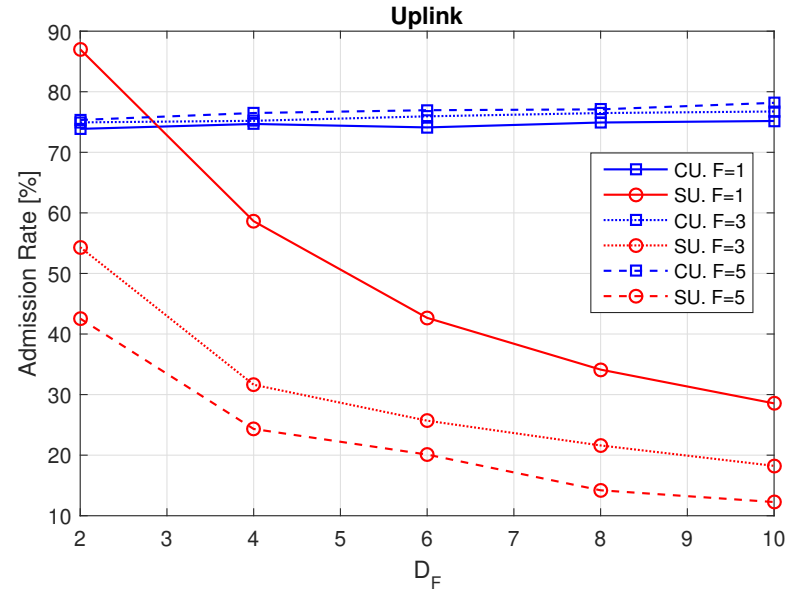

(a)

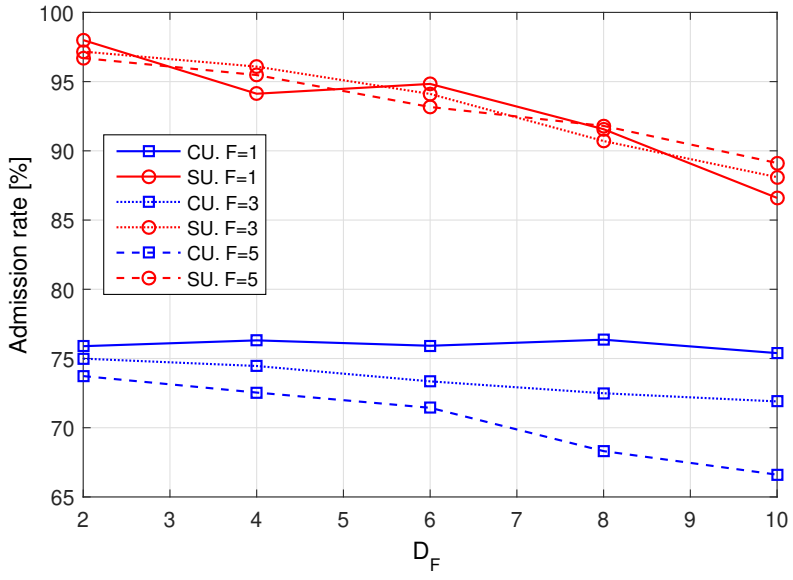

(b)

Figure 2.4: Admission rate (%) as function of the number of SUs per femtocells, with $\alpha = 1$, $K = 50$. (a) Uplink and (b) downlink.

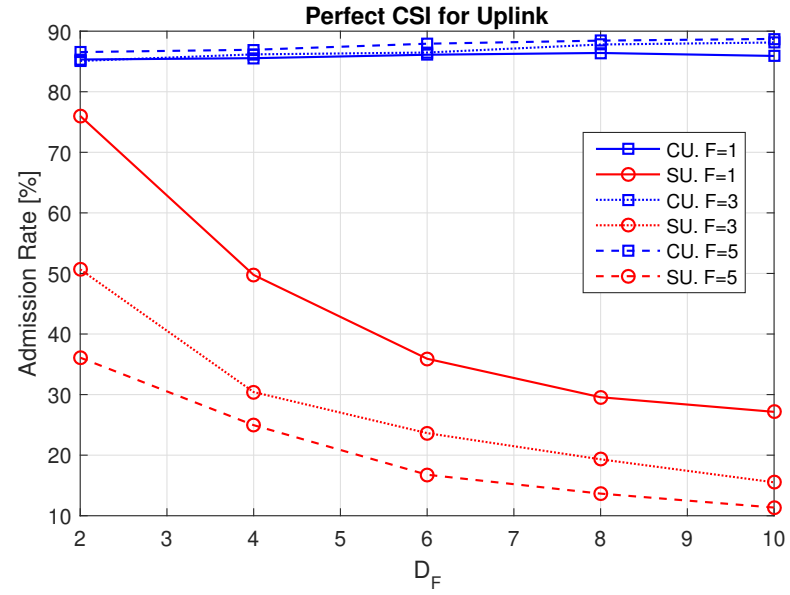

(a)

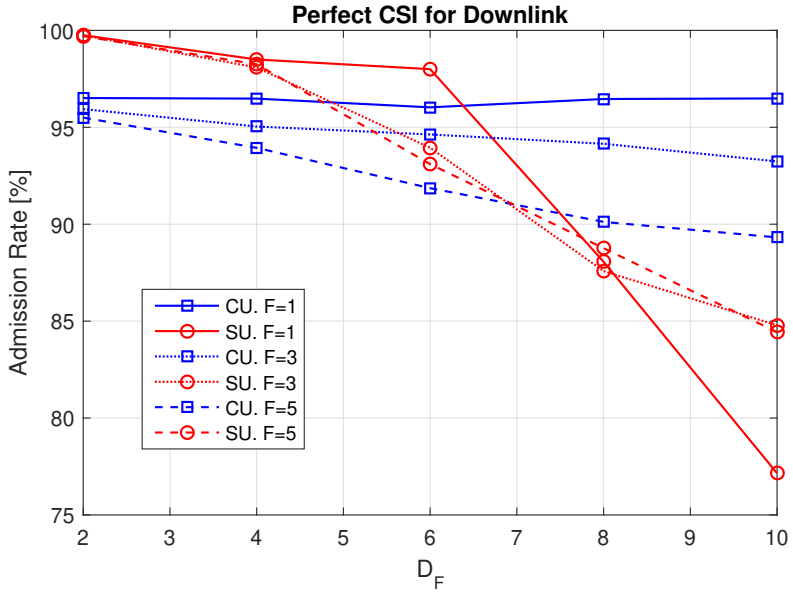

(b)

Figure 2.5: Admission rate (%) as function of the number of SUs per femtocells, with $\alpha = 1$, $K = 50$ and perfect CSI at the receiver. (a) Uplink and (b) downlink.

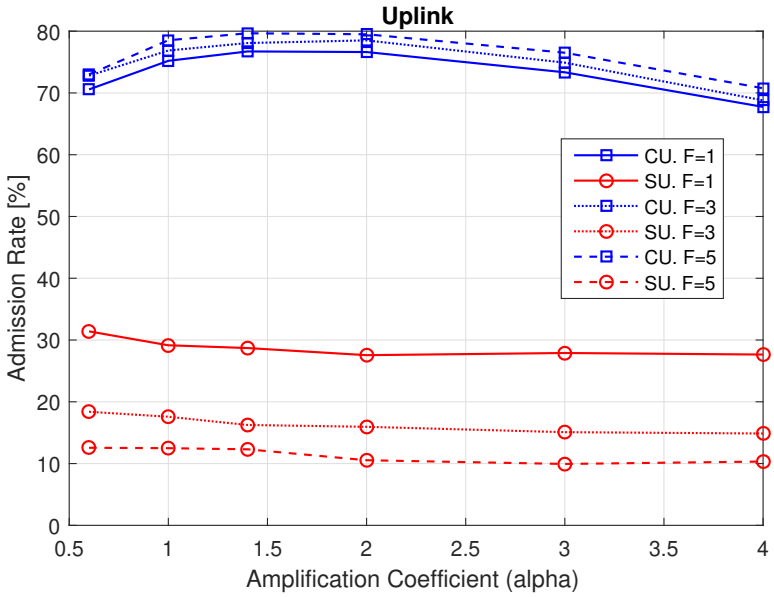

(a)

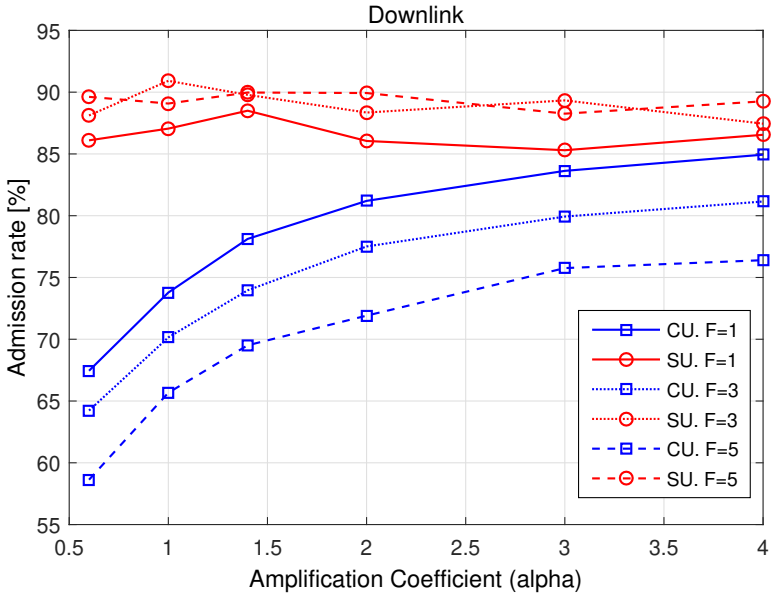

(b)

Figure 2.6: Admission rate (%) as function of the pilot amplification coefficient, with $D_F = 10$, $K = 50$. (a) Uplink and (b) downlink.

2.2.3 Capacity Analysis with Admission Control

Network capacity depends on the outcome of the AC algorithm that takes into account link-rate degradation due to channel estimation error and pilot-symbols overhead and it is shown in the Appenix A.

In order to evaluated the estimated capacity system, the AC algorithm considers the QoS-aware through the following expression $C_N \geq (R_C K + R_S D)q$. The estimated capacity not consider the effects of channel in time and frequency domain, however it can be observed that the effects of *multiuser-diversity* are introduced because in both case the capacity increases in function of the D_F users and F femtocells.

The Capacity Analysis when the system takes into in account the Admission Control Algorithm in presences of error and without error (perfect CSI), it shows that, with F=1,3,5 the capacity system in bps increases proportionately in terms of D_F of SUs per femtocell.

The Figure 2.7(a) and Figure 2.7(b) for uplink and downlink with perfect CSI can get to served around of 13Mbps and 22Mbps respectively when the number of femtocells increases to 5. This number is really important because in other words, the percentage of admitted users, both CU's and SU's (80%) achieve a speed higher than the limit given in the constraint optimization problem ($q = 256Kbps$).

For another hand, the same analysis can be established for the case with error, however the capacity is reduced due to interference caused by the users in the system. The results shown that in the Figures 2.8(a) and 2.8(b), the maximun capacity for $F = 1, 3, 5$ are 11.6/11/10.2Mbps and 20/16/12Mbps for Uplink and Downlink respectively.

In the results for both uplink and downlink, we have found that the impact of channel estimation error is not negligible and is especially relevant for downlink CUs. However, we have also shown that this degradation can be partially mitigated by allocating more power over pilot symbols. In this context, the best performance for both cases (uplink/downlink) with error and perfect CSI it turns out to be downlink in terms of capacity.

Obviously the capacity decreases in perfect CSI with respect to CSI. The gap between perfect&imperfect CSI with $F = 5$, is 20% in terms of capacity (bps) when $D_F = 10$. The results could change considerably when the effects of the channel and power allocation are considered.

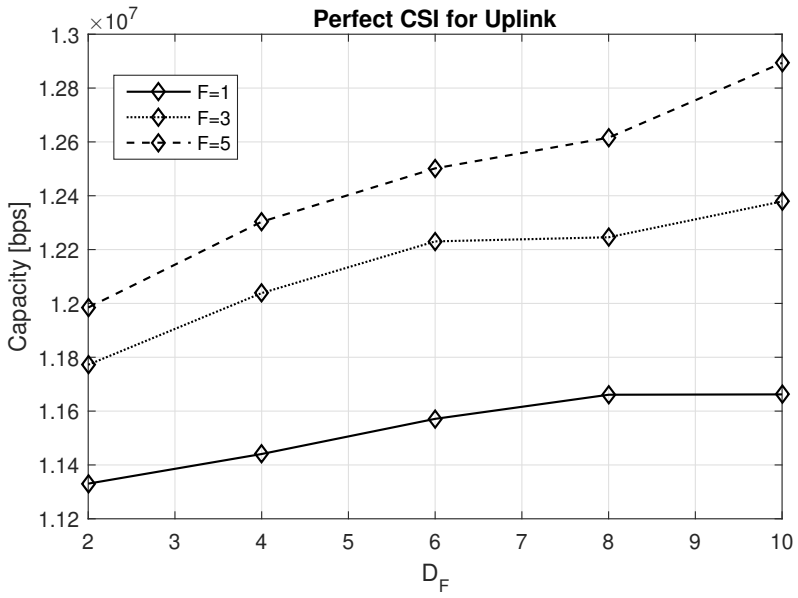

(a)

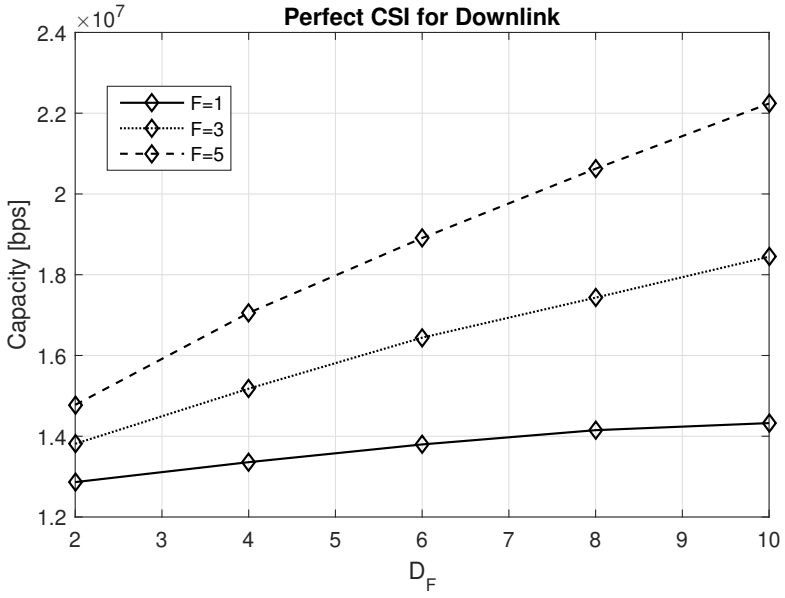

(b)

Figure 2.7: Capacity in Admission Control. (a) Uplink and (b) downlink.

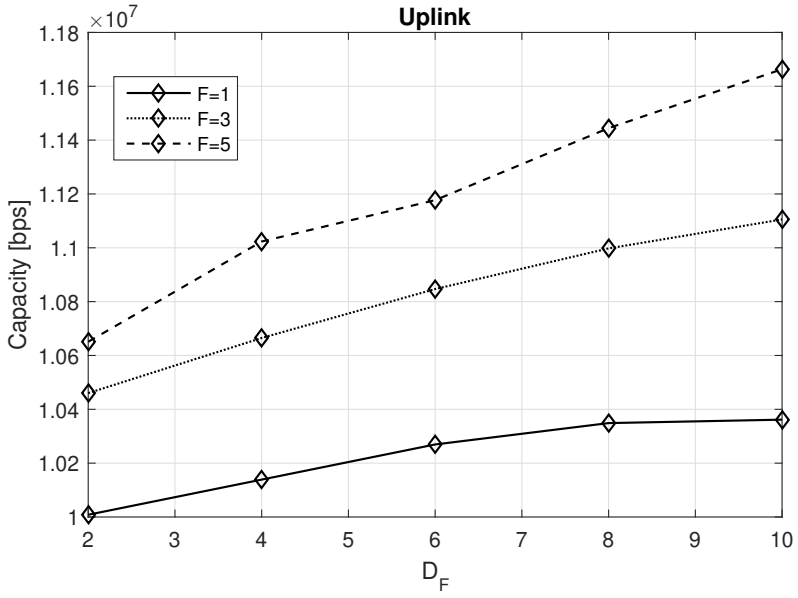

(a)

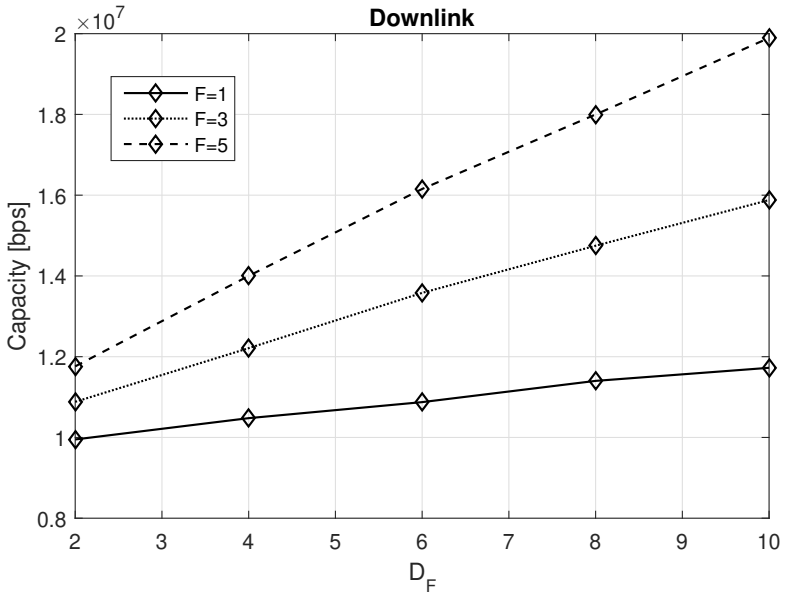

(b)

Figure 2.8: Capacity with Perfect CSI in Admission Control. (a) Uplink and (b) downlink.

Chapter 3

FiWi Networks: Network Planning and Optical Link Design

The deploying of FiWi networks is a problem that occurs often in real situations and needs to be is simplified through optimal planning. In this work we considered a scenario of urban dwellings with smart meters (SM), devices that need to be managed from a central office (CO) of an electric utility, with a advanced metering infrastructure such as a scenario 5G presented in previous chapter with HetNets, forming a neighborhood area network (NAN). Therefore, it has raised the need of a heuristic solution due to the property of a combinatorial problem. The Heuristics has an optimum location of cellular base stations (BS) for obtain the wireless connectivity to each Smart Meter (SM). In the same way, we can provide the service to mobile users or VANET' networks with the support of Core Network based on backhaul of fiber optic.

In the next step we proposed a solution for the optimal location of a CO with optical fiber link between each BS, and optical splitters that will be used for each section of fiber in order to achieve full connectivity of the BS to the point of metropolitan area network (MAN) equivalent to central office (CO). In this context, the algorithm searches the minimum cost of the fiber required in order to connect the CO with the different wireless nodes.

However, the fiber optic can not be only used as a bridge of transmission, for

this reason a strong processing on the fiber optic must be necessary in order to support the among of information for each branch that is shown in the Figure 3.1. In this context, a holistic 5G backhaul should provide a solutions with low latency, spectral efficiency and higher data rate transmission; guarantying in this way the network densification for other applications.

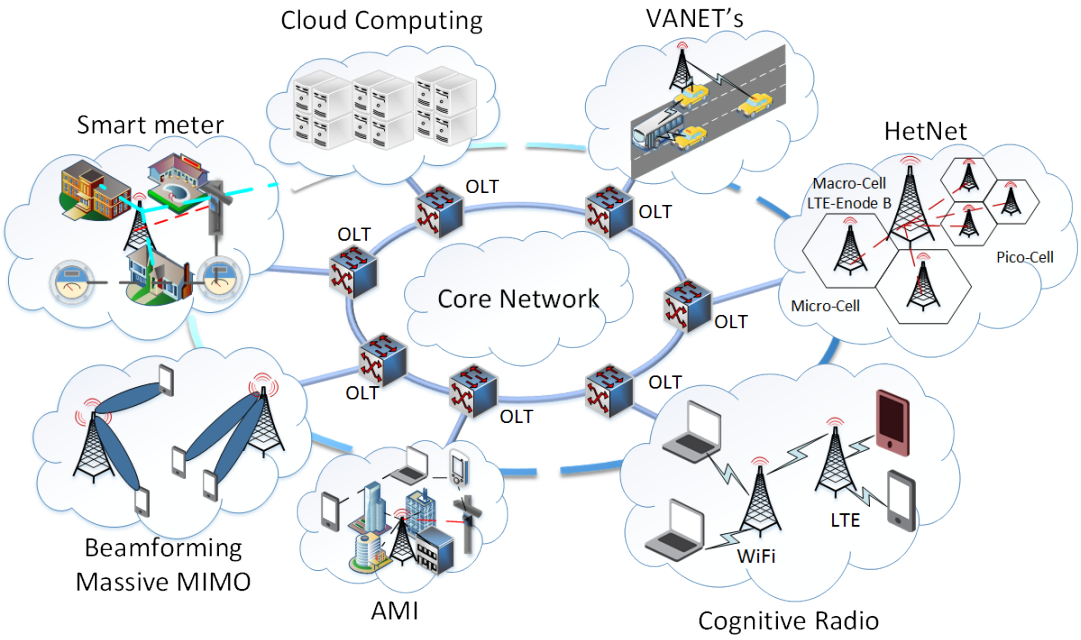

Figure 3.1: FiWi Holistic for 5G.

3.1 Optimal Planning for Deployment of FiWi Networks

The deployment for the last generation of access networks, must meet high requirements in terms of QoS, capacity, Spectral Efficiency (SE) and high transmission rates able to integrate the wireless services oriented towards 5G communications [63] with optical scalability as XG-PON (NG-PON1) *Next Generation PON*.

The Figure 3.2 has an advanced metering infrastructure and shows a small extract of Figure 3.1 where the service is oriented towards Urban - Neighborhood

area Network (NAN). In order to explain the scenario in better way, a heterogeneous network with Macro/Femto has been taken as previous Chapter. The system must guarantee the 100% of coverage to SM (smart meters) in each home give place to a new communication model for instant data reading in the cloud.

Therefore, this new proposal represents an investment costs for BS location and fiber cabling. For this reason, in this work is presented a planning model in order to minimize costs related to infrastructure resources for the deployment of FiWi networks [64].

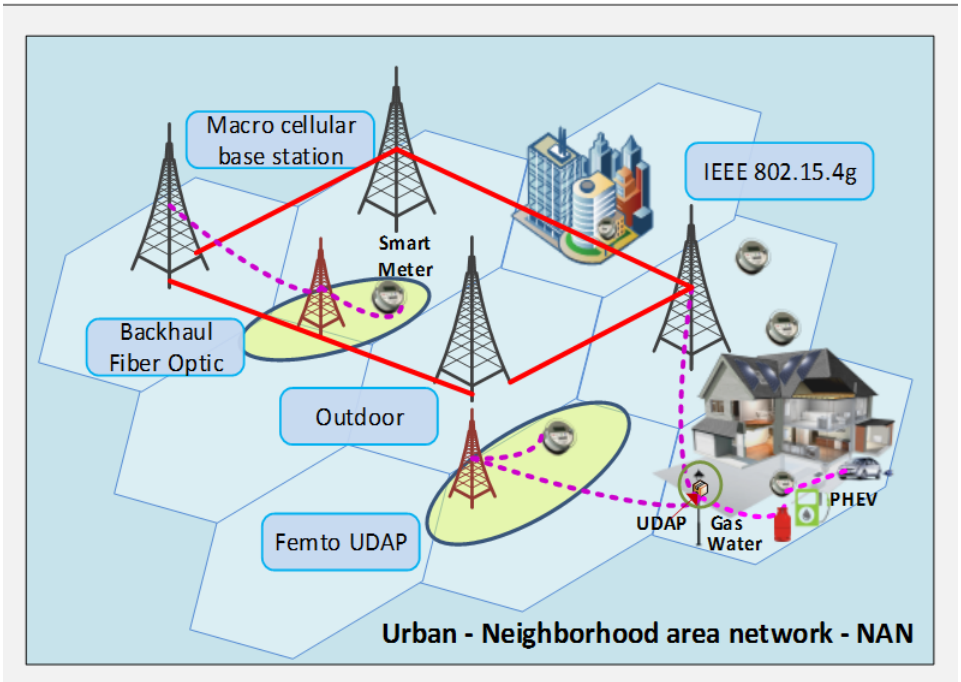

Figure 3.2: NAN Desnsification.

Thus, the set of SMs will be attended by the nearest BS, according to its coverage radius and restricted by its respective capacity.

The BS can be placed in any available space in the set of candidate sites. The sites are occupied by the houses which will not be used by the BS; subsequently, the sites that are available as "candidate sites" are considered as a location for optical splitters [65] [66].

In addition, the cost of optical fiber must be guaranteed to the minimum to interconnect the CO with BS. However, we must consider that the path from the CO to the BS contains a number of active optical devices that allow the exchange of information between the opto-electric standard.

The distances from CO to BS and the distances between each splitter are measured through the Euclidean distance.

The fiber path is restricted to the roadways of an urban zone [67]

Consequently, NAN networks are created from BS to SM's and the metropolitan area network (MAN) is formed by the interconnection of the central offices of each electric company [30][68]

For the deployment of the optical network, an automatic location of splitters through Steiner tree is proposed. For this scenario a real urban map is considered with delimitation of roads and ducts for the fiber. In this way, realistic scenario must be guaranteed with the necessary restrictions for the implementation of fiber into urban area.

In the Fig. 3.3 shows the proposed problem based on hybrid model with wireless and optical links distribution allowing its use as a backhaul for legacy networks. The goal will be to achieve the wireless connectivity for all SM's represented as houses where now we called NAN networks. Next, all BS's must connect via optical link to Central Office CO with the minimum distance using the Haversine formula. In this context we have a point of dis-aggregation called CO-NAN. The other dis-aggregation is achieved with optical link in order to build the MAN network called CO2-MAN. This optimization problem is solved with a Heuristic algorithm [30] called *"brute force"*, due to it analyzes all feasible points in a geo-referenced map in order to determinate the best location for SM's, BS's and optical splitters.

The technology for the access will depend of wavelengths allocation and processing deployment into the core network. Considering WDM as a base for access technology, we can combining different techniques as DWDM, Ultra-DWDM, CWDM that are already in literature. In the next section is explained the processing in order to achieved high data transmission and spectral efficiency with high

QAM-modulation.

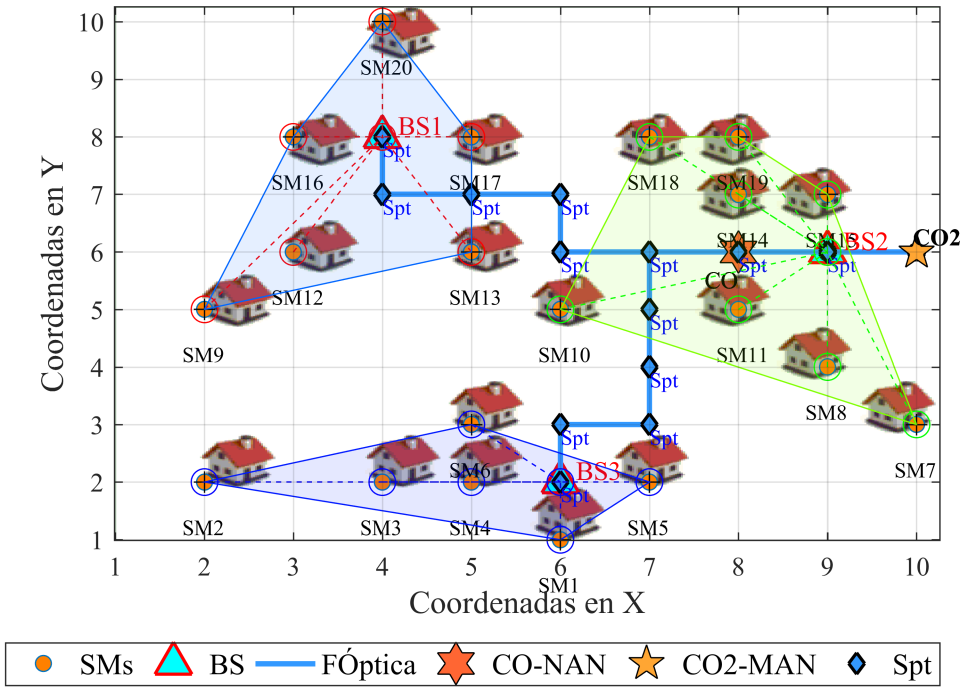

Figure 3.3: FiWi - AMI Network.

The optimization algorithm is described in the following Table 3.1 with the parameters used in Matlab:

Table 3.1: **List of parameters used in Matlab for FiWi Scenario**

C	set of residences
S	Set of Candidate Sites for BS
BS	Set of optimal base station
N	Number of Smart Meters
M	Number of Candidate sites for BS
V	Vertices of S
R	Ratio of BS's
CAP	Capacity of BS
P	Coverage probability
K	number of optimal BS
$d_{c_i - s_{i,k}}$	Distance between each residence and candidate sides
$cent$	$k-means$ centroids
$usNC$	Set of no-connected users
usC_k	Set of connected users with the clusters
BS_k	Feasible BS according $k-means$
V_k	Cadidates sites of k centroid
$V_{S_i,k}$	Site i of the neigbord sites for k centroid
$dist_{V_k - C_{i,k}}$	Distance between candidate site k and the i residence near to the cluster
$coordBS$	Optimized BS coordinate
$dist_{s_i - s_j}$	Distance among candidate sites and Central Ofice
CO	Central Ofice site
CO_2	CO site optimized
$borde$	Edge of candidate sites for CO
$scOC$	Set of candidate sites for CO
$scOC_q$	Set of q candidate sites for CO
$ruta_k$	Path from BS_k to CO

Algorithm 2 Wireless AMI Algorithm

Step 1 Input: $C = c_1, \ldots c_n, S = s, \ldots s_m, R, Cap, P$

Step 2 Output: $BS = bs_1, \ldots bs_3$
$coordBS = (bs_x1, bs_y1), \ldots (bs_x3, bs_y3)$

Step 3 Initialize: $K = 1, iter = 20, flag = 0, conta = 0, conta2 = 0, N = \|C\|, M = \|S\|, usC = 0, usNC = 0, d = 1hop$
$\Delta x_k \in \{-d, 0, d\} \wedge \Delta y_k \in \{-d, 0, d\}$

Step 4 set $d_{s_i - s_j} = dist(i, j), \forall j = 1 \rightarrow M$

Step 5 set $K | K * Cap < N$

Step 6 **while** $(flag = 0 \wedge conta < iter)$:
$cent = k - means\,(C, K)$;
set $usC_k = c_i$ conected to $cent_k$;
$usNC = usNC \cup \left(usC_k \backslash c_i \left| \max\left(d_{c_i - cent_k}\right)\right.\right)$;
$usNC = usNC \cup \left(usC_k \backslash \left| d_{c_i - cent_k} > R\right.\right)$;
$V = s_i \in S \left| \begin{array}{l} v_{x_k} = bs_{x_k} + \Delta x_k, v_{y_k} = bs_{y_k} + \Delta y_k \\ \wedge \left(dist_{V_k - C_{i,k}} \leq R\right) \wedge if\, s_i \neq BS \end{array} \right.$
$V_k = V_k \backslash V_{s_{i,k}} \left| dist\left(V_{s_{i,k}} - usNC_{p,k}\right) > R \right.$
while $\sum_{k=1}^{K} \|usC_k\| < Cap * P$:
forall $usNC_p$ whit 1 candidate $V_{s_{i,k}}$
if $\|usC_k\| \leq Cap * P$
$usC_k = usC_k \cup (usNC \backslash usNC_p)$;
endif
$BS_k = V_{S_i k}$
if cualquier otro $usNC_p$ tiene el mismo $V_{s_{i,k}}$:
$usC_k = usC_k \cup (usNC \backslash usNC_p)$;
set $V_{S_i k}$ as 1 candidate site only
endif
endforall
forall $usNC_p$ white more of 2 candidates $V_{s_{i,k}}$
if $\|usC_k\| \leq Cap * P$:
$BS_k = V_{S_i k}$

Algorithm 3 Optical Fiber -AMI Network Design

Step:1 Input:

$C = \{c_1, ..., c_n\}, S = \{s_1, ..., s_m\}, R, Cap, P$

$BS = \{bs_1, ..., bs_k\}$

$coordBS = \left\{\left(bs_{x_1}, bs_{y_1}\right), ..., \left(bs_{x_K}, bs_{y_K}\right)\right\};$

Step:2 Outout:$CO, CO2$

Step:3 Initialized:

$K = 1; N = ||C||; M = ||S||; ruta = \emptyset$

set $dc_i - s_j = dist(i; j), \forall i = 1 \rightarrow N, \forall j = 1$

set $ds_i - s_j = dist(i; j), \forall (i \wedge j) = 1 \rightarrow M$ set $borde = s_i \in S \mid \forall s_i$

Step:4 $scOC = S \setminus (C \cup BS)$

Step:5 **forall** $scOC_q \in scOC$ **do**

$ruta_k = dijkstra(ds_i - s_j, BS, scOK_q)$

endforall

Step:6 set $CO \left| \begin{array}{l} ruta_{OK} = \min\{ruta\} \, \forall BS_k \\ \wedge \\ \min\left(dist_{CO-borde_p}\right) \end{array} \right.$

Step:7 set $CO2 \left| \min\left(dijkstra(ds_i - s_j, CO2, borde_p)\right) \right.$

Step:8 return $CO, CO2$;

3.1.1 Heuristics Results

The model allows to find the optimal location of the BS that delivers the total coverage of the SMs of each residence and in this way the NAN network is formed. This is an exploratory analysis that finds the optimal location for the candidate sites in order to reduce the resource costs for the implementation. Figure 3.3 shows the final connectivity of SMs to each BS.

Subsequently, with the optimal locations of each BS, the heuristic model finds the optimal location of the central office (CO-NAN) using the minimum distance in order to allow the connection between the BS and the Central Office, by using a fiber optic link. The model is able to derive optimal Splitter's location considering the sites already used in the grid map with the aim to reach all the users in the network. The results are shown in the Figures 3.4 where the Capacity is the ability to host users in a BS and is evaluated from a range of 5 to 10 users with a maximum number of BS equal to 3. In the first figure the cost of fiber optic is reduced when the radio of BS increases due to amount of users that must be connected in the network. The algorithm converges exponentially with more interactions when the capacity and the radio of Base Station increase at the same time.

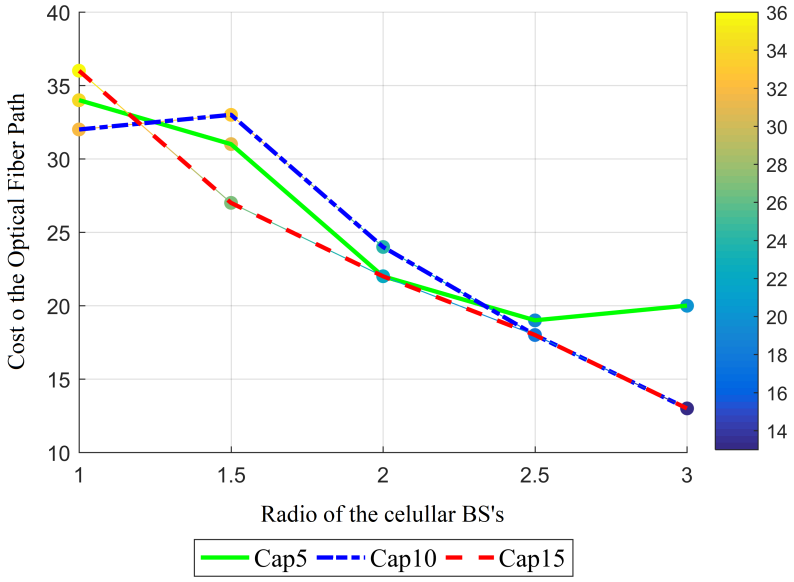

(a) Fiber vs Wireless link cost

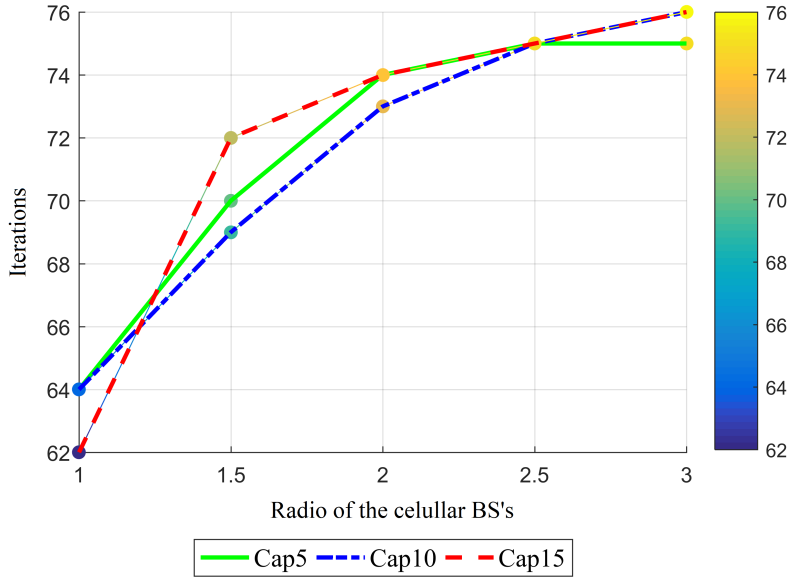

(b) Number of iterations vs. BS

Figure 3.4: Evaluation of costs and algorithm performance on FiWi networks.

3.2 Optimal Processing over Optical Communication

As we mentioned in the previous section, the deployment, processing and optimization on the wireless communications can not work without the support of a more robust network that allows higher bandwidths/rates/capacity with the possibility that users can access at great speeds to a data cloud and achieve experiences with optimal quality of services.

The problem for wireless networks is that the medium of transmission to and from the user – the air interface – is necessarily shared. In order to increase the bandwidth available to each user, fewer users must share the resource, which leads, in general, to a requirement for the size of ′ cells′ to decrease. The problem, then, is providing large amounts of bandwidth to larger numbers of small cells. The future communication networks need to marry the mobility offered by wireless connectivity to the high bandwidth provided by an optical distribution network.

In this context, the join processing between wireless systems and optical communications is is every day more imminent. There are different variants for the optical deployment of fiber-based next-generation access (NGA), but the main directions are: Point-to-Point and Passive Optical Networks. In this thesis, the next generation PON is described in terms of processing deployment with the aim to achieved high rate transmission.

WDM technology may allow its use as a backhaul for legacy wireless networks that they are being adopted for global operator by sharing its costs through several networks. In the next section is described a basical system with the principle of radio over fiber systems that involves the transport of an analog radio wave over a fiber link.

In order to get a flexible and adaptive optical transmission, a multilevel modulation is used to increase the spectral efficient through a coherent detection over optical systems [69]. Many structures proposes can be found to create different multilevel systems over the Mach-Zehnder modulator (MZM). In [70], a MZM is used in a monolithic silicon photonic 4-PAM device to produce a 56Gbps trans-

mission at 1310 nm wavelength. Furthermore, [71] describes the technique for a 16-QAM system using two MZM in parallel, called Dual-Drive configuration (DD-MZM). The system drives 4 binary signals, where the amplitude voltage values are handled through the MZM transfer function. Moreover, [72] uses a 64-QAM system with IQ-MZM driven by 4 binary electrical signals, proving a 240Gbps during the transmission.

In [73] a new Segmented Electrode over the wave guide of Mach-Zehnder (SEMZM) is proposed, in order to reduce the interconnection range and the power consumption, supporting in this way the higher data rates. In [74] a Integer Circuit CMOS is used to distributed the driver bit input for a low power consumption in a 4-PAM system for a 40Gbps transmission. In [75], the SEMZM to generate a 16-PAM signal at 160Gbps without an external DAC is used.

In [76] an experimental back-to-back (B2B) is set at 80 Km with DAC-less system using 16-QAM and 64-QAM transmissions over In Phase-Quadrature SEMZM (IQ-SEMZM). An integrated circuit Bipolar-CMOS (BiCMOS), and a hard-decision forward error correction (HD-FEC) is used, obtaining a BER= $3.8\text{x}10^{-3}$ measure in 64-QAM system at 37dB.

[31] shows a robust 256-QAM experiment for 32GBd with BiCMOS technology, over a 80km of distance, through two different LDPC codes in two stages with code rates of 1/2 and 2/3 with block dimensions of 1440x2880 and 2880x4320 respectively. The results show that the system achieves the best performance for the 2/3 code rate at OSNR=45dB a BER=10^{-4}. For the second stage,code rate at 1/2,the result is a BER=10^{-5} for an OSNR=27dB.

However, it is possible combining diversity techniques to generate a multilevel system [77], this method is proposed in [32], which uses a MZMs combinations in order to configure an OFDM-QPSK. In this context, the system can switch QPSK, 8-PSK, 8-QAM and 16-QAM in order to improve the spectral efficiency. Another proposal of multilevel modulation using DWDM systems is shown in [78] and [79], where HD-FEC using LDPC codes is development for DWDM schemes in the optical communications providing in this way a solution on the core network backbone. The advanced processing over optical communications enables the last

generation networks as XG-PON, where deployment of new and legacy networks are integrated by working at higher capacity and quickly data transmission on the same backhaul.

3.3 Solution in the Physical Layer

Several modulation methods have been used in the past. Single carrier (SC) modulation has been popular but ISI is a problem for which an equalizer is needed in the receiver at the output of the matched filter and sampler.

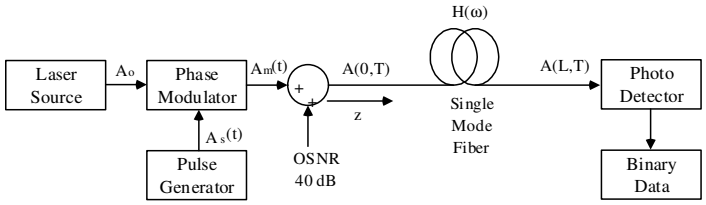

Figure 3.5: General structure for Physical Layer.

In the Figure 3.5 the laser source A_o is introduced to Phase Modulator with an amplitude equal to 1 using different wavelengths as (1310/1550)nm. The phase variation corresponding to the electrical driving voltage $A_s(t)$ is given as:

$$\varphi(t) = \pi \frac{A_s(t)}{V_p} \tag{3.1}$$

Where V_p is the voltage required in order to create a shift phase of 180 degrees on the light wave carrier [80], $A_s(t)$ represent the binary data in time-varying driving signal voltage and is given as:

$$A_s(t) = A_o \cdot s(t)\, e^{-\frac{1}{2}(1+j)t^2} \tag{3.2}$$

Where $s(t)$ are the binary pulses in the time domain and $e^{(1+j)}$ is the complex normalization of a periodic signal. Then, the complex-envelope representation of the optical field A_m at the output of EOPM (Electro-Optic Phase Modulation) is expressed as:

$$A_m(t) = e^{j\varphi(t)} - A_o \tag{3.3}$$

The Fig. 3.6 shows an overall system block diagram proposed in order to analyze a solution by RoF (Radio over Fiber) that it proposed a novel multilevel optical modulator in order to provide high data rate with high modulation index. On the electrical side, data from a binary source $b\,[n]$ first pass through LDPC encoder $R = n/k$ to obtain the coded bits $b\,[k]$. The LDPC decoder is constrained by Soft-Decision based on Sum-Product decoding algorithm (SPA), where is combined with Look-up-Table (LUT) and Gray Code in order to normalize the symbols according to set value of energy used in M-QAM modulation levels. The process of LDPC encoder/decoder design is referenced in [81] in order to obtain the probabilistic algorithm for SD-FEC.

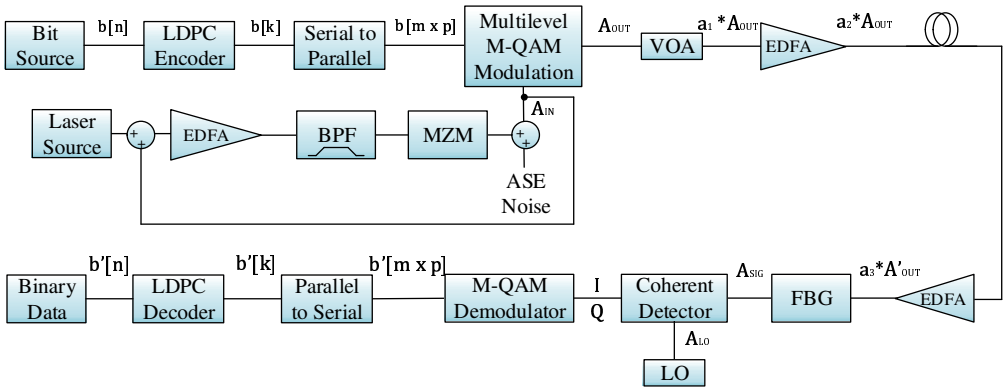

Figure 3.6: Block Diagram of M-QAM optical system.

Next, these bits are separated $b\,[m \times p]$ to obtain m outputs by a serial to parallel block to enter the Multi-Level M-QAM modulation that combines the electrical signals with an Actively Mode-Locked Fiber Ring, A_{IN} in order to generate the optical signal transmission A_{OUT}. Our approach is focused on the design of this modulator which is explained in the following section.

On another hand, the optical part is composed of an Actively Mode-Locked Fiber Ring Laser (MLFL), which includes the laser cavity design, active or gain medium (Erbium Doped Fiber Amplifier-EDFA), filter (BPF), and modulator mechanism (Mach-Zehnder Modulator-MZM). The noise generated in the system is due to ASE generated by EDFA. The filter provides stabilization against the energy fluctuation of the pulses propagating [26].

Next, the signal is insert through a Variable Optical Attenuator (VOA) to ensure that the optical power launched into the fiber or the receiver is at an appropriate level. The length of the fiber is normally 80 km whose attenuation is 20 dB. This attenuation can be equalized by the gain or typical EDFA. This means that, through VOA and EDFA is possible to combine different distances beyond 80km.

The DSP techniques are introduced in this scheme in order to compensate the linear and nonlinear impairments [82] for decision and recovery of the original data sequence. The resulting signal A_{sig}, is inserted in a coherent detection, which uses a phase shifter to change the phase over 0/90/180/270 degrees and combining with a Local Oscillator signal A_{LO}, outcoming four signals I_q described by (3.4).

$$l_q = \frac{1}{2}\left(A_{sig} + A_{LO}e^{i(q-1)\frac{\pi}{2}}\right), \quad q = 1, 2, 3, 4 \tag{3.4}$$

Where l_q is the electric field received by an optical detector where the interference between A_{sig} shifted and A_{LO} is taking place. And q represents the number of out coming signal for the result of the combination. The I and Q values are obtained when $I = l_1 - l_3$ and $Q = l_2 - l_4$. Furthermore, forward error coding (FEC) techniques have also been employed to enhance the BER with coding gain. The coherent detector result is processed through a M-QAM demodulation to return the symbol data to bit data. Next the Parallel to Serial block converts to stream data in order to decoded the signal by the LDPC decoder where the signal generated is finally recovered.

3.3.1 Multilevel Modulation Design

We simulate an Optical Multilevel M-QAM Modulation, based on 4 parallel Mach Zehnder Modulators using a commercially available dual drive IQ modulator driven by eight NRZ signals combining with different amplitudes.

This proposed design is of complex manufacture according to the authors, due to transceivers must have smaller footprints in order to reduce the power consumption. However, the simulated results show an interesting performance when the system is transmitted at 64-QAM up 80 km of distance. The BER performance achieves 10^{-04} at 27dB.

Our proposed is based on [71] and [32] to design a novel Multilevel M-QAM Modulation that allows to transmit on the optical fiber at different distances.

The Fig. 3.7 shows that Multilevel-QAM modulator scheme proposed. Each MZM is a dual drive MZM (DD-MZM) driven by eight NRZ signals (+1,-1) that decide the phase shifting and which in turn are multiplied by four levels of amplitude in the I-arm and Q-arm. These voltage levels will depend of the 4/16/64/256-QAM generation signals. In addition, a phase-offset of $\pi/2$ is added after of Q-arm in the modulator.

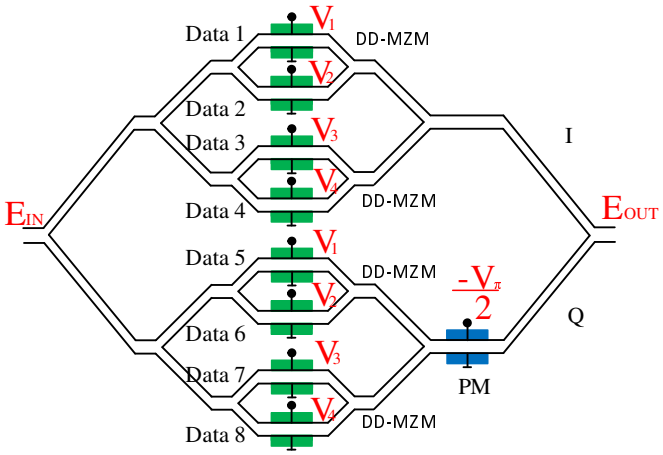

Figure 3.7: Multilevel M-QAM Modulator Design.

16-QAM Signal Generation The operating principle of the proposed 16-QAM transmitter is shown in Fig. 3.8. We will take the MZM in I arm of the IQ modulator to illustrate the 4-APSK generation in more detail. However the overall 16-QAM signal is generated by adding the two 4-APSK signals in the I-arm and Q-arm components. The MZM is operated in push-pull mode and biased at the Null point ($v_b = \pi$). The drive signals are two signals with amplitude v_H and v_L where ($v_H > v_L$), for the upper-arm and lower-arm respectively. Then, if $v_\pi = 2.5$ is a constant, four-level amplitude and phase-shift keying (4-APSK) signals are generated in this way: $v_H = 0.86v_\pi$ and $v_L = 0.44v_H$, where $v_1 = v_2 = \pm v_H/2$ and $v_3 = v_4 = \pm v_L/2$ in order to modulated the I and Q components. The transfer function of the dual drive MZM for 16-QAM is defined by:

$$\frac{A_{OUT}}{A_{IN}} = \mathbb{C}\left\{\frac{1}{2}\left[e^{j(\phi_1)} + e^{j(\phi_3)} + e^{-j(\phi_2)} + e^{-j(\phi_4)}\right]\right\} \tag{3.5}$$

Where:

$$\phi_n = \frac{\pm V_n}{2V_\pi}\pi + \frac{\pi}{2}, \qquad n = 1, 2, 3, 4 \tag{3.6}$$

and

$$\theta_n = \frac{\pm V_n}{2V_\pi}\pi, \qquad n = 1, 2, 3, 4 \tag{3.7}$$

Then, the overall 16-QAM signal generation with IQ components can be rewrite as:

$$\begin{aligned}\frac{A_{OUT}}{A_{IN}} = \frac{1}{2}\Bigg[\; e^{j\left(\frac{\pm V_1}{V_\pi}\pi+\frac{\pi}{2}\right)} + e^{-j\left(\frac{\pm V_2}{V_\pi}\pi+\frac{\pi}{2}\right)} + e^{j\left(\frac{\pm V_3}{V_\pi}\pi+\frac{\pi}{2}\right)} + e^{-j\left(\frac{\pm V_4}{V_\pi}\pi+\frac{\pi}{2}\right)} \;\Bigg] + \\ j\frac{1}{2}\Bigg[\; e^{j\left(\frac{\pm V_1}{V_\pi}\pi+\frac{\pi}{2}\right)} + e^{-j\left(\frac{\pm V_2}{V_\pi}\pi+\frac{\pi}{2}\right)} + e^{j\left(\frac{\pm V_3}{V_\pi}\pi+\frac{\pi}{2}\right)} + e^{-j\left(\frac{\pm V_4}{V_\pi}\pi+\frac{\pi}{2}\right)} \;\Bigg]\end{aligned} \tag{3.8}$$

The Transfer Function can be solved using some trigonometric identities in this way:

(3.9)

In 16-QAM mode, each DD-MZM uses a driving bit to achieve 10Gbps, resulting to four bits a data rate of 40Gbps.

According to the Fig. 3.8, the condition $d_1 = 2d_2$ is very important in order to obtain the distance among the constellation points through Eq. (3.10). This condition also allows obtaining the v_1 and v_2 voltage values, being already previously established.

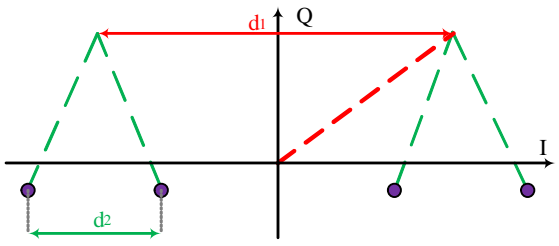

Figure 3.8: 4-APSK generation with DD-MZM, $v_1 = v_2$, $v_3 = v_4$.

$$d_n = 2sin\left(\frac{V_n}{V_\pi}\pi\right) \tag{3.10}$$

Table 3.2, 3.3 and 3.4 shows the allocation of the parallel bits in correspondence with the driver signals in order to be modulated according to the Transfer Function by each modulation. These bits coming out of S/P block, and they are function of the modulation index $k = \log 2(M)$.

	Diver	Bits
I-arm	v_1, v_2	1
	v_3, v_4	2
Q-arm	v_1, v_2	3
	v_3, v_4	4

Table 3.2: Driver Signals Allocation for 16-QAM.

64-QAM Signals Generation In order to obtain the overall 64-QAM signal, it also is used two 4-APSK signals in the I-am and Q-arm respectively. The upper DD-MZM use two different data inputs, and the lower DD-MZM only uses one data input in this way: $v_H = 0.57v_\pi$ and $v_L = 0.4246v_H$ for the upper-arm and lower-arm respectively. In this context, $v_1 = v_3 = v_4 = \pm v_H/2$ and $v_2 = \pm v_L/2$.

According to the Fig. 3.9, the condition for a square constellation is defined as $d_1 = 2d_2$ and $d_2 = 2d_3$, in order to obtain the amplitude of the drivers signals.

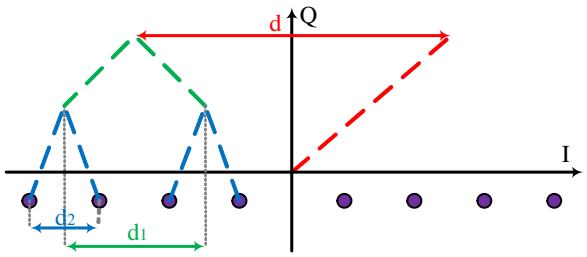

Figure 3.9: Constellation generated by the I arm for 64-QAM.

$$d_1 = 2sin\left(\frac{V_3}{2V_\pi}\pi\right) + 2sin\left(\frac{V_4}{2V_\pi}\pi\right) \tag{3.11}$$

Through the grouping of terms and trigonometric identities, the overall Transfer Function for 64-QAM signal generation results is as follows:

$$\frac{A_{OUT}}{A_{IN}} = \frac{1}{2}\left[e^{j\left(\frac{\pm V_H}{2V_\pi}\pi+\frac{\pi}{2}\right)} + e^{-j\left(\frac{\pm V_L}{2V_\pi}\pi+\frac{\pi}{2}\right)} + e^{j\left(\frac{\pm V_H}{2V_\pi}\pi+\frac{\pi}{2}\right)} + e^{-j\left(\frac{\pm V_H}{2V_\pi}\pi+\frac{\pi}{2}\right)} \right] + j\frac{1}{2}\left[e^{j\left(\frac{\pm V_H}{2V_\pi}\pi+\frac{\pi}{2}\right)} + e^{-j\left(\frac{\pm V_L}{2V_\pi}\pi+\frac{\pi}{2}\right)} + e^{j\left(\frac{\pm V_H}{2V_\pi}\pi+\frac{\pi}{2}\right)} + e^{-j\left(\frac{\pm V_H}{2V_\pi}\pi+\frac{\pi}{2}\right)} \right] \tag{3.12}$$

Where, the overall solve is as follow:

(3.13)

	Diver	Bits
I-arm	v_3, v_4	1
	v_1	2
	v_2	3
Q-arm	v_3, v_4	4
	v_1	5
	v_2	6

Table 3.3: Driver Signals Allocation for 64-QAM.

256-QAM Mode For 256-QAM signal generation, each MZM does not share information with any other, due to modulator uses its own amplitude drives. In this context, I-arm uses $v_1 = 0.57v_\pi$, $v_2 = 0.4246v_1$ for the first DD-MZM and $v_3 = 0.1028v_1$, $v_4 = 0.2069v_1$ for the second DD-MZM. The Q-arm uses the same values with respect to I-arm and consequently, the phase is changed in function of the bits that it arrive at the modulator.

The overall function transfer can be calculated through Eq. 3.8. The Table 3.4 specifies the allocation bits in accordance with the driver signals. Fig. 3.10 shows the calculated distance among the constellation points that is defined by $d_1 = 2d_2$, $d_2 = 2d_3$ and $d_3 = 2d_4$ according to Eq. (3.11).

3.3.2 Numerical Results on Optical Physical Layer

The overall simulations for the optical processing is done in Matlab, where the parameter settings are presented in the Table 3.5. In addition, the parameters

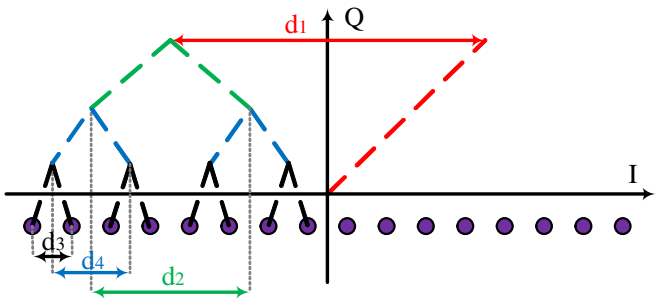

Figure 3.10: Constellation generated by the I arm for 256-QAM.

	Diver	Bits
I-arm	v_1	1
	v_2	2
	v_4	3
	v_3	4
Q-arm	v_1	5
	v_2	6
	v_4	7
	v_3	8

Table 3.4: Driver Signals Allocation for 256 -QAM.

settings used for LDPC coding are in the same way as the section 1.3.4 where the MZM plays the rol of converting the electrical signals to optical signals in order to insert the Modulation scheme and so this will be transmitted by the optical fiber.

Measurement BER vs. Transmission Distance Analysis This section presents the simulation results analyzed, using a LDPC coded/uncoded transmission in order to evaluated the best index modulation when the system is subjected to different distances up 100km.

When the BER performance is analyzed, the expected results are obtained in function of attenuation that is implicit in the OSNR signal. If the modulation index is increased, the noise report also increased. However, in our analysis the OSNR is fixed as a constant that is not implicit in the error probability. In this context,

Table 3.5: **List of parameters used in Matlab for Optical Processing**

Wavelength (λ)	1550nm
LDPC code rate ($R_n \times k$)	1/2
n	1024
k	2048
frequency of modulation (f_m) =40Ghz	
bandwith of the filter BW	1.2 nm
Amplifier Gain G_a	20 dB
Output Power P_out	10 dBm
Index of Modulation (M)	16 - 64 - 256 QAM
Number of pulse points by block (N)	1000
Sample Frequency (F_s)	$f_m * N$

the behavior of 16/64/256-QAM at 100km does not have an abrupt change with respect to the other distances as show in Fig. 3.11. 64-QAM mode presents the better transmission in terms of OSNR, considering that, the 16-QAM mode has the half of data stream than 64-QAM mode, but a bit error probability very close to 64QAM. The measured for 256-coded shows an error floor at BER=8x10-2 for an OSNR larger than 45 dB, being a disestablished transmission in this modulation format. However, in Fig 3.12. we analyzed BER vs. Transmission distance for pre-FEC and coded system. Our design shows that it is possible to transmit for a distance larger than 200 Km in each modulation format.

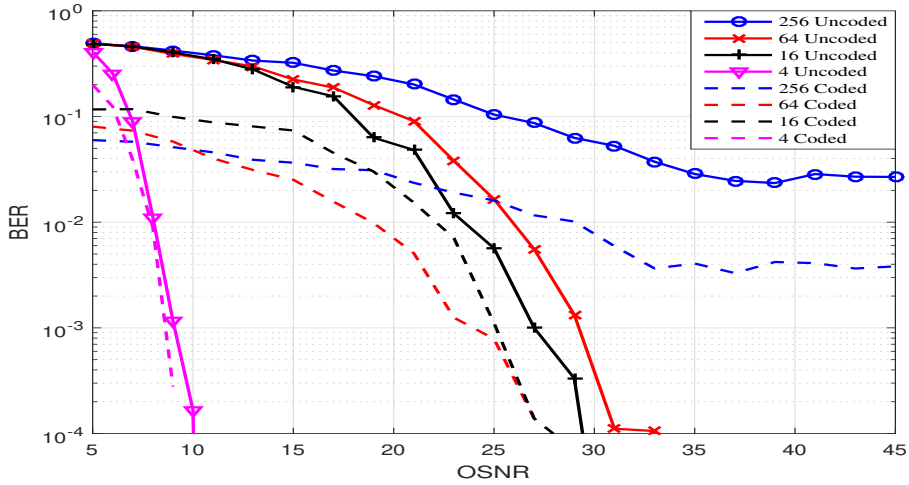

Figure 3.11: BER measure at 100 Km.

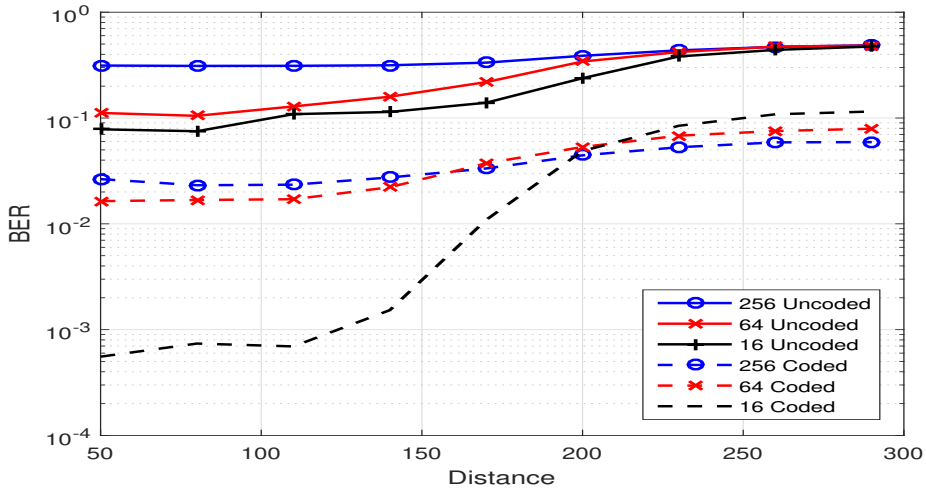

Figure 3.12: Measured BER vs Transmission Distance.

Pulse Propagation Analysis Fig. 3.13,3.14,3.15 shows the power transmission normalized of the pulse propagation for 50/80/100-Km of distance in 16/64/256-QAM respectively. The OSNR level is fixed at 20dB. The amplitude of pulse is decreased when the distance increases for all cases. The critical case is given when the distance arrives at 100km. The secondary pulses are attenuated due to

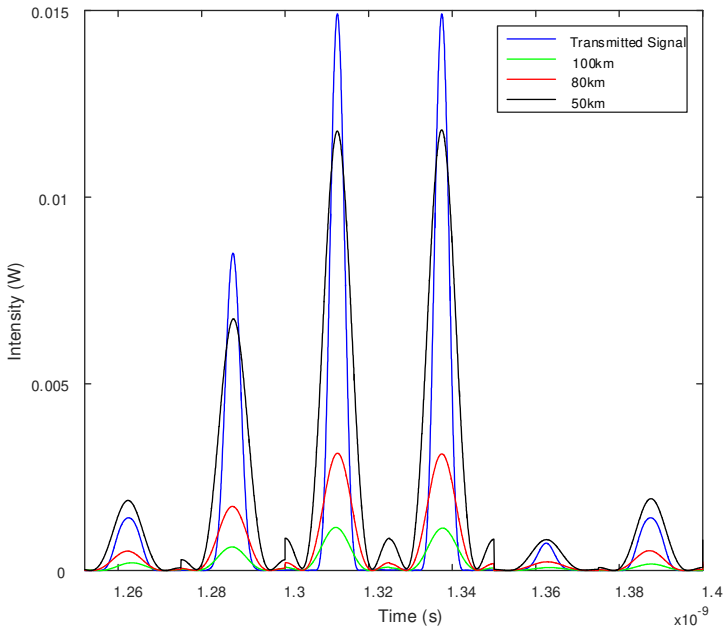

Figure 3.13: Pulse propagation by 16QAM, OSNR=20dB.

EDFA amplifier and consequently producing ISI.

The analysis can be extended with the eye diagram in order to show the reliability transmission in terms of ISI and determine the best conditions for the fiber.

Eye Diagram and Constellation Plots Analysis The Fig.3.16,3.17,3.18,3.19,3.20 shows the eye diagrams in-phase and quadrature for 16/64/256-QAM transmissions at 80km of distance. In the first case, 16-QAM works with an $OSNR = 20dB$ and the second case, 64-QAM increases the noise level with $OSNR = 40dB$, in order to evaluated the receiver behavior when increasing the noise, the distance and the index modulation.

Then, if the modulation index increases, the eye diagram closes and it increases the ISI, this is due to the saturation of the sampling time in each transmitted pulse. However our Multilevel-QAM Modulation design is able to support long distances up to 80km.

This statement can be very convincing with the Constellation Plots, where the

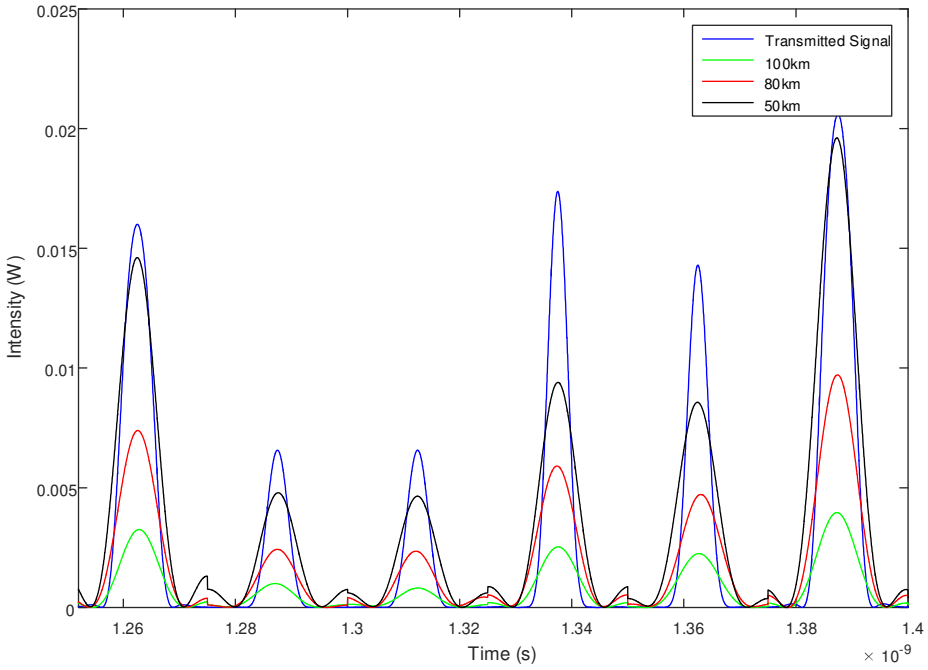

Figure 3.14: Pulse propagation by 64QAM, OSNR=20dB.

role of coherent detector can be clearly seen.

Finally, we demonstrated that it is possible to transmit up to 256QAM. Fig. 3.21 show the behavior of each modulation in the receiver. When the system is transmitted at 256-QAM it is very important to work with algorithms of optimization in the phase correction. On another hand, the rank of OSNR can improve the system performance when it is increased.

The sample time for each pulse is $250ps$, where the sample frequency is defined by $Fs = R * N$, being R the maximum rate transmission at 320Gbps and N the number of samples points established to 1000. The rate can increase according to the modulation index $R = fm * k$, being fm the modulation frequency set to 40GHz.

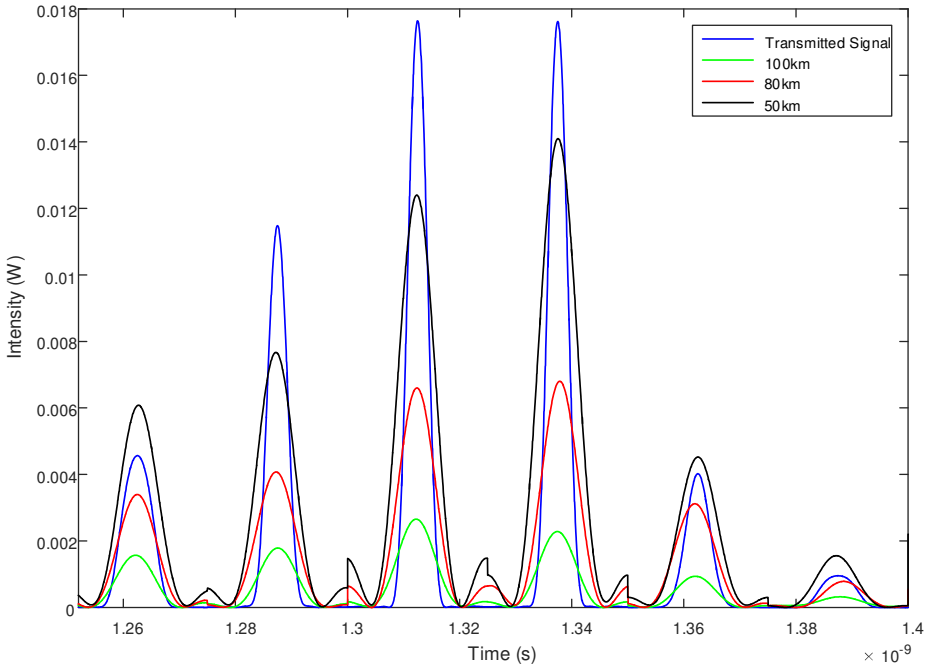

Figure 3.15: Pulse propagation by 256QAM, OSNR=20dB.

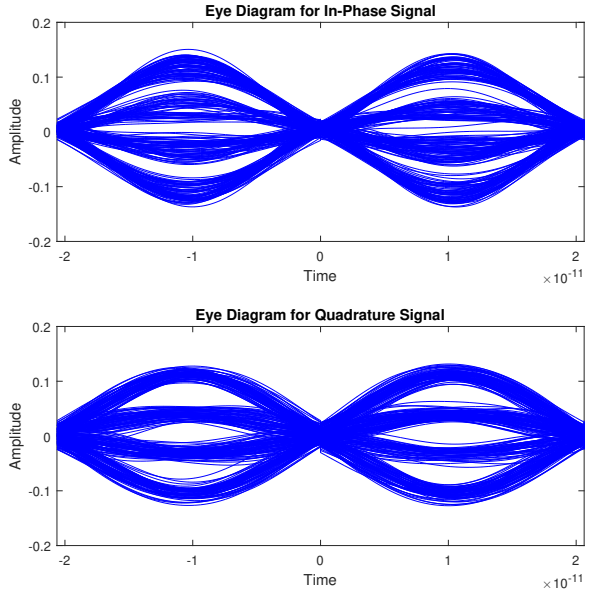

Figure 3.16: Eye diagram for 16-QAM with OSNR=20dB.

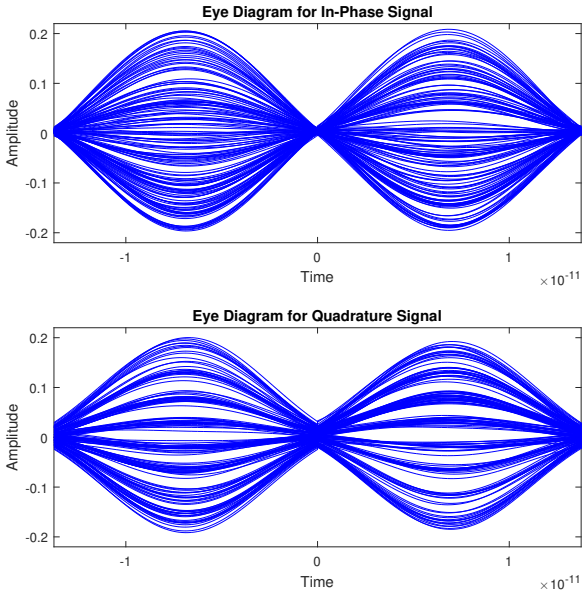

Figure 3.17: Eye diagram for 64-QAM with OSNR=40dB.

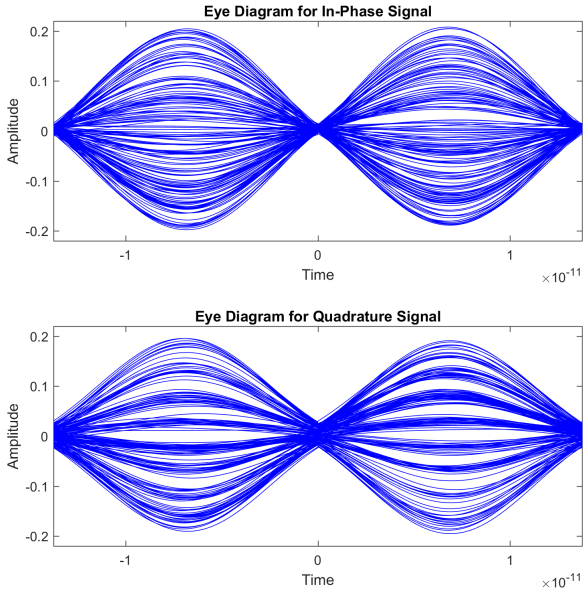

Figure 3.18: Eye diagram for 64-QAM with OSNR=20dB.

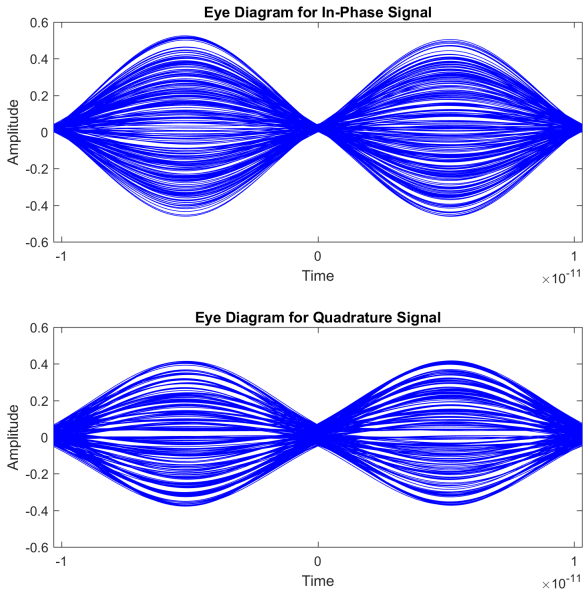

Figure 3.19: Eye diagram for 256-QAM, 50Km, OSNR=20dB.

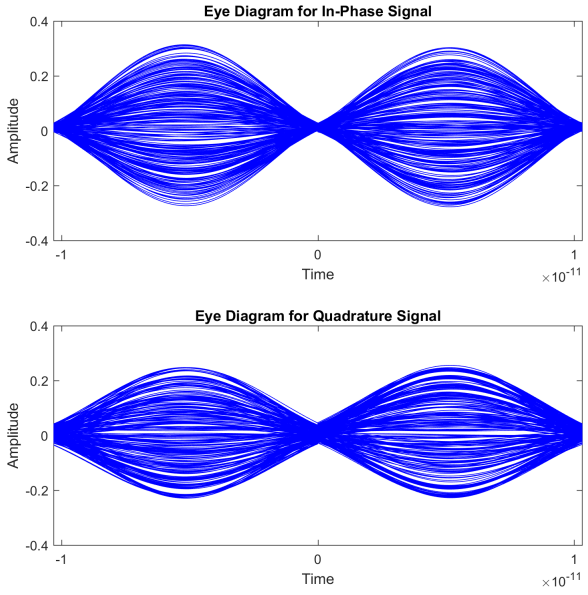

Figure 3.20: Eye diagram for 256-QAM, 80KM, OSNR=20dB.

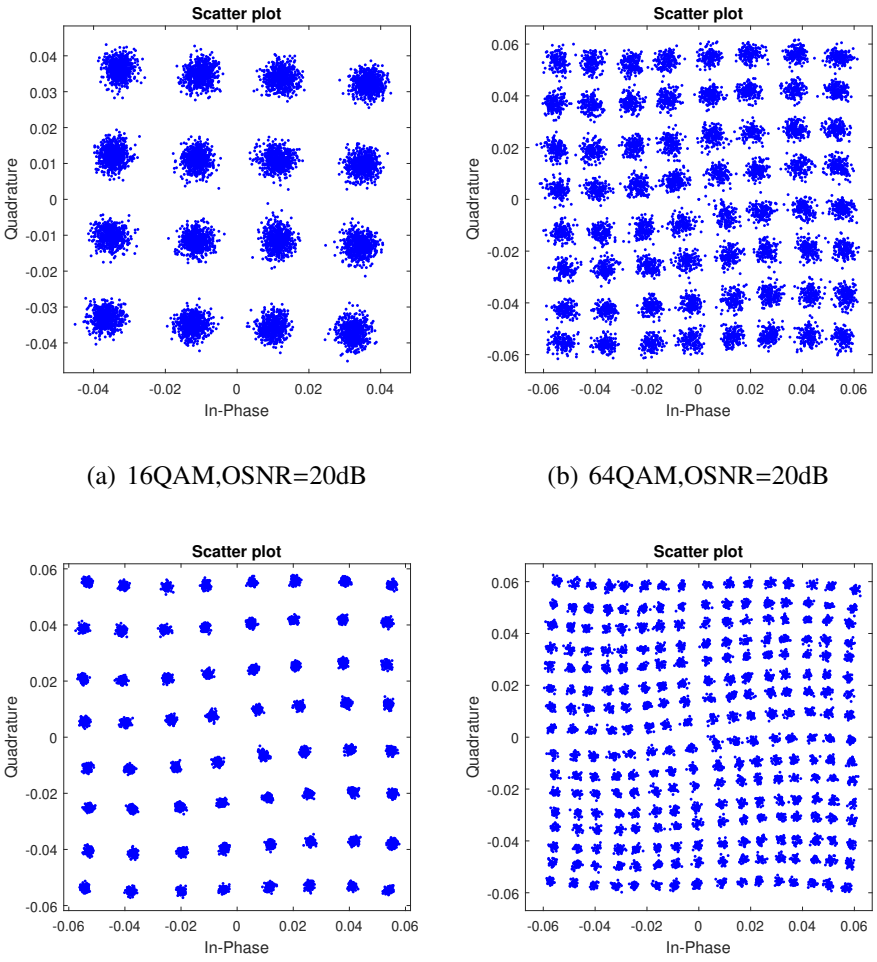

(a) 16QAM,OSNR=20dB

(b) 64QAM,OSNR=20dB

(c) 64QAM,OSNR=40dB

(d) 256QAM,OSNR=20dB

Figure 3.21: Scatter Plots.

Conclusions

This work presented a general framework for PHY layer processing and Network Access Optimization for 5G communications in order to satisfy the QoS requirements for the last generation networks, which is essential for many researches and developers.

The research framework includes a new multi-access scheme proposed for 5G namely Generalized-Frequency-Division-Multiplexing (GFDM), where its performance in presence of non-linear channel effects is evaluated, with the aim to explore the effectiveness of some PAPR reduction techniques to mitigate OOB radiation and error performance degradation. More specifically we have considered clipping techniques with iterative receiver and filtering, companding and selective mapping techniques, and also IFDMA for comparison.

The results suggest that a good technique for PAPR reduction in GFDM systems, which addresses to 5G systems requirements is clipping with CR between 1.5 and 2.5. In addition, this techniques allows the use of iterative detection schemes at the receiver that compensate for the nonlinear distortion. For comparison, IFDMA is able to maintain an acceptable performance level with low complexity in the receiver. It is less performing compared to GFDM with clipping techniques in terms of PAPR, but it has much better BER performance than GFDM in the nonlinear channel.

In this context, we also moved from theory to practice to test a last generation scheme that includes a SDR transmission with MIMO channel and LDPC coding we evaluated the system performance over Rayleigh channel. Currently, radio transmissions over SDR system are gaining a higher position in communi-

cation systems due to their flexibility, compatibility, scalability and high parallel processing for the deployment of more robust algorithms at the PHY layer level.

The results show that the implementation of the MIMO 3x4 technique with LDPC codes improves the systems over Rayleigh channel in terms of SNR and capacity. Our implementation show a gain of $13dB$ in terms of SNR and $6bps/Hz$ of gain in terms of capacity with respect to MIMO 2x2 when 16QAM modulation is used.

The performance of multi-access systems depends on the resource allocation; that is, on how the time, power, frequency, and spatial resources are divided among users. We have investigated the effects of pilot-aided channel estimation on the capacity of a two-tier HetNet with QoS-aware centralized AC and RRA that control the effects of cross-interference and optimize a service provider revenue. Network capacity depends on the outcome of the AC algorithm that takes into account link-rate degradation due to channel estimation error and pilot-symbols overhead.

In the results for both uplink and downlink, we have found that the impact of channel estimation error is not negligible and is especially relevant for downlink CUs. However, we have also shown that this degradation can be partially mitigated by allocating more power over pilot symbols.

We have also addressed the problem of network optimization in HetNet's due to network densification, it becomes important to develop a core network that provides the support for all the amount of information generated in the micro networks i.e. VANETS, SMART GRIDS accessing to a CORE NETWORK using to optical 5G backhauls.

For this thesis we developed of 5G backhaul solutions, through the design of a multilevel M-QAM modulator capable of transmitting at large distances with a good performance using digital processing over fiber optical. The simulation results present a small difference between the 16 and 64 QAM modes in the uncoded system. A BER=1x10e-04 the OSNR difference between them are of 4/4.5/2 dB for link lengths of 50/80/100 Km. 64-QAM may be a modulation format suitable for long-distance transmissions that allow greater spectral efficiency when the amount of information to be transfered is large.

As future work we plan to test a complete access scheme that combines diversity techniques with a strong parallel processing. In addition the HetNet should be optimized as a of multi-cell system with beamforming and coordination problems among base stations.

Finally, our optical link can be combined with DWDM technology in order to achieve a better performance. Additionally, the modulation formats investigated can evolve towards multidimensional-modulations. The simulation has shown that our proposed system can be implemented in a practical way through SE-MZM.

Appendix A

Greedy Algorithm for Admission Control

Here, the algorithm for Admission Control is illustrated. It is obtained from [53] by adapting it to HetNet scenario.
The key-idea is to build clusters of CU users having the maximum value of a suitably defined objective function and to select them for admission in the cellular system until constraint holds. This objective function includes both the utility, i.e., the total revenue of a CU cluster, and the total cost, i.e., the amount of RBs required to achieve the required QoS for each CU in the cluster.

A cluster $C = \mathcal{K}' \cup \mathcal{D}'$ is defined as a subset of CUs and SUs that includes at least one CU. The cost of cluster C is given by $\Psi C = \Psi(x,\beta) = \sum_{k \in K} x_k \left[\frac{q_k}{c_k^{(0)}} + \sum_{d \in D} \beta_d^{(k)} \left(1 - \frac{c_k^{(d)}}{c_k^{(0)}} \right) \right]$, while objective function is defined as:

$$f_C(\beta) = U(x,z) - \mathcal{F}\Psi(x,\beta) \tag{A.1}$$

where $x_k = 1$, $z_d = 1$, if $k \in \mathcal{K}'$, $d \in \mathcal{D}'$ respectively, and $x_k = 0$, $z_d = 0$ otherwise. The parameter $\mathcal{F}$ is a positive scaling factor. A cluster is said to be optimized if $\beta = \beta^*$ such that the objective function achieves the maximum value $f_C(\beta^*)$, given the constraints (2.2), (2.3), (2.4) and (2.5) that they are described in

the Chapter 2. The optimum β^* is then the solution of the following problem:

$$\min_{\beta} \sum_{k \in \mathcal{K}'} \sum_{d \in \mathcal{D}'} \beta_d^{(k)} \left(1 - \frac{c_k^{(d)}}{c_k^{(0)}} \right) \tag{A.2}$$

This is a simple LP problem which can be optimally solved with polynomial complexity, e.g., by using the interior-point or dual-simplex methods, which also evaluates the feasibility of the problem. If the problem is unfeasible, cluster C is said to be not optimized. If the problem is feasible, it may happen that some $k' \in \mathcal{K}'$ exist such that $\beta_d^{(k')} = 0, \forall d \in \mathcal{D}'$.

This means that the CU k' does not support resource sharing with the SU in C. Hence, we finally define the minimal cluster $\overline{C}$ that supports resource sharing with SUs in C as $\overline{C} = \mathcal{D}' \cup \mathcal{K}'\ k \in \mathcal{K}' : \beta_d^{(k)} = 0, \forall d \in \mathcal{D}'$.

The details of the AC algorithm are illustrated as follows:

Algorithm 4 Greedy Algorithm for Admission Control

Step 1 Input: Initialize the set $\mathcal{A}$ of admitted CUs to 0. Define the marginal cost (objective) of a cluster C as the cost (objective) of the cluster C minus the cost (objective) of the cluster $C \cup \mathcal{A}$.

Step 2 Sort the CUs in the set $\mathcal{K}$ in decreasing order according to the individual objective function. For each $k \in \mathcal{K}$ build the cluster C_k^0 with $\mathcal{K}' = k' = 1, \ldots k$ and $\mathcal{D}' = 0$.

Step 3 For each SU d, build the cluster C_d^h with $\mathcal{K}' = \mathcal{K}$ and $\mathcal{D}' = d$. If the optimized cluster of C_d^h exists, derive the minimal cluster $\overline{C}_d^h$ of C_d^h and set it as admissible.

Step 4 Compute the marginal cost and the marginal objective of all the admissible clusters C_k^0 and $\overline{C}_d^h$. If the marginal cost of cluster $\overline{C}_d^h$ plus the cost of $\mathcal{A}$ is larger than S, then set the cluster $\overline{C}_d^h$ as not admissible.

Step 5 Find the cluster $\overline{C}_{d^*}^h$ with minimum marginal cost among the admissible clusters $\overline{C}_d^h$. If some clusters C_k^0 have both a larger marginal objective and a smaller marginal cost with respect to $C_{d^*}^h$, select the cluster C_k^0 with minimum k and include it in $\mathcal{A}$, otherwise build the cluster $C^{temp} = \overline{C}_{d^*}^h \cup \mathcal{A}$. If the minimal cluster $\overline{C}^{temp}1$ exists and its cost is smaller than S, include cluster $C_{d^*}^h$ in $\mathcal{A}$.

Step 6 Go to step 4 until there is no admissible clusters.

Step 7 Iteratively admit the not yet admitted CUs if the total cost does not exceed S.

Bibliography

[1] K. Au, L. Zhang, H. Nikopour, E. Yi, A. Bayesteh, U. Vilaipornsawai, J. Ma, and P. Zhu, "Uplink contention based SCMA for 5G radio access," in *2014 IEEE Globecom Workshops, GC Wkshps 2014*, 2014, pp. 900–905.

[2] P. Banelli, S. Buzzi, G. Colavolpe, A. Modenini, F. Rusek, and A. Ugolini, "Modulation Formats and Waveforms for 5G Networks: Who Will Be the Heir of OFDM?: An overview of alternative modulation schemes for improved spectral efficiency," *Signal Processing Magazine, IEEE*, no. October, pp. 80–93, 2014.

[3] C. G. K. Yong Soo Cho, Jaekwon Kim, Won Young Yang, *Mimo Ofdm Wireless Communications With Matlab*, 2010.

[4] P. Mishra, G. Singh, R. Vij, and G. Chandil, "BER Analysis of Alamouti Space Time Block Coded 2x2 MIMO Systems using Rayleigh Dent Mobile Radio Channel," pp. 154–158, 2012.

[5] G. S. S. Priya and B. Senthil, "An efficient scheme for PAPR reduction in Alamouti MIMO-OFDM systems," *2014 International Conference on Information Communication and Embedded Systems, ICICES 2014*, no. 978, 2015.

[6] H. Futaki and T. Ohtsuki, "Low-density parity-check (LDPC) coded MIMO systems with iterative turbo decoding," *2003 IEEE 58th Vehicular Technology Conference. VTC 2003-Fall (IEEE Cat. No.03CH37484)*, vol. 1, pp. 342–346, 2003.

[7] J. Hou, P. Siegel, L. Milstein, and H. Pfister, "Capacity-approaching bandwidth-efficient coded modulation schemes based on low-density parity-check codes," *IEEE Transactions on Information Theory*, vol. 49, no. 9, pp. 2141–2155, sep 2003.

[8] C. Rachinger, R. Müller, and J. Huber, "Low Latency-Constrained High Rate Coding: LDPC Codes vs. Convolutional Codes," *Symposium on Turbo Codes and Iterative Information Processing (ISTC), 2014 8th International*, no. 2, pp. 218–222, 2014.

[9] T. Lestable, E. Zimmerman, M. H. Hamon, and S. Stiglmayr, "Block-LDPC Codes vs Duo-Binary Turbo-Codes for European Next Generation Wireless Systems," *Ieee Vehicular Technology Conference*, pp. 1–5, 2006. [Online]. Available: http://ieeexplore.ieee.org/lpdocs/epic03/wrapper.htm?arnumber=4109550

[10] R. Pyndiah, a. Picart, and a. Glavieux, "Performance of block turbo coded 16-QAM and 64-QAM modulations," *Proceedings of GLOBECOM '95*, vol. 2, pp. 1039–1043, 1995.

[11] M. Taherzadeh, H. Nikopour, A. Bayesteh, and H. Baligh, "SCMA Codebook Design." Vancouver, BC, Canada: Vehicular Technology Conference (VTC Fall), 2014 IEEE 80th, 2014.

[12] U. Sorger, I. D. Broeck, and M. Schnel, "Interleaved FDMA-a new spread-spectrum multiple-access scheme," in *Communications, 1998. ICC 98. Conference Record. 1998 IEEE International Conference on*, 1998, pp. 1013–1017.

[13] G. Fettweis, M. Krondorf, and S. Bittner, "GFDM - Generalized frequency division multiplexing," *IEEE Vehicular Technology Conference*, pp. 1–4, 2009.

[14] R. Datta and G. Fettweis, "FBMC and GFDM Interference Cancellation Schemes for Flexible Digital Radio PHY Design," in *Digital System Design (DSD), 2011 14th Euromicro Conference on*, 2011, pp. 335–339.

[15] S. Das and S. Tiwari, "Discrete Fourier transform spreading-based generalised frequency division multiplexing," *Electronics Letters*, vol. 51, no. 10, pp. 789–791, 2015. [Online]. Available: http://digital-library.theiet.org/content/journals/10.1049/el.2014.3833

[16] N. Chiurtu, L. Gasser, P. Roud, and B. Rimoldi, "Software-defined radio implementation of multiple antenna systems using low-density parity-check codes," *Wireless Communications and Networking Conference, 2005 IEEE*, vol. 1, pp. 527—-531 Vol. 1, 2005.

[17] Z. He, S. Roy, and P. Fortier, "Adaptive LDPC codes for MIMO transceiver with adaptive spectral efficiency," *24th Biennial Symposium on Communications, BSC 2008*, pp. 120–123, 2008.

[18] N. Michailow, L. Mendes, M. Matthe, I. Gaspar, A. Festag, and G. Fettweis, "Robust WHT-GFDM for the next generation of wireless networks," *IEEE Communications Letters*, vol. 19, no. 1, pp. 106–109, 2015.

[19] K. S. Masaaki Fuse, "Non-orthogonal Multiple Access and Massive MIMO for Improved Spectrum Efficiency," vol. 19, no. 91, pp. 19–30, 2016.

[20] F. Fang, H. Zhang, J. Cheng, and V. C. M. Leung, "Energy Efficiency of Resource Scheduling for Non-Orthogonal Multiple Access (NOMA) Wireless Network," *2016 IEEE International Conference on Communications (ICC)*, 2016.

[21] J. Oviedo and H. Sadjadpour, "A new NOMA approach for fair power allocation," in *Proceedings - IEEE INFOCOM*, vol. 2016-Septe, 2016, pp. 843–847.

[22] Y. Han, L. Jiang, and C. He, "Resource sharing optimization for device-to-device wireless system with femtocells," in *IEEE International Conference on Communications*, vol. 2015-Septe, 2015, pp. 2535–2540.

[23] J. G. Andrews, F. Baccelli, and R. K. Ganti, "A tractable approach to coverage and rate in cellular networks," *IEEE Transactions on Communications*, vol. 59, no. 11, pp. 3122–3134, 2011.

[24] C.-h. Yu, K. Doppler, B. Ribeiro, and O. Tirkkonen, "Resource Sharing Optimization for Device-to-Device Communication Underlaying Cellular Networks," vol. 10, no. 8, pp. 2752–2763, 2011.

[25] N. Q. Ngo and Others, *Ultra-fast fiber lasers: Principles and applications with MATLAB{®} models*. CRC Press, 2010.

[26] H. Feng, W. Zhao, S. Yan, and X. P. Xie, "Generation of 10-GHz ultra-short pulses with low time jitter in an actively mode-locked fiber laser," *Laser Physics*, vol. 21, no. 2, pp. 404–409, 2011.

[27] A. Ortega, L. Fabbri, and T. Velio, "Performance evaluation of GFDM over nonlinear channel," in *2016 International Conference on Information and Communication Technology Convergence (ICTC)*, 2016, pp. 12–17.

[28] R. Prieto, A. Abril, and A. Ortega, "Experimental Alamouti-STBC using LDPC codes for MIMO channels over SDR systems," *Canadian Conference on Electrical and Computer Engineering*, pp. 1166–1170, 2017.

[29] A. Ortega, S. Negrini, and V. Tralli, "On the effects of pilot-aided channel estimation on the capacity of QoS-aware heterogeneous OFDMA networks," in *IEEE 13th Malaysian International Conference on Communications*, 2017.

[30] E. Inga-Ortega, A. Peralta-Sevilla, R. C. Hincapie, F. Amaya, and I. Tafur Monroy, "Optimal dimensioning of FiWi networks over advanced metering infrastructure for the smart grid," *2015 IEEE PES Innovative Smart Grid Technologies Latin America, ISGT LATAM 2015*, pp. 30–35, 2016.

[31] A. Aimone, F. Frey, R. Elschner, I. G. Lopez, G. Fiol, P. Rito, M. Gruner, A. C. Ulusoy, D. Kissinger, J. K. Fischer, C. Schubert, and M. Schell, "DAC-Less 32-GBd PDM-256-QAM Using Low-Power InP IQ Segmented MZM," *IEEE Photonics Technology Letters*, vol. 29, no. 2, pp. 221–223, 2017.

[32] H. Yamazaki, T. Yamada, T. Goh, and S. Mino, "Multilevel optical modulator with PLC and LiNbO 3 hybrid integrated circuit," in *Optical Fiber Communication Conference and Exposition (OFC/NFOEC), 2011 and the National Fiber Optic Engineers Conference*. IEEE, 2011, pp. 1–3.

[33] B. Penafiel and O. Andres, "A joint multilevel modulator and robust LDPC codes Processing over Optical Systems by providing solutions for holistc 5G backhaul," in *IEEE 13th Malaysian International Conference on Communications*, 2017, pp. 1–6.

[34] N. Michailow, S. Krone, M. Lentmaier, and G. Fettweis, "Bit Error Rate Performance of Generalized Frequency Division Multiplexing," *2012 IEEE Vehicular Technology Conference (VTC Fall)*, pp. 1–5, 2012. [Online]. Available: http://ieeexplore.ieee.org/lpdocs/epic03/wrapper.htm?arnumber=6399305

[35] N. Thi and T. Trang, "POWER EFFICIENCY 1MPROVEMENT BY PAPR FEDUCTION AND PREDISTORTER IN MIMO-OFDM SYSTEM," in *The 7th International Conference on Advanced Communication Technology, 2005, ICACT 2005.*, 2005.

[36] L. X and C. L, "Effects of clipping and filtering on the performance of OFDM," in *IEEE 47th Vehicular Technology Conference. Technology in Motion*, no. C, 1997, pp. 2005–2008.

[37] A. Conti D. Dardari ; V. Tralli, "On the performance of CDMA systems with nonlinear amplifier and AWGN," in *Sixth International Symposium on Spread Spectrum Techniques and Applications, 2000 IEEE*, vol. 00, no. Mc 240, 2000.

[38] L. Sendrei, S. Marchevsk, N. Michailow, and G. Fettweis, "Iterative Receiver for Clipped GFDM Signals," in *Radioelektronika (RADIOELEKTRONIKA), 2014 24th International Conference*, no. 1, 2014, pp. 14–17.

[39] N. Michailow, R. Datta, S. Krone, M. Lentmaier, and G. Fettweis, "Generalized Frequency DivisionMultiplexing for 5th Generation Cellular Networks Nicola," *IEEE Transactions on Communications*, vol. 62, no. 9, pp. 3045–3060, 2014.

[40] C. An, B. Kim, and H. G. Ryu, "Design of W-OFDM and nonlinear performance comparison for 5G waveform," *2016 International Conference on Information and Communication Technology Convergence, ICTC 2016*, pp. 1006–1009, 2016.

[41] Z. Sharifian, M. J. Omidi, A. Farhang, and H. Saeedi-Sourck, "Polynomial based compressing and iterative expanding for PAPR reduction in GFDM," *To appear in Proc. of ICEE'15*, pp. 518–523, 2015.

[42] M. Matthe, N. Michailow, I. Gaspar, and G. Fettweis, "Influence of pulse shaping on bit error rate performance and out of band radiation of Generalized Frequency Division Multiplexing," in *2014 IEEE International Conference on Communications Workshops, ICC 2014*, 2014, pp. 43–48.

[43] D. Cuji and P. Chasi, "Frame Synchronization Through Barker Codes Using SDRs in a Real Wireless Link," in *2016 International Conference on Electronics, Communications and Computers (CONIELECOMP)*, no. 2, 2016, pp. 68–72.

[44] S. T. Brink, G. Kramer, and a. Ashikhmin, "Design of low-density parity-check codes for modulation and detection," *IEEE Transactions on Communications*, vol. 52, no. 4, pp. 670–678, 2004.

[45] X.-Y. Hu, E. Eleftheriou, D. Arnold, and a. Dholakia, "Efficient implementations of the sum-product algorithm for decoding\nLDPC codes,"

GLOBECOM'01. IEEE Global Telecommunications Conference (Cat. No.01CH37270), vol. 2, pp. 1–6, 2001.

[46] T. J. Richardson and R. L. Urbanke, "The capacity of low-density parity-check codes under message-passing decoding," *IEEE Transactions on Information Theory*, vol. 47, no. 2, pp. 599–618, 2001.

[47] M. Baldi, F. Chiaraluce, and G. Cancellieri, "Finite-Precision Analysis of Demappers and Decoders for LDPC-Coded M-QAM Systems," *IEEE Transactions on Broadcasting*, vol. 55, no. 2, pp. 239–250, jun 2009.

[48] S. Lai, R. Cheng, K. Letaief, and R. Murch, "Adaptive trellis coded MQAM and power optimization for OFDM transmission," *1999 IEEE 49th Vehicular Technology Conference (Cat. No.99CH36363)*, pp. 290–294, 1999.

[49] Z. Ding, R. Schober, and H. V. Poor, "On the design of MIMO-NOMA downlink and uplink transmission," in *2016 IEEE International Conference on Communications, ICC 2016*, vol. 1, 2016.

[50] S. Pietrzyk, G. J. M. Janssen, R. Unit, and P. Warsaw, "Multiuser Subcarrier Allocation for QoS Provision in the OFDMA Systems," *in IEEE 56th Vehicular Technology Conference*, vol. 2, no. 1, pp. 1077–1081, 2002.

[51] C. Y. Wong, R. S. Cheng, K. B. Letaief, and R. D. Murch, "Multiuser OFDM with adaptive subcarrier, bit, and power allocation," *IEEE Journal on Selected Areas in Communications*, vol. 17, no. 10, pp. 1747–1758, 1999.

[52] C. H. Yu, O. Tirkkonen, K. Doppler, and C. Ribeiro, "Power optimization of device-to-device communication underlaying cellular communication," in *IEEE International Conference on Communications*, 2009, pp. 1–5.

[53] S. Cicaló and V. Tralli, "Joint Admission Control and Resource Allocation for D2D Communications with QoS Constraints," in *2015 IEEE Globecom Workshops (GC Wkshps)*, 2015.

[54] M. Kaneko, T. Nakano, and K. Hayashi, "Distributed Resource Allocation With Local CSI Overhearing and Scheduling Prediction for OFDMA Heterogeneous Networks," *IEEE Transactions on Vehicular Technology*, vol. 66, no. 2, pp. 1186–1199, 2017.

[55] M. Bacha, Y. Wu, and B. Clerckx, "Downlink and Uplink Decoupling in Two-Tier Heterogeneous Networks With Multi- Antenna Base Stations," *IEEE Transactions on Wireless Communications*, vol. 16, no. 5, pp. 2760–2775, 2017.

[56] D. Verenzuela and G. Miao, "Scalable D2D Communications for," *IEEE Transactions on Wireless Communications*, vol. 16, no. 6, pp. 3435–3447, 2017.

[57] S. Ohno and G. B. Giannakis, "Capacity Maximizing MMSE-Optimal Pilots for Wireless OFDM Over Frequency-Selective Block Rayleigh-Fading Channels," *IEEE Transactions on Information Theory*, vol. 50, no. 9, pp. 2138–2145, 2004.

[58] X. Cai and G. B. Giannakis, "Error probability minimizing pilots for OFDM with M-PSK modulation over Rayleigh-fading channels," *IEEE Transactions on Vehicular Technology*, vol. 53, no. 1, pp. 146–155, 2004.

[59] M. Anas, C. Rosa, F. D. Calabrese, P. H. Michaelsen, K. I. Pedersen, and P. E. Mogensen, "QoS-Aware Single Cell Admission Control for UTRAN LTE Uplink," in *Vehicular Technology Conference, 2008. VTC Spring 2008. IEEE*, vol. 1, no. 1, 2008, pp. 2487–2491.

[60] G. Song and Y. G. Li, "Cross-Layer Optimization for OFDM Wireless Networks — Part I : Theoretical Framework," *IEEE Transactions on Wireless Communications*, vol. 4, no. 2, pp. 614–624, 2005.

[61] H. Weingarten; Y. Steinberg; S. Shamai, "Gaussian Codes and the Scaled Nearest Neighbor Decoder in Fading Multi-Antenna Channels," in *Proceedings IEEE International Symposium on Information Theory*, 2002, p. 7803.

[62] R. M. A. Ghosh, J. Zhang, J. G. Andrews, *"Fundamentals of LTE"*. Prentice Hall, 2010.

[63] M. Jaber, M. Imran, R. Tafazolli, and A. Tukmanov, "5G Backhaul Challenges and Emerging Research - A survey," *IEEE Access*, vol. 3536, no. c, pp. 1–1, 2016. [Online]. Available: http://ieeexplore.ieee.org/lpdocs/epic03/wrapper.htm?arnumber=7456186

[64] N. Ghazisaidi and M. Maier, "Fiber-wireless (FiWi) access networks: Challenges and opportunities," *IEEE Network*, vol. 25, no. 1, pp. 36–42, 2011.

[65] M. Lévesque, M. Maier, and M. Mttr, "Probabilistic Availability Quantification of PON and WiMAX Based FiWi Access Networks for Future Smart Grid Applications," vol. 62, no. 6, pp. 1958–1969, 2014.

[66] A. Peralta-Sevilla, E. Inga, R. Cumbal, and R. Hincapié, "Optimum deployment of FiWi Networks using wireless sensors based on Universal Data Aggregation Points," in *IEEE Colombian Conference on Communications and Computing, COLCOM 2015 - Conference Proceedings*. IEEE, 2015, pp. 1–6.

[67] Q. Dai, G. Shou, Y. Hu, and Z. Guo, "A General Model for Hybrid Fiber-Wireless (FiWi) Access Network Virtualization," pp. 858–862, 2013.

[68] A. Peralta, E. Inga, and R. Hincapié, "FiWi Network Planning for Smart Metering Based on Multistage Stochastic Programming," *Latin America Transactions, IEEE (Revista IEEE America Latina)*, vol. 13, no. 12, pp. 3838–3843, 2015.

[69] E. Ip, A. P. T. Lau, D. J. F. Barros, and J. M. Kahn, "Coherent detection in optical fiber systems," 2008.

[70] C. Xiong, D. M. Gill, J. E. Proesel, J. S. Orcutt, W. Haensch, and W. M. J. Green, "Monolithic 56 Gb/s silicon photonic pulse-amplitude modulation transmitter," *Optica*, vol. 3, no. 10, pp. 1060–1065, 2016.

[71] S. Yan, D. Wang, Y. Gao, C. Lu, A. Lau, L. Liu, and X. Xu, "Generation of square or hexagonal 16-QAM signals using a single dual drive IQ modulator driven by binary signals," in *Optical Fiber Communication Conference and Exposition (OFC/NFOEC), 2012 and the National Fiber Optic Engineers Conference*. IEEE, 2012, pp. 1–3.

[72] S. Yan, D. Wang, Y. Gao, C. Lu, A. Lau, Y. Zhu, Y. Dai, and X. Xu, "Generation of 64-QAM signals using a single dual-drive IQ modulator driven by 4-level and binary electrical signals," in *Optical Fiber Communication Conference and Exposition and the National Fiber Optic Engineers Conference (OFC/NFOEC), 2013*. IEEE, 2013, pp. 1–3.

[73] S. S. Azadeh, J. Müller, F. Merget, S. Romero-García, B. Shen, and J. Witzens, "Advances in Silicon Photonics Segmented Electrode Mach-Zehnder Modulators and Peaking Enhanced Resonant Devices," in *Proc. Of SPIE Vol*, vol. 9288, 2014, pp. 928 811–928 817.

[74] T. N. Huynh, N. Dupuis, R. Rimolo-Donadio, J. E. Proesel, D. M. Gill, C. W. Baks, A. V. Rylyakov, C. L. Schow, W. M. J. Green, and B. G. Lee, "Flexible Transmitter Employing Silicon-Segmented Mach–Zehnder Modulator With 32-nm CMOS Distributed Driver," *Journal of Lightwave Technology*, vol. 34, no. 22, pp. 5129–5136, 2016.

[75] I. G. Lopez, P. Rito, L. Zimmermann, D. Kissinger, and A. C. Ulusoy, "A 40 Gbaud SiGe:C BiCMOS driver for InP segmented MZMs with integrated DAC functionality for PAM-16 generation," in *IEEE MTT-S International Microwave Symposium Digest*, vol. 2016-Augus, no. 99, 2016, pp. 3–6.

[76] A. Aimone, I. García López, S. Alreesh, P. Rito, T. Brast, V. Höhns, G. Fiol, M. Gruner, J. K. Fischer, J. Honecker, A. G. Steffan, D. Kissinger, A. C. Ulusoy, and M. Schell, "DAC-free Ultra-Low-Power Dual-Polarization 64-QAM Transmission with InP IQ Segmented MZM Module," *Ofc 2016*, vol. 1, pp. 15–17, 2016.

[77] T. Pinto, D. Mello, D. Arantes, and L. Carvalho, "System evaluation of optical M-QAM modulation driven by multilevel and binary waveforms," in *Communications (LATINCOM), 2016 8th IEEE Latin-American Conference on*. IEEE, 2016, pp. 1–5.

[78] H. Y. Choi, T. Tsuritani, H. Takahashi, W.-R. Peng, and I. Morita, "Generation and detection of 240-Gb/s PDM-64QAM using optical binary synthesizing approach and phase-folded decision-directed equalization," *Opt. Express*, vol. 20, no. 25, pp. 27 933–27 940, 2012.

[79] L. Cuzco, J. Arias, and A. Ortega, "LDPC-DWDM processing for Optical communications using polymer fiber," in *Communications and Computing (COLCOM), 2016 IEEE Colombian Conference on*. IEEE, 2016, pp. 1–5.

[80] L. N. Binh and N. Q. Ngo, *Ultra-Fast Fiber Lasers: Principles Applications with MATLAB Models*, 2011. [Online]. Available: http://www.lavoisier.fr/livre/notice.asp?id=RK2W6SARR3SOWL

[81] A. Ortega and J. Bravo, "Combining LDPC codes, M-QAM modulations, and IFDMA multiple-access to achieve 5G requirements," in *Electronics, Communications and Computers (CONIELECOMP), 2017 International Conference on*. IEEE, 2017, pp. 1–5.

[82] A. Rostamiand and A. Yazdanpanah-Goharrizi, "Optical transfer function: A new proposal for identification of complex brag gratings using genetic algorithm (optimization)," *Journal of Electromagnetic Waves and Applications*, vol. 22, no. 4, pp. 599–613, 2008.

Acknowledgments

Innanzitutto voglio ringraziare Dio per il dono della vita e della salute e per il coraggio che mi ha dato per portare a termine questa parte di percorso della mia vita. Ringrazio l'UPS per aver creduto in me. Ringrazio il mio Tutor Velio perché è stato come una guida per me: lo ringrazio soprattutto per la sua pazienza, per la sua umiltà e per gli infiniti consigli. Ricorderò sempre le sue parole: "La ricerca non finisce mai!".

Voglio ringraziare tutte le persone del Dipartimento: docenti, colleghi ed amici da cui ho imparato e condiviso tante cose bellissime proprio dell'Ingegneria.

Ringrazio il Dott. Cicalò che è stato una delle prime persone che mi ha aiutato e fornito supporto in questo lungo percorso che, mi sarebbe piaciuto continuare a fare ricerca insieme a Lui.

Ringrazio Chisci: non solo un collega ma anche un amico che ho avuto il piacere di conoscere veramente; ti ringrazio in modo particolare per tutte l'esperienza che abbiamo condiviso insieme. Inoltre i miei amici dell'Ecuador a Ferrara che mi hanno sempre sostenuto e ci sono sempre stati nei momenti più difficili.

Ed infine, il più importante, ringrazio la mia Famiglia che purtroppo è molto lontana da me: tutti voi siete il mio tesoro meraviglioso, la cosa più bella che un uomo possa avere nella sua vita. Senza affetto non c'è nulla e voi, in questi lunghi mesi, mi avete riempito di calore facendomi sentire sempre vicino a voi.

Grazie fratelli Juano & Diego, grazie Gozalito-Carmita, grazie Mami Sara, grazie Tebo-Mary, grazie Cognati..

Grazie ancora a tutti Voi!!!